

H24/3485

se of
s for

er

may

or in

owing

eds to
ng the

Eng, Monash Uni

garding
n to the

12/02

MONASH UNIVERSITY
THESIS ACCEPTED IN SATISFACTION OF THE
REQUIREMENTS FOR THE DEGREE OF
DOCTOR OF PHILOSOPHY

ON..... 15 April 2003

Sec. Research Graduate School Committee

Under the copyright Act 1968, this thesis must be used only under the normal conditions of scholarly fair dealing for the purposes of research, criticism or review. In particular no results or conclusions should be extracted from it, nor should it be copied or closely paraphrased in whole or in part without the written consent of the author. Proper written acknowledgement should be made for any assistance obtained from this thesis.

MULTIMODAL VORTEX-INDUCED VIBRATION

**Dissertation submitted in partial fulfilment
of the requirements for the degree of
Doctor of Philosophy at Monash University**

by

**Hayden Marcollo
B.Sc. B.E. (Hons)**

**Department of Mechanical Engineering
Monash University
Victoria, Australia 3800**

December 2002

SUMMARY

A long flexible riser exposed to ocean currents is known to undergo Vortex-Induced Vibration (VIV). In a spatially sheared flow the response of a riser to VIV can vary from single mode lock-in to multimodal. The purpose of this thesis was to determine important issues in the area of VIV prediction in shear flow and then address these issues through an experimental investigation.

A literature review revealed three important areas lacking in knowledge. The areas were:

- The accuracy of short rigid cylinder results for long flexible cylinder cases.
- In-line motion and its effect on cross-flow response.
- Modal competition and dominant response behaviour.

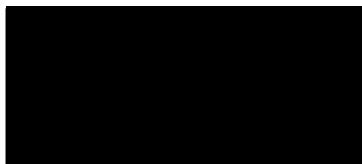
A new experimental facility was designed and built to investigate the above mentioned areas. The facility consisted of a long flexible cylinder (modelling a riser) in a uniform and a simplified spatially sheared flow. The simplified shear flow was a 2-Slab flow, with each slab having uniform velocity. The cylinder was simultaneously forced at resonant from both regions to investigate modal competition issues and multimodal response patterns. Variables that were subject to the investigation were the relative length of each of the slabs and the spacings of natural frequencies.

Through the use of direct local fluid force measurement at two locations on the cylinder as well as accelerometers spaced along the cylinder axis several important results were obtained. The results were:

- Short rigid cylinder results predict added mass of long flexible cylinders well and location (as a function of reduced velocity) of peak response poorly.
- In-line lock-in can dominate cross-flow lock-in in regions where the in-line response is associated with another region's higher frequency cross-flow response.
- The development of empirical relationships between dominant modal response with power-in length and spacing of natural frequencies.

STATEMENT OF ORIGINALITY

This thesis does not contain any material previously published either for a degree or diploma in any university; and to the best of my knowledge it does not incorporate any material published by another person except where due reference is made in the text of this thesis.



Hayden Marcollo

12 December 2002

Tham
and
(APA
The
Depa
My
Fina

ACKNOWLEDGEMENTS

Thank you to my Supervisor, A/Prof Jon B. Hinwood, for fostering my ideas and encouraging me through the thesis. The Australian Postgraduate Award (APA) scholarship program for its financial support during my candidature. The various graduate students and staff of the Mechanical Engineering Department at Monash University for the technical resources made available. My family and friends for their help and understanding of the commitment. Finally, my wife, Bianca, whose support made it all possible.

TABLE OF CONTENTS

1.	INTRODUCTION	1
1.1.	MOTIVATION	1
1.2.	HISTORY OF PROJECT	3
1.3.	ORGANISATION OF THE THESIS	4
2.	LITERATURE REVIEW	6
2.1.	INTRODUCTION	6
2.2.	STEADY FLOW AROUND A CYLINDER	7
2.3.	THE VORTEX SHEDDING PROCESS	9
2.3.1.	Roughness	11
2.3.2.	Turbulence	12
2.4.	VORTEX SHEDDING FORCES ON A CYLINDER IN STEADY FLOW	12
2.5.	VORTEX-INDUCED VIBRATIONS (VIV)	15
2.5.1.	Basic System Parameters	16
2.5.2.	Basic Force Analysis	17
2.5.3.	Reduced Velocity	19
2.5.4.	Lock-in; Air Experiments	19
2.5.5.	Width of Lock-in Region	21
2.5.6.	Differences in Water	22
2.5.7.	Added Mass Effects	24
2.5.8.	Amplitudes of VIV	27
2.5.9.	Correlation	29
2.5.10.	In-line response	30
2.6.	RISER STRUCTURAL DYNAMICS	33
2.6.1.	Damping of Excitation Waves	35
2.6.2.	Quantifying Force on Flexible Cylinders	35
2.7.	VIV IN SHEAR CURRENT	36
2.7.1.	Number of Possible Modes	37
2.7.2.	Lock-in Characteristics	38
2.7.3.	Damping in Shear Flow	38
2.7.4.	Amount of Shear	42
2.8.	LATEST OBSERVATIONS	45
2.9.	CONCLUDING THE LITERATURE REVIEW	46
2.10.	THESIS OBJECTIVES	47
2.11.	EXPERIMENTAL FACILITY REQUIREMENTS	48
3.	DESCRIPTION OF THE EXPERIMENTS	50
3.1.	DESIGN OF APPARATUS AND FACILITIES	50
3.1.1.	The Facilities	50
3.1.2.	The Use of a Constriction for the Flow	51
3.1.3.	Two-flow Field	53

.....1	3.1.4. The Riser Model	55
.....1	3.1.5. Model Scale and Testing Effects	60
.....3	3.1.6. Instrumentation.....	62
.....4	3.1.7. Signal Acquisition.....	70
.....6	3.2. EXPERIMENTAL DESIGN AND VELOCITY PROFILES	71
.....6	3.2.1. Experimental Design	71
.....7	3.2.2. Flow Profile.....	74
.....9	3.3. PROBLEMS ENCOUNTERED.....	81
.....11	4. STATIONARY FLOW RESULTS AND LIFT	
.....12	FORCE CORRECTION.....	85
.....12	4.1. STILL WATER NATURAL FREQUENCIES.....	85
.....15	4.1.1. Vibration Technique	85
.....16	4.2. STRUCTURAL DAMPING VALUES	88
.....17	4.2.1. Effect of Mode Number and End Tension.....	89
.....19	4.3. LIFT FORCE CORRECTION MODEL.....	91
.....19	4.3.1. Correction Model from Stationary Cylinder.....	91
.....21	4.4. CONCLUDING THE CHAPTER.....	94
.....22	5. UNIFORM FLOW RESULTS	95
.....24	5.1. LIFT FORCE COEFFICIENTS	95
.....27	5.2. UNIFORM FLOW RESPONSE	100
.....29	5.2.1. Modal Displacement.....	102
.....30	5.3. CROSS-FLOW DYNAMICS	106
.....33	5.3.1. Amplitude of Response.....	107
.....35	5.3.2. Frequency of Vibration and Added Mass	109
.....35	5.3.3. Lift Force.....	113
.....36	5.3.4. Effects of Spacing of Natural Frequencies.....	121
.....37	5.3.5. Hysteresis	122
.....38	5.4. IN-LINE RESPONSE	124
.....38	5.4.1. Mode 1 In-line.....	125
.....42	5.4.2. Higher In-line Modes	126
.....45	5.5. SUMMARY OF CHAPTER.....	133
.....46	6. 2-SLAB FLOW RESULTS.....	134
.....47	6.1. VARIABLE EXAMINED.....	134
.....48	6.2. AMPLITUDE OF RESPONSE.....	135
.....50	6.3. FREQUENCY OF RESPONSE.....	144
.....50	6.4. CROSS-FLOW FORCE	149
.....50	6.4.1. Forces and Coefficients from Original Time Series.....	151
.....51	6.4.2. Forces and Coefficients from Filtered Time Series.....	156
.....53	6.5. EFFECT OF DIFFERENT SPACING OF NATURAL FREQUENCIES.....	163
	6.6. PREDICTION OF RESPONSE.....	168
	6.6.1. Contributions from the Non-favoured Regions	168
	6.6.2. Applicability of coefficients.....	177

pproach.....	178
ENDATIONS	
.....	179
.....	179
.....	180
ORK.....	185
.....	187

LIST OF FIGURES

Figure 2-1 Evolution of vortex shedding patterns with increasing Reynolds number (Sumer and Fredsoe 1997).....	9
Figure 2-2 One shear layer drawing the opposite shear layer across the near wake and rolling up into vortices.....	10
Figure 2-3 Strouhal number vs Reynolds number, $St = St(Re)$ (Blevins 1977).	11
Figure 2-4 Drag and lift traces obtained from measured pressure distributions (Drescher (1956) as reported by Sumer and Fredsoe (1997)).....	13
Figure 2-5 One third of a cycle of vortex shedding showing a sequence of simultaneous surface pressure fields and wake forms at $Re = 112,000$ (Drescher (1956) as reported by Blevins (1977)).	15
Figure 2-6 Simple model of short section cylinder undergoing VIV showing parameters relevant to the equation of motion.	17
Figure 2-7 Feng's data showing the phenomenon of lock-in to the system's natural frequency (Feng (1968) as reported by Blevins (1977)).....	20
Figure 2-8 Regions in which the cylinder motion controls the shedding frequency (Koopman (1967) as reported by Blevins (1977)).....	22
Figure 2-9 The different transverse amplitude response of a cylinder in water and in air vs reduced velocity (Griffin and Ramberg 1982).....	23
Figure 2-10 Rising lock-in frequency phenomenon due to a low mass ratio ($m^* = 2.4$) (Khalak and Williamson 1999).	24
Figure 2-11 The 'Griffin' plot revealing different modes of response by using a log-linear scale instead of a traditional log-log scale (Khalak and Williamson 1999).....	27
Figure 2-12 Correlation length vs amplitude and frequency for an oscillating cylinder. a) Strouhal frequency to cylinder frequency = 1.25; b) Strouhal frequency to cylinder frequency = 1.0 (Toebe 1969).....	30
Figure 2-13 In-line VIV response of a marine pile model against reduced velocity (King 1973).	31
Figure 2-14 Spanwise distribution of Strouhal number (with velocity defined from mid-span value) in a shear flow for a) stationary cylinder, and b) oscillating cylinder with amplitude $A/D = 0.06$ (Stansby 1976).....	37
Figure 2-15 Power flow model for the second mode of vibration of a flexible riser in shear current (Vandiver 1993).	40
Figure 2-16 Hypothesis on how strong shear can lead to single mode dominance (Vandiver <i>et al.</i> 1996).....	44
Figure 2-17 Helland-Hansen full-scale riser response data showing modal participation factors time series and spectra (Kaasen 2000).	46
Figure 3-1 Above: One of the six walls forming the constriction prior to installation showing the depth of testing section. Below: A view of the constriction from above. The flow is from top to bottom of photo. The narrowed testing section is 320 mm wide and 4 m deep.....	53
Figure 3-2 A sketch of the experimental set-up in the constriction. Flow is from left to right.	54
Figure 3-3 The riser model out of the water.....	60

ipe.	Figure 5-15 Mode 2 time series at $Ur_{n=2} = 3$ for previous Ur value of a) $Ur = 3$;	
....64	b) $Ur \gg 3$, c) $Ur \ll 3$	123
id	Figure 5-16 Qualitative low Ur Mode 1 in-line response shown as a function of	
t	Mode 1 cross-flow reduced velocity.	125
....67	Figure 5-17 Mode 1 and Mode 2 in-line response together with Mode 1 cross-	
....76	flow response.....	126
...77	Figure 5-18 Modal participation time series and power spectra for cross-flow	
...79	Mode 1 and 2 and in-line Mode 1 and 2.	127
...80	Figure 5-19 Oscillation frequencies of in-line Mode 1 and 2 as well as the	
the	driving frequency.....	129
...87	Figure 5-20 In-line added mass value for the persistence of Mode 1.....	130
...89	Figure 5-21 Uniform flow riser trajectories for a) $Ur = 4$; b) $Ur = 6$; c) $Ur = 9$.	
...90	132
...93	Figure 6-1 Conceptual sketch of a typical profile considered in Chapter 6. ...	134
rce	Figure 6-2 Time series of Mode 1 and 2 for a typical competing modes test.	135
...93	Figure 6-3 Modal response vs reduced velocity for a power-in length of 40 %	
ries	shown as a) Mode 1; b) Mode 2; c) Mode 2 divided by Mode 1 for each	
.105	individual test.....	137
it	Figure 6-4 Modal response vs reduced velocity for a power-in length of 35 %	
st	shown as a) Mode 1; b) Mode 2; c) Mode 2 divided by Mode 1 for each	
.107	individual test.....	139
cy,	Figure 6-5 Modal response vs reduced velocity for a power-in length of 30 %	
.110	shown as a) Mode 1; b) Mode 2; c) Mode 2 divided by Mode 1 for each	
n	individual test.....	139
.111	Figure 6-6 Kurtosis of Mode 1 and Mode 2 amplitude response as a function	
.112	of Mode 2 reduced velocity for different l^*	141
set	Figure 6-7 Amplitude of response against Mode 2 reduced velocity for each	
.113	individual mode and each power in length (shown in legend). Cross-flow	
al	Mode 1 and 2 are on the L.H.S. while in-line Mode 1, 2 and 3 are on the	
.114	R.H.S.	143
nt	Figure 6-8 Central response frequency for each mode as a function of reduced	
.115	velocity.....	144
for	Figure 6-9 Frequency of response against Mode 2 reduced velocity for each	
.116	individual mode and each power in length (shown in legend). Cross-flow	
.118	Mode 1 and 2 are on the L.H.S. while in-line Mode 1, 2 and 3 are on the	
,	R.H.S.	146
.118	Figure 6-10 Global cross-flow added mass (based purely on response	
.118	frequency) of each mode as a function of each mode's reduced velocity	
.119	for various values of l^*	148
.121	Figure 6-11 $C_{L,V}$, the average lift coefficient in phase with cylinder velocity	
	from the faster and slower regions as a function of Mode 2 reduced	
	velocity.....	152
	Figure 6-12 $C_{L,A}$, the local lift coefficient in phase with acceleration in the	
	faster and slower regions as a function of Mode 2 reduced velocity.	154
	Figure 6-13 Ca , the local added mass for the faster and slower regions as a	
	function of Mode 2 reduced velocity.	154
	Figure 6-14 Slower and faster flow region's $C_{L,V}$ Mode 1 and $C_{L,V}$ Mode 2	
	characteristics.	158

Figure 6-15 Slower and faster flow regions' C_{LA} Mode 1 and C_{LA} Mode 2 characteristics.	160
Figure 6-16 Slower and faster flow regions' Ca Mode 1 and Ca Mode 2 characteristics	161
Figure 6-17 The range coverage of Mode 1 (hollow circles) and Mode 2 (solid circles) reduced velocities. Each pair of lines represents a test series for the ratio of natural frequencies given (w_2/w_1), with each circle representing a test.	164
Figure 6-18 Mode 2 Peak A/D response as a function of the Mode 2 reduced velocity.....	165
Figure 6-19 Mode 1 Peak A/D response as a function of the Mode 1 reduced velocity.....	166
Figure 6-20 Mode 1 Peak A/D response as a function of the Mode 2 reduced velocity.....	166
Figure 6-21 The power transfer in the 'non-favoured' regions for Mode 1 (M1 P.O.) and Mode 2 (M2 P.O.), along with response (q_2/q_1) as a function of reduced velocity.....	169
Figure 6-22 Motion of the model relative to ambient fluid through the slower flow region of fluid for a) less than Mode 2 lock-in ($Ur_{n=2} = 6.8$ for faster region) ; b) Mode 2 lock-in ($Ur_{n=2} = 7.63$); c) greater than Mode 2 lock-in ($Ur_{n=2} = 8.44$).	171
Figure 6-23 Peak cross-correlation values as a function of Mode 2 reduced velocity for a) all modes correlated with the higher frequency force in the slower region b) Mode 1 and Mode 2 correlated with their respective excitation and damping forces. Also shown is Mode 2 / Mode 1 response.	174
Figure 6-24 In-line VIV in the slower flow region against reduced velocity.	175

LIST OF TABLES

ode 2
160
 2
161
 e 2 (solid
 ries for
164
 educed
165
 educed
166
 educed
166
 de 1 (M1
 nction of
169
 e slower
 or faster
 lock-in
171
 educed
 rce in the
 ective
 response.
174
 ocity. 175

Table 3-1 The physical properties of the model.....59
Table 3-2 Predicted nat. frequencies of the model for selected end tensions
59

NOMENCLATURE

All units are based on the SI system

ζ	Damping ratio
ζ_c	Critical damping ratio
ρ	Density of fluid, unless otherwise specified
ρ_{xy}	Peak cross correlation coefficient of variables x and y
ω	Angular frequency
ϕ	Modeshape
φ	Phase angle
β	Shear parameter
τ	Time lag used for correlation
ν	Kinematic viscosity
μ	Viscosity
σ_g	Specific gravity
A	Amplitude
A/D	Peak non-dimensional amplitude
A/D_{rms}	rms non-dimensional amplitude
<i>C.F.</i>	Cross Flow
Ca	Added mass coefficient
Cd	Drag force coefficient
Cdo	Drag force coefficient for stationary cylinder ($A/D=0$)
C_L	Total Lift force coefficient
$C_{L,A}$	Lift force coefficient in phase with acceleration
$C_{L,V}$	Lift force coefficient in phase with velocity
C_{xy}	Correlation coefficient between x and y
D	Diameter
E	Young's Modulus (elastic)
f	Frequency in Hz
\hat{f}	Nondimensional frequency
F_o	Drag force
F_L	Lift force
$F_{L,V}$	Lift force in phase with body velocity
F_{Lrms}	Root mean square value of lift force
f_n	Natural frequency in still water
f_{osc}	Frequency of oscillation
f_v	Frequency of vortex shedding for a stationary cylinder
F_o	Peak force in cycle
I	Area moment of Inertia
<i>I.L.</i>	In Line
K	Kurtosis
k_p	Pressure drop coefficient
k	Stiffness
k^*_{eff}	Effective stiffness

L
 l^*
 l_n
 l_{total}
 L_v
 m
 m^*
 N_s
 P
 q_n
 q_{no}
 rms
 Re
 Re_c
 R_u
 SG
 St
 std
 t
 U
 Ur
 $Ur_{n=1}$
 $Ur_{n=2}$
 U_{TR}
 $w2/w$
 y
 z

L	Length
I^*	Non-dimensional power-in length
I_n	Power-in length of Mode n
l_{total}	Total length of riser
L_u	Macrolength scale of turbulence
m	Mass
m^*	Mass ratio
N_s	Number of possibly excited modes
P	End tension
q_n	Modal participation factor for Mode n
q_{no}	Peak value of modal participation factor in cycle for Mode n
rms	Root mean square
Re	Reynolds number
Re_c	Critical Reynolds number
R_u	Autocorrelation
S_G	Reduced damping
St	Strouhal number
std	Standard deviation
t	Time
U	Velocity
U_r	Reduced velocity - general
$U_{r_{n=1}}$	Reduced velocity based on Mode 1 still water natural frequency
$U_{r_{n=2}}$	Reduced velocity based on Mode 2 still water natural frequency
U_{TR}	True reduced velocity
w_2/w_1	Ratio of 2 nd natural frequency to 1 st natural frequency
y	Local cross-flow displacement of riser model
z	Height along axis of riser model

1. INTRODUCTION

The following chapter highlights the motivation for the current reported research effort into Multi-modal Vortex-Induced-Vibration (VIV). A history of the project is then presented. To conclude the chapter, the structure of the thesis is outlined.

1.1. MOTIVATION

Long flexible pipelines used in the offshore industry can be subject to VIV. Drilling and production risers as well as umbilicals are the most affected by VIV which leads to increases in their hydrodynamic loading and reduction in their service life due to fatigue. The offshore industry is moving into deeper waters in the search for new oil reserves. In July 2002 there were some 89 deepwater drill ships operating in waters deeper than 1,000 m (Harding 2002). The exploration for oil continues to go deeper as the technology increases through the years with drilling exploration rigs being designed for depths up to 4,000 m. As the relative length of a riser subjected to VIV from current sources becomes larger the need to understand VIV is more critical. Risers of any diameter can experience VIV.

Single frequency, single mode response is a typical characteristic for structures subjected to VIV from a uniform flow profile. In the ocean however, risers are generally exposed to a shear current profile over their

depth. Determining the total response is not as simple as summing individual different depth contributions. Shear flow leads to a complex non-linear mechanism. The shedding frequency does not linearly vary over the length of the riser, but rather vortices are shed in cells due to a weak span-wise coupling of the vortices. The situation is made more difficult due to the feedback from the riser structure and interaction of end tensions.

The most undesirable form of VIV for the offshore industry is termed *lock-in*. Lock-in is used to describe an elastic structure's ability to control the shedding process in a bandwidth around its resonant frequency. Associated with lock-in is a larger amplitude of excitation increasing unwanted effects. Lock-in has been observed in shear flow both in model tests and on operational risers. Establishing the boundaries of lock-in and determining the necessary conditions to avoid it is a critical area of research.

The dominant mode and modal amplitude will vary along the riser in a shear flow and may vary over time at a given point on a riser. Prediction of the dominant mode is now generally made on the basis of energy exchanges considering each mode's excitation and damping. Hydrodynamic damping is thought to be the main driver in determining likely modal responses. A damping model by Venugopal (1996) independently tested by Vikestad, Vandiver and Larsen (2000) has provided a means to sum each mode's damping contributions across a riser. The latest VIV prediction tools, Shear7 and VIVANA, calculate damping on a mode-by-mode basis to formulate

overall r
lock-in a
principa
and to c
energies

1.2.

In 1997,
period
major r
allowe
differen
latest d
gradua

To date
on she
require
sparse
exper
(length
cellula
reason

overall riser response. The conditions necessary for the ability of one mode to lock-in a large portion of the riser's response are still somewhat unclear. The principal aim of the current research is to address modal competition issues and to determine conditions leading to dominant modes along with their energies and amplitudes.

1.2. HISTORY OF PROJECT

In 1997, A/Prof Jon Hinwood was involved in the Deeper project. He spent a period of time at the headquarters of this project in Trondheim, Norway. A major research effort was completed called the 'rotating rig'. The rotating rig allowed simultaneous exposure of a long flexible cylinder to a range of different vortex shedding frequencies. As a result of exposure to some of the latest developments in VIV in shear current A/Prof Hinwood proposed a post graduate study into Multimodal VIV. This thesis was then born.

To date there has been a lot of investigative research into the dynamics of VIV on short rigid cylinders due to the relatively small laboratory facilities required. Experiments conducted on long flexible cylinders and cables are sparse compared to short rigid cylinder ones. Usually long cylinder and cable experiments are required to be conducted in the field where the aspect ratio (length to diameter) can be of large enough scale to sufficiently model the cellular nature of the vortex shedding that happens on the pipelines. For this reason, the understanding of the VIV of short rigid cylinders is becoming

relatively advanced while the applicability of the results to long flexible cylinders is not receiving much attention. The large flume facilities at Monash University are somewhat unique and allow a relatively long cylinder to be subjected to large volumes of water flow (up to 850 litres/sec), while the cylinder can still be of sufficient diameter to fit complex instrumentation inside it.

1.3. ORGANISATION OF THE THESIS

Following the introduction, the thesis begins with a literature review in Chapter 2 that surveys the current levels of understanding that are relevant to VIV on long flexible cylinders. As a result of the literature review several key areas of importance and lack of understanding are highlighted. A need to conduct experimental research is identified. The thesis objectives are highlighted that form the basis of the research effort. The experimental section is then presented in Chapter 3 which details the experiments conducted, the facilities and apparatus used and the flow profiles incorporated into the testing program. Enough detail is given to enable replication of the experiments if so required. The results of the experiments are presented in the next three chapters (Chapters 4, 5 and 6). The first of the results chapters deals with some preliminaries; decay tests in air, still water experiment results and verification of some of the instrumentation. The following results chapter (Chapter 5) presents the results of uniform flow conditions. Where possible other researcher's data is compared to the uniform flow results. The final

results chapter (Chapter 6) is the results of the 2-Slab flow experiments which force the flexible cylinder to simultaneously respond to different excitation regimes. Relationships of response variables with dependent parameters are presented as are any interesting features that were not predicted a priori to commencement of the experiments. The key results to improving the ability to predict multi-modal VIV are identified. The thesis finishes with a Conclusions and Recommendations for Future Work section.

2. LITERATURE REVIEW

2.1. INTRODUCTION

The literature review starts by introducing the concepts of steady flow around a cylinder considering only concepts relevant to risers. Oscillating flow is neglected as the research is only aimed toward VIV from steady current sources. Forces from flow around a cylinder are discussed next with VIV being introduced. The basics are now formed for a more probing examination of vibrations of short rigid cylinders and the phenomenon of lock-in that is so often talked about in this field. The review then looks at extending the multitude of data from short cylinder experiments to understand the VIV effects of long flexible cylinders. At this point a brief transgression into riser structural dynamics takes place to familiarise the reader with relevant concepts. Shear current across a long flexible cylinder is then presented with the latest ideas on what parameters are important in predicting response. The review is finalised by discussing the approaches of the dominant research bodies presently trying to more accurately predict response of risers due to VIV in a shear current.

2.2. STEADY FLOW AROUND A CYLINDER

The classification of steady flow around a fixed cylinder is best presented in terms of the Reynolds number (Re)

$$Re = \frac{UD}{\nu}, \quad (2.1)$$

where U is the flow velocity, D the cylinder diameter, and ν the kinematic viscosity.

In an idealised, disturbance-free situation it is the Reynolds number Re that is the governing parameter describing flow around a cylinder. At certain critical values of Reynolds number, Re_c , the flow transitions from laminar to turbulent. Disturbances from other effects can change this value of Re_c . Such effects might be surface roughness, turbulence and any cylinder oscillations (Zdravkovich 1997).

The flow around a smooth cylinder can be classified into different states that are dependent on the governing Re parameter (Zdravkovich 1997). These are shown in Figure 2-1.

Figure 2-1 a), b), c) *Laminar*, $0 < Re < 180-200$ - No turbulence in the flow. In the neighbourhood of $Re = 40$ periodicity first appears in the wake.

Figure 2-1 d) *Transition- in-wake state of flow*, $180-200 < Re < 350-400$. The flow undergoes transition to turbulence in the wake of the cylinder.

Figure 2-1 e) *Transition-in-shear-layers (Subcritical state)*. $350-400 < Re < 100k-200k$. The transition to turbulent flow takes place in the free shear layers after the flow through the boundary layers, of which remains laminar.

Figure 2-1 f), g), h) *Transition-in-boundary-layers (Critical state)*. $100k-200k < Re < \text{above } 6M$. Describing the state when transition to turbulence takes place in the boundary layers. For lower Re , the point of transition is after the laminar separation of the boundary layer from the cylinder. At certain values in this critical state the flow can reattach after becoming turbulent. For higher Re , one side of the cylinder can have a completely turbulent boundary layer.

Figure 2-1 i) *Fully Turbulent, above $6M < Re < \infty$* . When all regions of flow around the cylinder that are not part of the free-stream are turbulent.

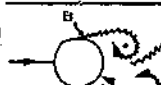
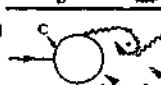
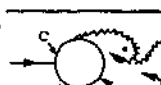
a)		No separation. Creeping flow
b)		A fixed pair of symmetric vortices
c)		Laminar vortex street
d)		Transition to turbulence in the wake
e)		Wake completely turbulent. A: Laminar boundary layer separation
f)		A: Laminar boundary layer separation B: Turbulent boundary layer separation; but boundary layer laminar
g)		B: Turbulent boundary layer separation; the boundary layer partly laminar partly turbulent
h)		C: Boundary layer com- pletely turbulent at one side
i)		C: Boundary layer comple- tely turbulent at two sides

Figure 2-1 Evolution of vortex shedding patterns with increasing Reynolds number (Sumer and Fredsoe 1997).

2.3. THE VORTEX SHEDDING PROCESS

The phenomenon of vortex shedding in the wake of a cylinder is the basis for the effects studied in this research. The onset of vortex shedding is at Re roughly 40 and continues right through to fully turbulent flow states. The phenomenon is an instability intrinsic to the flow itself. It is a consequence of

the interaction between shear layers, base pressure, diffusion and dissipation of vorticity (Sarpkaya 1979). Gerrard (1966) explains the fundamentals of vortex shedding as a result of mutual interaction between two separating shear layers. A vortex grows (see Figure 2-2) from its own connected shear layer until it is strong enough to draw the opposing shear layer across the near wake. In doing so it rolls up into a new vortex and cuts off the opposite, now further downstream one.



Figure 2-2 One shear layer drawing the opposite shear layer across the near wake and rolling up into vortices.

The rate at which vortex shedding takes place is a function of the flow velocity, U , cylinder diameter, D , and the Strouhal number, St . Equation 3.2 presents these parameters all in terms of the normalised vortex shedding frequency, f_v :

$$f_v = St \frac{U}{D}. \quad (2.2)$$

At first the Strouhal number was thought to be constant, but this was only because subcritical Reynolds numbers were being investigated. Figure 2-3 shows how St is now considered to vary with Re .

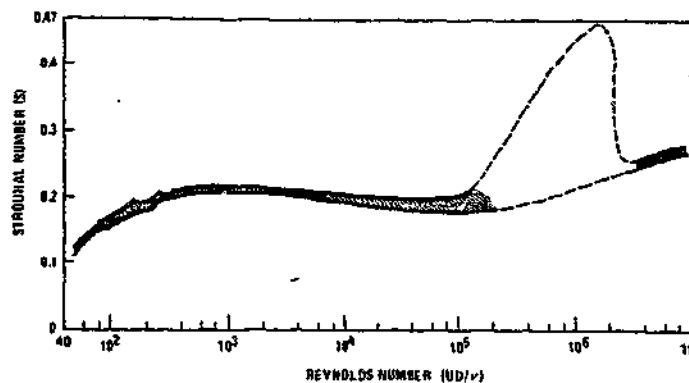


Figure 2-3 Strouhal number vs Reynolds number, $St = St(Re)$ (Blevins 1977).

Note that in Figure 2-3 for a given Re there is a band of values for St . Some of the influencing parameters that determine the actual value for St are described below.

2.3.1. Roughness

The roughness on the cylinder has an effect on St , with the largest effect being in the critical Re region. The greater the roughness the lower the value of St in the critical region, likewise for a smooth cylinder, St is seen to more than double in this region. (Achenbach and Heinecke 1981).

2.3.2. Turbulence

Incoming turbulence also plays a role in determining St similar to the effect of surface roughness. In experiments looking at Re number regions, Cheung (1983) found the turbulence with a length scale of the order of the boundary layer thickness had an effect on Re_c . If the intensity of this turbulence increased, Re_c would assume a lower value as a result of the earlier transition to turbulence in the boundary layer.

2.4. VORTEX SHEDDING FORCES ON A CYLINDER IN STEADY FLOW

During vortex shedding the resulting pressure distribution on the cylinder periodically changes thereby exerting a periodic net force on the cylinder. The net force can be split into two components, the in-line (drag) and the transverse (lift). Both of the forces fluctuate periodically, however it is the fluctuating lift force about a zero-mean value that is largest in amplitude.

Figure 2-4 shows the typical values of the instantaneous drag coefficients in both directions. The lift force coefficient is seen to approximate harmonic variation.

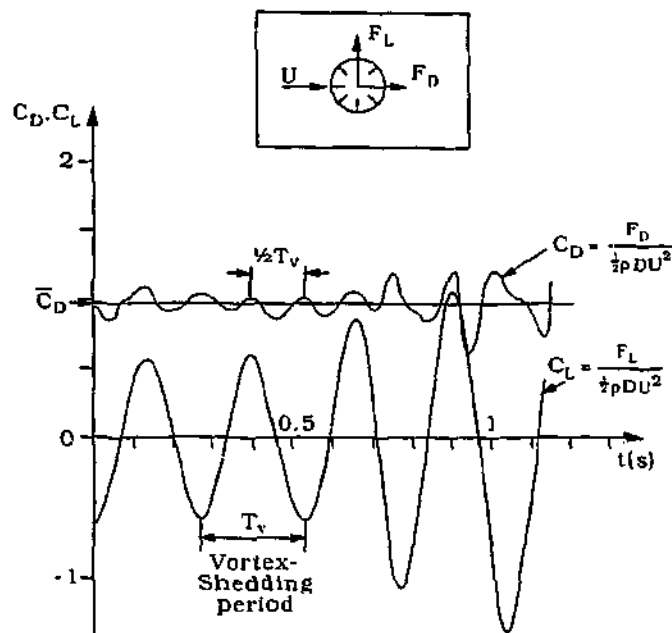


Figure 2-4 Drag and lift traces obtained from measured pressure distributions (Drescher (1956) as reported by Sumer and Fredsoe (1997)).

Also shown in Figure 2-4 is that the lift force oscillates at the vortex shedding frequency while the drag force oscillates at twice the vortex shedding frequency. The cylinder experiences a force in the in-line direction each time a vortex is shed, whereas the transverse force alternates from side to side each vortex shedding event.

Figure 2-5 shows the development of a vortex shedding cycle (one-third of a cycle). The pressure fields around the cylinder show what the cylinder experiences. By integrating the instantaneous pressure around the circumference an instantaneous net force is resolved. The net force can then

be resolved into a lift and drag component (as explained earlier in this section). The figure shows the instantaneous sizes of the lift and drag forces and by comparing these with the state of vortex growth one can determine how the effects of shedding influence the force. The most important conclusion from Figure 2-5 is that maximum lift force occurs just prior to a vortex being shed on the opposite side of the cylinder (shown in step 1).

Fig

si

2.

A cyl

patter

of the

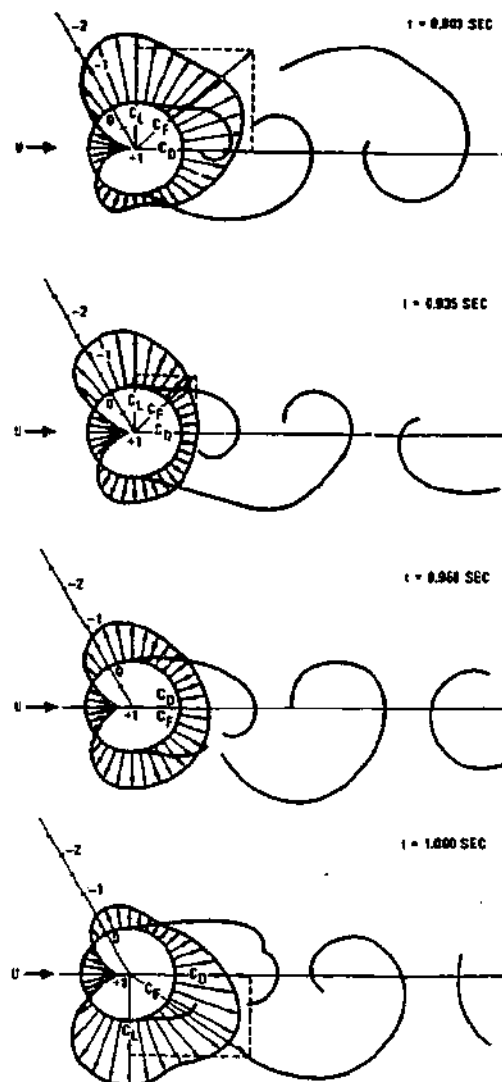


Figure 2-5 One third of a cycle of vortex shedding showing a sequence of simultaneous surface pressure fields and wake forms at $Re = 112,000$ (Drescher (1956) as reported by Blevins (1977)).

2.5. VORTEX-INDUCED VIBRATIONS (VIV)

A cylinder oscillating in a stream can dramatically alter the vortex shedding pattern. The oscillations provide a means for coupling the flow along the span of the body, and this can lead to a large increase in the correlation length of

the vortex (Bearman 1984). Induced oscillations due to a fluctuating lift force are termed VIV. VIV is sometimes a problem in wind and offshore engineering, not only because of the direct transverse vibration from the vortex forces, but because transverse sweeping may increase the in-line drag force by a factor of three.

After investigating stationary cylinders, researchers turned their attention to freely oscillating cylinders to better understand the effects of VIV. Early experiments showed that the resulting flow field changed rapidly with velocity of flow and amplitude of motion. Since varying the velocity changes the amplitude, some researchers then performed forced cylinder experiments to uncouple the two effects. A thorough summary of short cylinder tests for stationary, freely oscillating and forced oscillation conditions is presented in Pantazopoulos (1994).

2.5.1. Basic System Parameters

VIV of a short rigid cylinder section is best analysed by considering the equation of motion of the system. Figure 2-6 shows the typical parameters that are important.

Figur

The e

becom

 $F_L(t)$ k the

only

prop

The l

prev

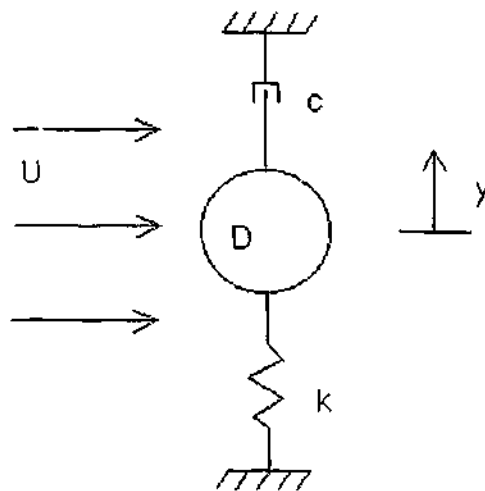


Figure 2-6 Simple model of short section cylinder undergoing VIV showing parameters relevant to the equation of motion.

The equation of transverse motion in terms of the parameters in Figure 2-6 becomes:

$$m \ddot{y} + c \dot{y} + ky = F_L(t). \quad (2.3)$$

$F_L(t)$ is the lift force on the cylinder, m the mass of the cylinder, c the damping, k the system stiffness, y the transverse direction. For reasons described later only structural parts of the model are on the left-hand side. All fluid dynamic properties are best kept on the right hand side.

2.5.2. Basic Force Analysis

The lift force, $F_L(t)$, can be modelled as a harmonic function of time, as shown previously in the results of Figure 2-4.

$$F_L(t) = F_o \sin(\omega t + \varphi) \quad (2.4)$$

ω_s is the vortex shedding frequency, F_o the force amplitude and φ the phase angle between lift force and body displacement. Since there is a phase difference between the lift force and the body motion a common way of gaining a physical understanding of the fluid-structure interaction is to split the force into two components. The force in phase with the body velocity is termed excitation or damping force, depending on its sign and the force in phase with body acceleration is used to calculate the effective added mass.

Effective added mass is only an artifice to account for the pressure distribution. Recent discussion is leading towards the elimination of this method of description (Sarpkaya 2000). Nevertheless, the use of 'added mass' to describe 'effective added mass' will continue throughout this thesis to make use of previous conventions in the literature.

A problem that can sometimes occur with measuring sectional force directly is that if the shedding is not correlated along the section, then adjacent cells of opposite forcing tend to cancel each other. Accurate flow visualisation can help to substantiate these results however. Measuring sectional forces with pressure tappings around the circumference obviously provides a more reliable result of the local sectional force.

Many experiments have estimated values for all the coefficients and a useful summary is contained in Pantazopoulos (1994). One has to be careful when calculating the fluid forces that the structural inertia forces have been subtracted.

2.5.3. Reduced Velocity

$$U_r = \frac{U}{f_n D} \quad (2.5)$$

The reduced velocity, U_r , is an important parameter to help predict response to VIV.

Given a system's natural frequency, f_n (assumed fixed at this stage), the reduced velocity is then a function of only U/D . At low U_r values ($U_r < 4$), there is little vibration present with vortex shedding taking place at the shedding frequency determined from the St relationship, as if the cylinder were fixed.

2.5.4. Lock-in; Air Experiments

As the vortex shedding frequency approaches the system natural frequency (approx. $U_r = 5$) the system takes control and locks on the vortex shedding frequency. The St relationship doesn't hold through this range for experiments in air. In most systems the peak resonance response is for $5 < U_r < 7$. In this whole range, the system will choose to vibrate at its

resonant frequency. Damping by the vortices limits the amplitudes thereby avoiding divergent behaviour and quick structural failure.

The experiments of Feng shown in Figure 2-7 show a lock-in phenomenon. The Re number range that Feng tested in was subcritical. Different ranges of Re can alter the lift coefficients and would thus change the amplitude of the response in Feng's diagram.

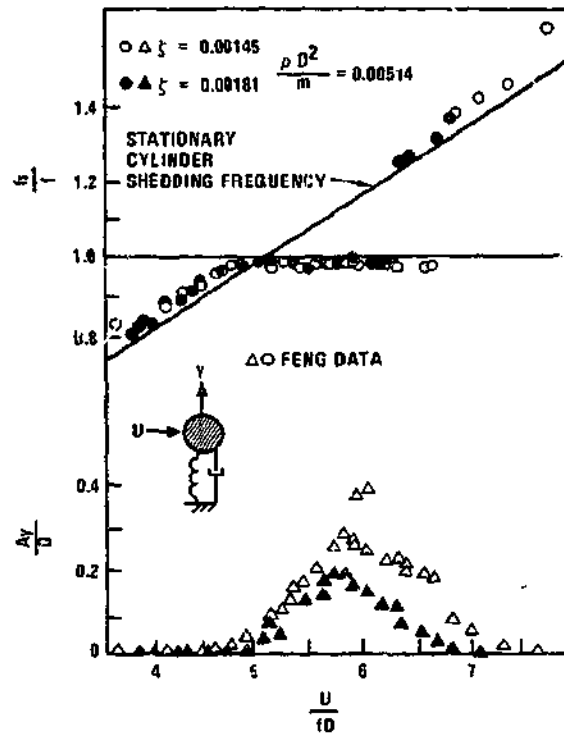


Figure 2-7 Feng's data showing the phenomenon of lock-in to the system's natural frequency (Feng (1968) as reported by Blevins (1977)).

The top portion of Figure 2-7 shows f/f_n (or Feng's parameters, f_s/f) which is a measure of the shedding frequency to the natural frequency. Feng found that the shedding frequency followed the straight line until $Ur = 5$. The behaviour

of the shedding frequency with further increases in velocity is then determined by the natural frequency until about $Ur = 7$ where it then deviates back to the stationary cylinder values, determined from the St relationship.

Feng also discovered that higher amplitudes were achieved only when reduced velocity was increased rather than decreased. The discovery of this hysteresis effect has lead researchers in recent times to perform flow visualisation on the vortex shedding. In 1988, Williamson and Roshko put forth a map of wake pattern behaviour with amplitude of motion and the reduced velocity as the variables (Williamson and Roshko 1988). It was found that the vortices can be shed in single groups, pairs or alternating single and pair groups.

2.5.5. Width of Lock-in Region

Figure 2-8 shows the ability of the system to take control of the vortex shedding process. For moderate values of amplitude the system will lock-on when the Strouhal frequency comes within $\pm 20\%$ of the system natural frequency. The width of the lock-in range is also dependent on the vibration amplitude. The larger the amplitude the wider the lock-in range. Koopman's early results are often used nowadays in complex models to determine the boundaries of lock-in. The results of Koopman are at low Re and show that Re has an influence. Stansby (1976) observed the same characteristics of the Koopman's $Re = 300$ case with a Re number roughly 10 times larger.

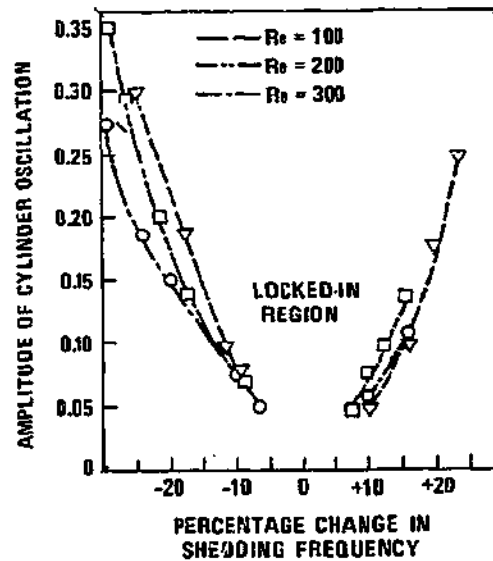


Figure 2-8 Regions in which the cylinder motion controls the shedding frequency (Koopman (1967) as reported by Blevins (1977)).

2.5.6. Differences in Water

When cylinders are immersed in water as compared to air, the most obvious difference is the ratio of the cylinder's mass to the fluid's mass. Termed the mass ratio, m^* , it is defined as the ratio of the body mass, m , to displaced fluid masses ($\rho_f D^2$) multiplied by a constant, $\pi/4$, so that $m^* = m/\rho_f D^2$.

Griffin and Ramberg (1982) have compared the responses of a circular cylinder in air and water. Shown in Figure 2-9 is the transverse amplitude versus the reduced velocity for both cases. For the water case, the reduced velocity has been based on the still water natural frequency. The most

interesting observation from this work is that the response either side of the peaks is quite different. They have chosen to compare similar values of the combined 'response' parameter. They define the response parameter as the product of the mass ratio, m^* , and the damping ratio, ζ (where $\zeta = r/2\omega m$, r being the damping constant per unit length). As the experiments were performed in water and air then the mass ratios are very different. Consequently, to have similar values of response parameter in both water and air involves having very different damping ratio parameters. In conclusion, for the same value of response parameter, a greater damping ratio, or a smaller mass ratio leads to a much broader response band.

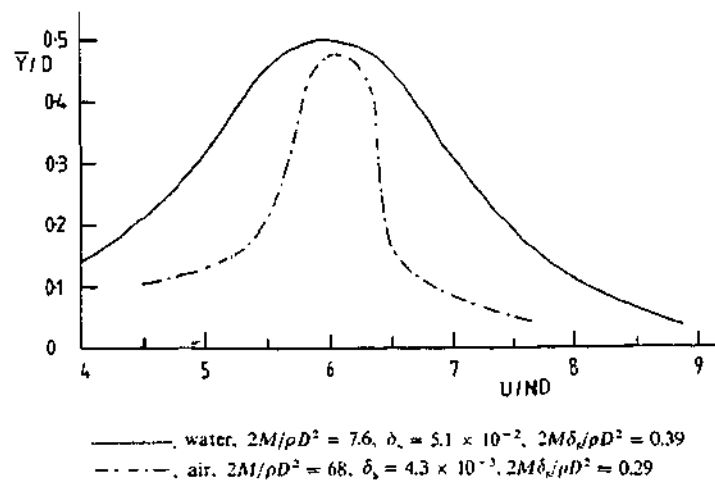


Figure 2-9 The different transverse amplitude response of a cylinder in water and in air vs reduced velocity (Griffin and Ramberg 1982).

2.5.7. Added Mass Effects

Griffin and Ramberg, as do many researchers, base the calculations of the reduced velocity, Ur , for water experiments, on the still water natural frequency, f_n . Although using f_n seems a reasonable approach, Moe and Wu (1990) showed that for small mass ratios in the lock-in bandwidth, the frequency of lock-in changes. An illustration of the rising lock-in phenomenon is shown in Figure 2-10 and taken from Khalak and Williamson (1999). Unlike air experiments, the natural frequency does not have a fixed value in the lock-in region. It also cannot be said that a lock-in effect does not occur as the gradient line depicts what the shedding frequency would be for a stationary cylinder if the shedding were governed by the Strouhal relationship.

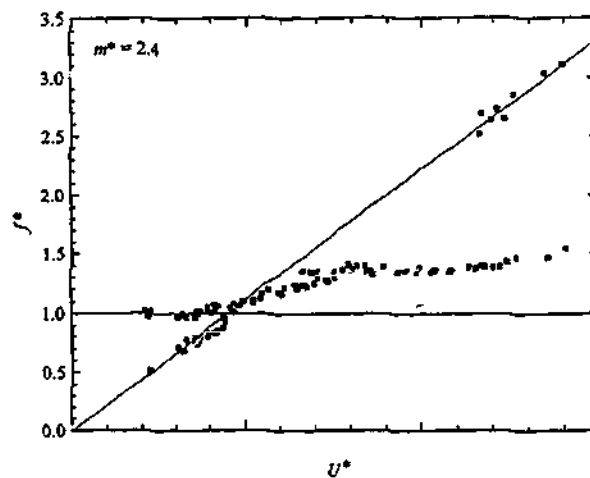


Figure 2-10 Rising lock-in frequency phenomenon due to a low mass ratio
($m^* = 2.4$) (Khalak and Williamson 1999).

For a changing natural frequency to be observed, by definition, there has to be either a changing mass or stiffness. As fluid has little stiffness then the effect is attributed to a changing mass, or an effective 'added mass'.

In setting up system vibration equations some models include the added mass in the 'structural' part of the equation but Sarpkaya (1979) argues that these fluid dynamic effects should all be incorporated into the 'fluid' part of the model from the outset.

Sarpkaya (1979) found added mass coefficients by performing driven cylinder experiments (the applicability of extrapolating driven cylinder experimental data to responding flexible structures has been questioned (Vikestad *et al.* 2000)). The added mass was found to be very large for low values of Ur and as lock-in regions were approached a sharp decrease in added mass to small negative values appeared. The added mass then rises, but still stays below zero for high Ur . Sarpkaya also found that the added mass coefficient is sensitive to the amplitude.

To deal with the seemingly improper definition of Ur based on the still water natural frequency, Sarpkaya (1995) changed the definition of natural frequency from the still water value to the body oscillation frequency, f_{osc} , throughout the lock-in zone. Moe and Wu (1990) use a similar concept in proposing the use of 'true reduced velocity', U_{TR} :

$$U_{TR} = \frac{U}{f_{osc} D} \qquad U_r = \frac{U}{f_n D} \qquad (2.6)$$

'True U_r '

'Nominal U_r '

Gharib (1999) makes use of the original definition of Ur with f_n , and builds his thesis around the postulate that large amplitudes of vibration can be experienced for low m^* cases when not in the lock-in region. In defining the lock-in region with f_n he has based it on a fixed natural frequency. As has been discussed previously, the natural frequency varies in the lock-on region which leads to some ambiguity in his definition of the 'not locked in' region. Nevertheless, he proposes the amplitude of vibration to be a function of the effective stiffness, k_{eff}^* , such that in the absence of damping, amplitude is given by

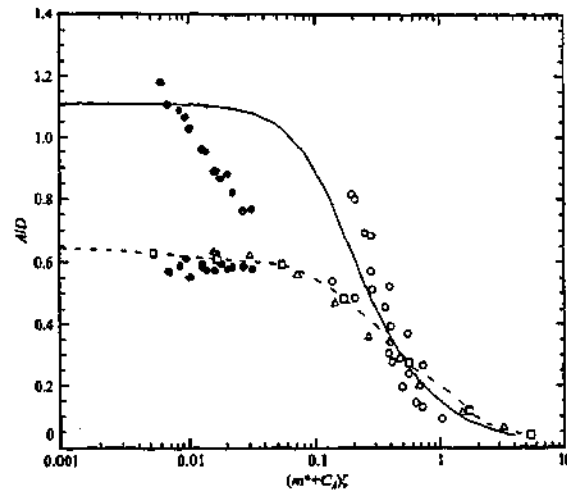
$$\frac{A}{D} = \frac{C_y}{k_{\text{eff}}^*} = \frac{C_y U^2}{m^* \left\{ 1 - \left(\frac{f_{\text{osc}}}{f_n} \right)^2 \right\}}, \quad (2.7)$$

where A/D is dimensionless amplitude (made up of A , measured amplitude and D , diameter), C_y is the lift force coefficient, m^* is mass ratio, f is oscillation frequency.

Classically, VIV has only been observed during lock-in conditions for high mass ratios. Under Gharib's aforementioned hypothesis, lock-in ($f \sim f_n$) is not a necessary condition for VIV at low mass ratios. Experiments that formed part of Gharib's thesis found that the system responded when not near the shedding frequency, but in a different mode when the effective stiffness was minimised.

2.5.8. Amplitudes of VIV

The maximum attainable amplitude of a system undergoing VIV at resonance was investigated by Griffin *et al.* (1975). A compilation of different investigations was put together on a log-log graph showing dimensionless amplitude versus a parameter representing the system mass and damping, $S_G = 2\pi^3 St^2 m^* \zeta$. More recently different branches, representing different modes of vortex shedding have been identified on a log-linear plot, as shown in Figure 2-11 (Khalak and Williamson 1999).



●, Present data; ○, data compiled by Griffin (1980); —, Skop & Balasubramanian (1997); △, Blackburn & Karniadakis (1993); -□-, Newman & Karniadakis (1996).

Figure 2-11 The 'Griffin' plot revealing different modes of response by using a log-linear scale instead of a traditional log-log scale (Khalak and Williamson 1999).

The largest amplitude of oscillation found to date for a short rigid cylinder is $A/D = 1.2$ (as shown in Figure 2-11) in experiments on cantilevered cylinders

at very low damping. In fact, the amplitudes of this size are not present in conditions of high m^* but in low m^* , and are only obtainable when Ur is increasing. In conditions of high Ur , another mode of vortex shedding takes place where instead of two single vortices shed per cycle (2S), four vortices are shed per cycle in two groups of pairs (2P) (Khalak and Williamson 1999).

The amplitude of response for a long flexible cylinder was measured by Koch (1985 (taken from Vandiver 1993)) as a function of systematic variation in reduced velocity for Mode 1 response in uniform flow conditions. Koch's data represents the amplitude of Mode 1 response of a neutrally buoyant Aluminium tube of mass ratio = 0.78 (specific gravity ratio = 1). Koch's data is presented in Figure 5-2 (later in the results section) and shows that an amplitude of $A/D = 1.35$ is possible at the antinodes of a flexible structure.

The previously mentioned parameter, S_G , representing mass and damping of the system (first proposed by Skop in 1974) has come under increasing scrutiny in recent times. It represents a type of system damping from structural sources always applied at resonant conditions for the single cylinder. Clearly, for low values, the highest amplitudes are obtained. Zdradkovich (1990) stated that a combined mass-damping parameter is useful for air experiments but in water experiments (low mass ratio) mass and damping have to be considered separately. Sarpkaya (1979) also states that response is governed separately by mass and damping. Khalak and Williamson (1999) have since found that the combined mass-damping

parameter works well for water experiments at least down to the lowest values presented in Figure 2-11.

Vandiver (1993) showed that S_G , known variously as the 'reduced damping', the 'stability parameter', or 'response parameter', reduces to the following expression:

$$S_G = r\omega / (\rho_f V^2). \quad (2.8)$$

This shows that for uniform flow conditions, S_G is independent of cylinder mass, revealing the misleading use of the name 'mass-damping' for this parameter. Hereafter it is referred to as 'reduced damping'.

2.5.9. Correlation

When the cylinder oscillation frequency differs from the shedding frequency the length of the cells of shedding (correlation length) is reduced. Toebes (1969) presents results from experiments in air (Figure 2-12), where the amplitude of vibration is also shown to have an effect. Figure 2-12 a) shows that for a shedding frequency equal to 1.25 times the cylinder frequency the correlation length is not greatly affected by amplitude. Figure 2-12 b) shows the correlation length is affected by amplitude and for high amplitude values (shown in the figure) is much longer at resonance (shedding frequency matches oscillation frequency). Correlation of the lift force is thus shown to have a maximum value during lock-in ($f_v = f_n$). The influence of Re on the correlation length is presented by King (1977). Even in the predominantly

constant St number region of subcritical Re the correlation length decreases as Re increases.

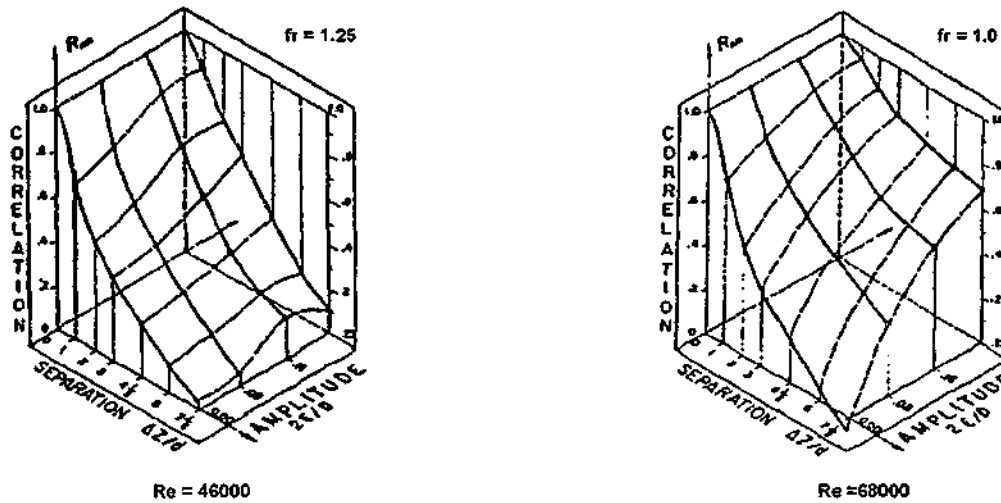


Figure 2-12 Correlation length vs amplitude and frequency for an oscillating cylinder. a) Strouhal frequency to cylinder frequency = 1.25; b) Strouhal frequency to cylinder frequency = 1.0 (Toebes 1969).

2.5.10. In-line response

Often the in-line responses of elastically mounted cylinders are neglected in experimental studies of vortex shedding as the cross-flow response amplitude is seen to dominate the total response. An inspection of the in-line response can reveal some fundamental characteristics of the inter-dependent relationship to cross-flow response.

In the absence of cross-flow response, the in-line response of flexible cylinders is reported to occur, in the range $1.5 < Ur < 3.5$. Figure 2-13 shows the in-line response of a marine pile model oscillating in water in the flexible cantilever mode as a function of reduced velocity. The two regions of response have been identified as being caused by two different flow instabilities (King *et al.* 1973). The first region features two symmetric vortices shedding, while the second region features asymmetric vortex shedding.

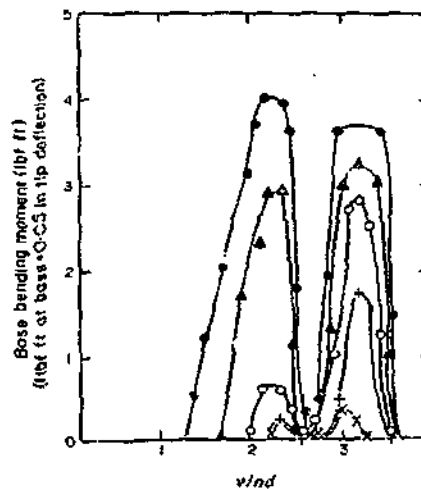


Figure 2-13 In-line VIV response of a marine pile model against reduced velocity (King 1973).

King states that the onset of in-line VIV response occurs at a Ur that is $\frac{1}{4}$ the value of the cross-flow lock-in one.

Free vibration experiments performed by Moe and Wu (1990) consisted of a short rigid cylinder allowed to vibrate in both the in-line and transverse flow

directions. The in-line natural frequency in-air was set at twice that of the cross-flow natural frequency for the apparatus. Additionally, in a separate experiment, the in-line direction motion was constrained. Moe and Wu found greater cross-flow amplitudes in the free in-line case compared to the constrained in-line case, although the location of peak response differed between the two cases by a factor of 1.5 on the reduced velocity scale. Sarpkaya (1995) and Huse *et al.* (2002) found similar trends in response to Moe and Wu with their respective short rigid cylinder experiments, although Huse *et al.* did not plot the same higher levels of reduced velocity as the other two researchers and hence has not shown the maximum response in the in-line direction that the other two found.

Huse *et al.* (2002) performed a novel experiment with two short rigid cylinders coupled together. The experiment was aimed towards finding out how cross-flow and in-line VIV interact when the in-line VIV is considered to be active at twice the frequency and approximately twice the mode number. The experiment allowed a cylinder to choose its own in-line phase of VIV and then coupled two cylinders together to understand the effects of 180 degree out of phase in-line movement between the two cylinders (a situation that would be occurring over sections spanning half the riser length). The results showed the cases of 180 degree out of phase motion reduced the amplitude response levels of cross-flow VIV beyond $Ur = 5$ compared to both the free in-line and constrained in-line cases. Additionally, prior to the amplitude increasing significantly near lock-in, the in-line and transverse vibrations 'live

independent lives'. Huse also points out that often the in-line direction has higher dynamic curvature than the cross-flow direction, which leads to a greater contribution to fatigue damage.

Vandiver and Jong (1987) performed analyses on cable strumming experiments to determine relationships between cross-flow and in-line VIV. They found a strong quadratic correlation between the in-line and transverse VIV. An important hypothesis that came out of their paper was that odd in-line mode numbers are excited in preference to even ones. The reason was attributed to the fact that drag (in-line) fluctuations (occurring at double the transverse frequency) will be symmetrically distributed about the cylinder midpoint and odd in-line mode numbers are always symmetrical about the midpoint.

In summary, important points of in-line response are:

- In-line response occurs prior to cross-flow in the range $1.5 < Ur < 3.5$.
- In the cross-flow dominated regions the in-line response takes the form of odd mode numbers.

2.6. RISER STRUCTURAL DYNAMICS

In extending the results of single cylinder tests to long flexible risers one first needs to consider the fundamental behaviour of long flexible structures. Risers with differing physical and geometrical properties can behave very differently in the same fluid loading conditions. The two most common forms

of risers are drilling tensioned risers and export catenary risers. Both the previous two risers generally have aspect ratios (L/D , where L is length, D is diameter) greater than 100.

The natural frequencies of risers are commonly used to predict their response in currents. A riser can behave like a beam (lateral stiffness dominated by bending stiffness) or a cable (lateral stiffness dominated by axial tension) depending on its physical and geometrical properties.

The natural frequencies for a tensioned cable are directly proportional to the mode number; $\omega_n \propto n$ (where n is the mode number and ω_n the natural frequency); while for a beam they are proportional to the square of the mode number; $\omega_n \propto n^2$. The result is that for a beam there appears more and more bandwidth between natural frequencies for higher mode numbers than for a cable.

Risers with some combination of both end tension and bending stiffness have their natural frequencies computed using a combination as follows:

$$\omega_n = \frac{\pi^2}{l^2} \sqrt{\frac{EI}{m_L} \left(n^4 + \frac{n^2 P^2}{\pi^2 EI} \right)}, \quad (2.9)$$

where l is the length, m_L is the mass per unit length, P the tension, E the Young's Modulus and I the moment of Inertia (Rao 1990).

Equation 2.9 can be used to determine the natural frequencies in air. The most common way of using the equation for water cases is to use effective added mass data (as in the previously stated data of Sarpkaya). For the lock-in region ($Ur \approx 5$) the added mass used is usually $Ca = 1$.

2.6.1. Damping of Excitation Waves

If the excitation of a riser is located in just one small section along its length then it would commonly be expected that if the damping was higher than a certain value, vibration could be damped out before the excitation travels to the ends of the riser and sets up a standing wave pattern. To determine the likelihood of the waves being travelling waves (otherwise termed infinite cable behaviour) or standing waves, Vandiver (1993) uses the product of the mode number and the mode damping ratio, $n\zeta_n$ (where ζ_n is the damping ratio for mode n). A recommended guide is when the product is greater than 2.0, infinite cable behaviour results, less than 0.2 and standing wave patterns results. For $0.2 < n\zeta_n < 2.0$, a combined behaviour results.

2.6.2. Quantifying Force on Flexible Cylinders

Detailed force data on long flexible cylinders is not available. The problems with attempting to measure sectional forces on moving structures have proved overwhelming to date. Commonly, the responses are measured via accelerometers placed at strategic points as in Lie *et al.* (1997). As results do

not contain forcing information, designing prediction models that deal with the fluid structure interactions based on the results of these experiments is very difficult.

2.7. VIV IN SHEAR CURRENT

While extensive attention has been paid to uniform cylinders in uniform flow, only recently has the effect of shear in the approach flow been given attention. Ocean currents commonly consist of depth varying velocities and thus understanding shear flows is vital to understanding riser responses.

Shear flow results in a varying shedding frequency along the length of the cylinder. In experiments on a cylinder in air, Stansby (1976) found that the shedding occurs in cells that extend much longer spanwise if the cylinder is allowed to vibrate. His results are presented in Figure 2-14. The transition between cells concur with the results of the higher Re cases of Koopman (presented earlier in Figure 2-8). Interestingly, Stansby found there to be some quantitative correspondence between the boundary situations in uniform and shear flow.

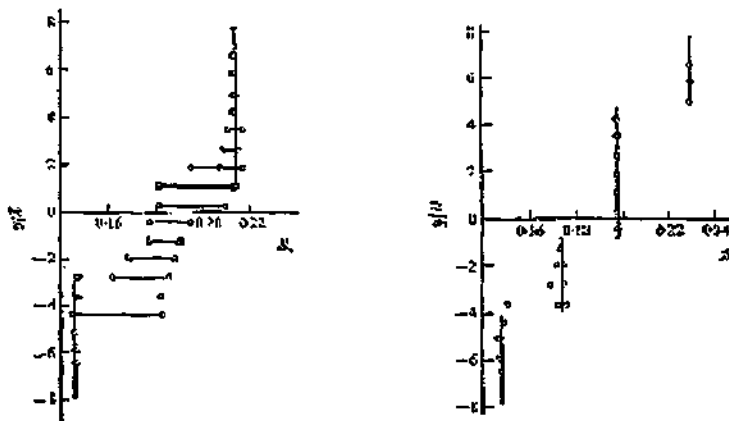


Figure 2-14 Spanwise distribution of Strouhal number (with velocity defined from mid-span value) in a shear flow for a) stationary cylinder, and b) oscillating cylinder with amplitude $A/D = 0.06$ (Stansby 1976).

For a varying flow velocity, certain bandwidths of shedding frequencies will be acting within a close range of natural frequencies of the riser structure. Most commonly the results presented in Figure 2-8 (earlier) are extrapolated in this case to assume that the shedding cells will lock-in to a natural frequency of the riser if the flow speed shedding frequency is anywhere within a 25% band around resonance (Vandiver 1993).

2.7.1. Number of Possible Modes

In describing the variation in flow velocities over the length of the riser, one is able to infer the lowest shedding frequency at the slowest velocity end and the highest shedding frequency at the fastest velocity end. Using the bounds of shedding frequencies as a guide, it is then possible to calculate how many natural frequencies of the riser could be expected to respond. The term N_s

(Kim *et al.* 1986) describes the number of possible modes excitable. It has been hypothesised that if the number of possible excitable modes is too high then there is less likelihood of single mode lock-in (Vandiver 1993).

2.7.2. Lock-in Characteristics

A statistical tool may be used to classify the response of a riser into multimode or single mode lock-in. The tool is the Kurtosis and is particularly useful for examining vast quantities of data expediently, but may also serve as a means of classification. The kurtosis (or the 'variance of the variance'), K_{qi} of Mode i is calculated from the modal amplitude time series $q_i(t)$,

$$K_{qi} = \frac{\langle q_i^4 \rangle}{\langle q_i^2 \rangle^2}, \quad (2.10)$$

where $\langle \rangle$ represents the mean. Vandiver (2000) showed that multimodal type response of risers is well modelled as a Gaussian noise behaviour which takes on the value $K_{qi} = 3.0$, whereas single mode lock-in takes on a more sinusoidal response form where $K_{qi} = 1.5$.

2.7.3. Damping in Shear Flow

Damping as a whole can be described by the structural and hydrodynamic components. For a single cylinder in uniform flow at resonance the structural damping (via 'reduced damping' parameter) has been shown to be adequate in predicting response. It is usually determined from decay tests in air, if possible. For tensioned risers the structural component is so small compared

to the hydrodynamic component that it is rarely used in predicting riser response in shear flow. Under shear conditions, regions of the riser that are not locked in contribute very large hydrodynamic damping.

Several discussions on modelling damping in shear flow follow. The first model of this type was presented in Vandiver (1993). It examines each mode of excitation and applies damping where the shedding frequency does not match the natural frequency. A simple 'proportional to velocity' damping model is then applied. The following equation shows this hydrodynamic damping, $\zeta_{h,n}$, for each mode, n

$$\zeta_{h,n} = C_D \omega_{s,max} / \left[4\pi^2 St \omega_n (\sigma_g + Ca) \right], \quad (2.11)$$

where σ_g is the specific gravity, $\omega_{s,max}$ is the maximum shedding frequency and C_D is the drag coefficient.

A damping model, such as the one just presented, provides a method of calculation that can be employed in riser dynamics models. Most industry accepted empirical based prediction models calculate response on a mode-by-mode basis using a formulation as that in Equation 2.11 for estimation of each mode's damping. Examples of such programs are VIVANA and SHEAR7 (Larsen 2002).

A generalised form of the response (damping) parameter, S_G , has been developed by Vandiver (1985). It originates from the earlier presented expression for uniform flow, Equation 2.8, which that reveals S_G is the ratio of

damping force per unit length over exciting force per unit length. The newer form of S_G for shear flow conditions accounts for separate power in and power out zones for each mode as shown in Figure 2-15.

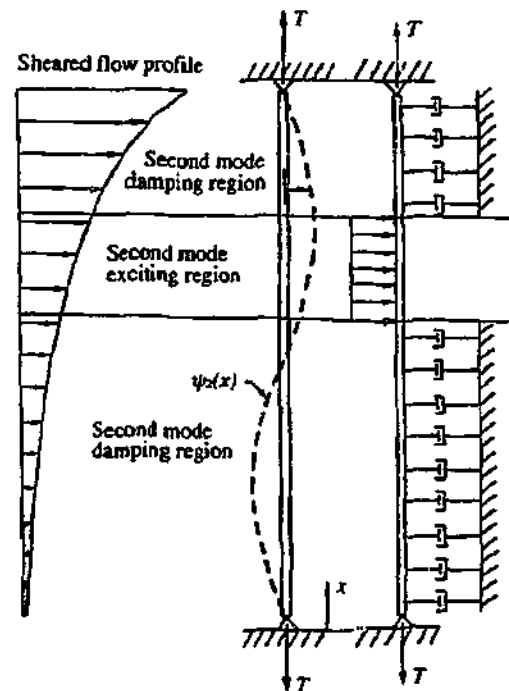


Figure 2-15 Power flow model for the second mode of vibration of a flexible riser in shear current (Van Diver 1993).

Gopalkrishnan (1993) conducted the most extensive forced oscillation tests to date of a short rigid cylinder. The lift force was measured as a function of A/D and nondimensional frequency, \hat{f} . The lift force was then decomposed into coefficients in phase with velocity and acceleration. Gopalkrishnan's results now provide the basis of most empirical VIV prediction programs and are of most importance in estimating the response of structures away from their lock-in region, such as the damping regions in a shear flow. The empirical based VIV prediction programs apply Gopalkrishnan's short rigid cylinder

results to cases of long flexible structures with limited knowledge on how modal competition affects the response.

Most of the current modal analysis techniques involve a modal damping ratio unique to each mode. Frequency analysis is then carried out. However, instantaneous superposition of the different frequency results would seem to be the wrong approach, as this does not involve any history of the motion. Simple models such as that presented in Chaplin (1999) shows that the motion history of a cylinder is important. It is suggested that a time domain or single frequency analysis would provide a more accurate modeling approach, based on the premise that vortex shedding is a single frequency phenomenon and so only a single frequency should dominate the response.

The current state of the art damping model was developed by Venugopal (1996) and subsequently verified by Vikestad *et al.* (2000). The damping model consists of two forms, one for regions with reduced velocities above the natural frequency (high U_r model) and one for regions with reduced velocities below the natural frequency (low U_r model). Each natural frequency of the system is examined in turn and hence the model assumes that there is one shape of displacement (modeshape) for each natural frequency. The damping models are functions of diameter, velocity, mass ratio and still water damping values with empirically determined lift coefficients.

Testing of cylinders was confined to stationary, forced or free vibrations until Vikestad (1998) performed driven spring mounted cylinder tests. His apparatus measured the damping and exciting forces on cylinders in flow when they were excited through a spring mount at different frequencies and amplitudes to what the fluid would determine. The idea behind performing these tests was to model the physical case of a riser in shear flow being excited in one region by the local vortex shedding, while at the same time another region's different frequency of excitation is present. Vikestad fixed the plane of the cylinder so that it could only vibrate cross-flow which may have produced a different shedding pattern to a two-dimensionally free cylinder. He varied flow velocity, support displacement and frequency of support excitation. High amplitudes of response in low reduced velocity regions were reported. Thus indicating that significant vibration could be occurring in the lower 'non-locked-in' region of the riser and supporting the locked-in region. Significant contributions were made to the field in the understanding of damping from other regions.

2.7.4. Amount of Shear

A simple shear fraction is the simplest method of quantifying the amount of global shear present and is described as

$$\text{Shear Fraction} = \frac{\Delta U}{U_{\max}}, \quad (2.12)$$

where $\Delta U = U_{\max} - U_{\min}$ is the change in flow speed over the spanwise length.

The maximum shear fraction is 1.0, indicating that all frequencies up to the

maximum determined by the St relationship are possible. The total number of eigenfrequencies possible being N_s . A low shear fraction would indicate that the excitation frequencies are close to the maximum shedding frequency.

Griffin (1985) classifies the amount of shear in a flow through the use of the shear parameter:

$$\beta = \left(\frac{D}{U_{ref}} \right) \frac{dU}{dx} = \left(\frac{D}{L} \right) \frac{\Delta U}{U_{ref}}, \quad (2.13)$$

where U_{ref} is any velocity chosen as reference, L the length of the cylinder in the x direction.

A more useful parameter is described in Vandiver (1993), termed the local shear steepness

$$\beta_x = \frac{D}{\omega_s} \frac{d\omega_s}{dx} = \frac{D}{U(x)} \frac{dU}{dx}, \quad (2.14)$$

where $U(x)$ is the local flow velocity at position x along the cylinder. β_x is more useful as it indicates the likely correlation length at a given point. If the flow is assumed linear ($dU/dx = \text{constant}$) then β_x is smallest for the highest velocity region and thus has the longest correlation length. Having the longest correlation length means the region is more dominant in the response than other regions.

Until 1996 it was thought that too large a shear would prevent single mode lock-in as the hydrodynamic damping would be too great from the non-preferred lock-in regions. Experiments performed on cantilevered cylinders in

highly sheared flow showed that lock-in could occur (Vandiver *et al.* 1996). The hypothesis explaining this effect by the group of researchers was based on the relationship that power delivered to the riser is roughly proportional to the flow speed cubed. With a larger amount of shear in a flow there would be a larger power variation from the low to the high speed regions. It is this relative difference in power that is able to allow the higher speed region to dominate the lower speed region and lock on the whole cylinder. Figure 2-16 shows the relative 'power profiles' for the differing shear cases and the likely response from the hypothesis.

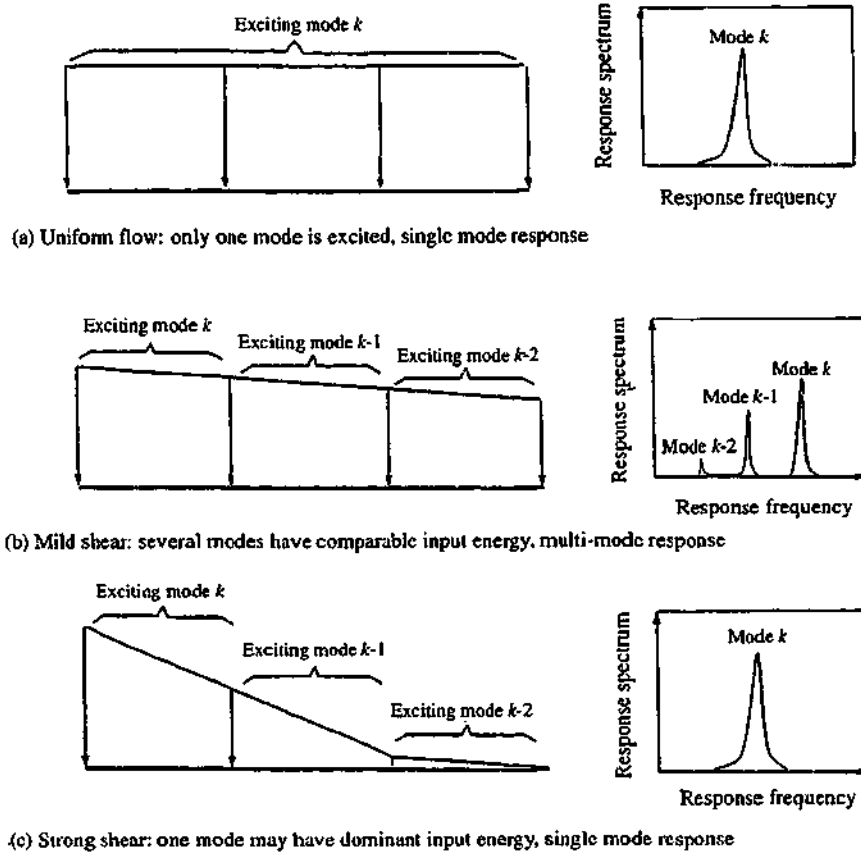


Figure 2-16 Hypothesis on how strong shear can lead to single mode dominance (Vandiver *et al.* 1996).

One method of presenting the boundaries of lock-in (single mode dominance) and multimode is to present it in N_s vs β space (Vandiver *et al.* 1996). Results in other experiments have somewhat clouded the boundaries (Lie *et al.* 1997) and much more data needs to be collected to clarify whether this is an accurate method.

2.8. LATEST OBSERVATIONS

Experiments performed on a flexible model riser (Lie *et al.* 1997) were the first real experimental tests to examine modal behaviour and frequency dominance under an extensive matrix of linear shear flow conditions. Unfortunately a substantial length of the model riser was in air causing a non-uniform mass distribution. The results obtained proved difficult to extract any real meaning or new hypotheses on predicting modal behaviour even though the experiment was cleverly designed. An observable characteristic in the results was the appearance of different modeshapes at the same frequency. In the papers published as a result of these series of experiments this was attributed to each modeshape 'experiencing' a different added mass. In very recent times data that supports the results of the rotating rig experiments has been obtained from full-scale riser tests (Kaasen 2000) as shown in

Figure 2-17. In Figure 2-17 the same characteristic of one dominant or resonant frequency with many different modeshapes excited (found by using

standard modal analysis) is present. The reason behind different modeshapes appearing at the same frequency is unclear and in need of further research.

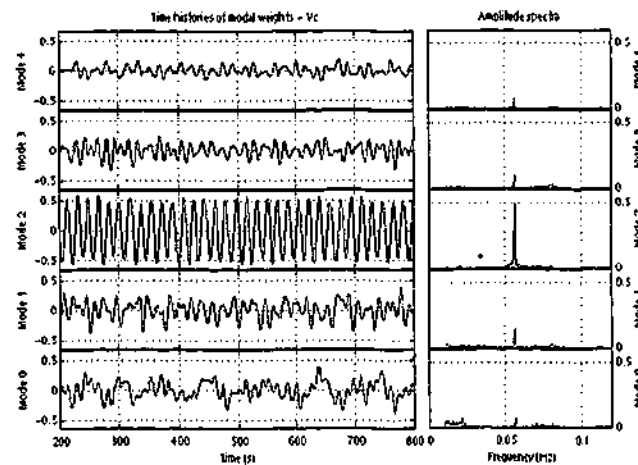


Figure 2-17 Helland-Hansen full-scale riser response data showing modal participation factors time series and spectra (Kaasen 2000).

2.9. CONCLUDING THE LITERATURE REVIEW

We have seen that the understanding of the response of short rigid cylinder sections has been well advanced over the past 30 years. The mass ratio of the cylinder has been shown to be important, implying that the significant body of data that exists for cylinders in air is of little use for the prediction of responses of marine risers. Study of uniform flow conditions over long flexible cylinders in water has made use of short cylinder results to predict response. In-line response was noted as being a significant contributor to fatigue damage in its own right. Determining the response of long flexible cylinders in shear flow is still in its infancy. The discoveries of Stansby on shear flow in 1976 have only been

progressed a little in the last few years. Most shear flow research of recent times has been aimed at developing numerical prediction tools with a plethora of programs being developed in the last three years. Importantly, there has been very little data gathered from long flexible cylinders in shear flow. Long elastic risers in sheared currents will generally experience multimodal VIV. To date multi-mode VIV is solved simply by considering each mode independently with the assumption that there is no interdependence and applying the results of short rigid cylinder experiments.

2.10. THESIS OBJECTIVES

From a review of the literature in this chapter the VIV prediction of long flexible cylinders in shear flow conditions, relative to the understanding of short rigid cylinder VIV, is shown to still be in its infancy. Accurate prediction of long flexible cylinder shear flow VIV response is paramount for the offshore industry. The areas of greatest uncertainty are:

The accuracy of short rigid cylinder results for long flexible cylinder cases. A relatively large amount of data exists for the results of short rigid cylinder cases yet there are very few results reported on long flexible cylinder VIV against which short cylinder predictions may be compared. Fundamentals knowledge of the behaviour, including modeshape effects, are lacking even for simple scenarios.

In-line motion and its effect on cross-flow response. The application of constrained in-line direction rigid cylinder experiments does not address in-line response issues; yet all short rigid cylinder experiments show a substantial difference in response when freedom in both directions is allowed. In-line response is significant in its own right as it frequently may be the main cause of fatigue damage.

Modal competition and dominant response behaviour. The results of short rigid cylinder experiments are applied to calculate multimodal response in shear flow conditions with limited knowledge of how modal competition affects either the individual response, the partitioning of response or the affect on hydrodynamic coefficients associated with each mode. Boundaries of single mode response conditions are also unclear.

2.11. EXPERIMENTAL FACILITY REQUIREMENTS

With numerous numerical modelling attempts currently underway in the same area it was decided that the most value can be added to the area through an experimental modelling program. An experimental program can also serve as a fundamental check for numerical modelling attempts.

With the thesis objectives in mind, the following requirements were determined for an experimental facility:

- Studies of fixed rigid cylinders cannot simulate the flow around moving cylinders or predict forces on moving cylinders, hence a dynamic moving model was necessary.
- A dynamic model must be capable of transverse and in-line motion.
- Long flexible cylinder models more closely match the offshore engineering applications of long spanning pipelines where VIV problems are widespread.
- Quantitative evaluation of linear shear flow experiments is inherently difficult and subjective because the damping and excitation are different at every point along the riser. Simplifying the shear flow effect is desirable.
- Direct measurement of some of the local added mass and force coefficients on the model would help connect to the knowledge from previous research into short rigid cylinder VIV.

With the previous objectives in mind, an experimental facility was designed and research conducted as described in the next chapter.

3. DESCRIPTION OF THE EXPERIMENTS

The following chapter starts with an overview of the design of the experimental apparatus including the riser model and the facilities used for the testwork. The detailed assembly and the calibration of the instrumentation is then discussed to assist the reader reconstruct the experiments if so required. The experimental design and velocity profile conditions that the model was subjected to are next shown. Finally the problems encountered are discussed.

3.1. DESIGN OF APPARATUS AND FACILITIES

3.1.1. The Facilities

The Monash University large wave flume was used for the experiments. The depth of the flume is 4 m with a shallow working section of 2.5 m at one end. The flume is fitted with a large wave paddle, although this feature was not used as this study is focusing on current only effects. Two large recirculating pumps combine to give a maximum capacity of 850 Litres/second. The width of the tank throughout its whole length is 2.14 m. The current testing program was conducted at a location half way along the flume total length, which is 80 m.

3.1.2. The Use of a Constriction for the Flow

There were many trade off points in designing the flow characteristics and the model physical properties. The design objectives are listed below:

- The model needed to be excited in its first 3 natural modes of vibration underwater over at least part of its length.
- The model needed to have pressure tapings to derive forces and accelerometers to measure responses.

A smaller diameter pipe could easily reach its first 3 natural frequencies with the given flow spanning the whole flume width (being a relatively slow flow of 0.1 m/s). A pipe capable of generating a high enough vortex shedding frequency such that it matches its third harmonic in a flow of 0.1 m/s could be around 5 mm diameter. Such a small size would be impractical to fit instrumentation into.

The amount of instrumentation and associated cabling was then the constraint that set minimum internal diameter of the model pipe. With six pressure transmitter cables and five accelerometer leads all requiring to pass by the last accelerometer the minimum ID was decided to be about 30 mm. Some gains could be made by passing some of the instrumentation leads through the other opening of the pipe, but this was decided against for ease of installation and removal, an activity that was required almost daily.

With the minimum ID of the pipe now fixed, as low a bending stiffness (EI , where E is the elastic material modulus and I is the moment of inertia) as possible was required to reach higher natural frequencies. EI was minimised with a small wall thickness and selection of High Density Polyethylene (HDPE) as the pipe material.

The flow had to be sped up by constricting the width of the flume in order to maximise the Strouhal frequency. Calculations showed that the width was required to be as small as possible (while not having any undue hydrodynamic effects) in order to achieve the 3rd natural frequency, given the physical parameters already decided upon. Constriction of the width of the flume was achieved with temporary wooden walls as shown in Figure 3-1. A minimum 2D (2 Diameter) clearance either side of the greatest amplitude was maintained for reasons explained in Section 3.1.5. The total width of the constriction is then 7D, made up from a possible 1D maximum amplitude of vibration either side of the mean and then a 2D clearance from the maximum position. A 7D flow width gives a blockage of 14.3 %. While a 14.3 % blockage is considered relatively high, the physical limitations of the facility require this amount to obtain enough flow speed. Blockage corrections are performed on the mean velocity data as the velocity is measured in the absence of the model. In order to achieve the highest frequency of shedding possible, the pipe had to be at its smallest possible practical outside diameter which was 40 mm.

Fig
ins
cor

The tv
of a fle

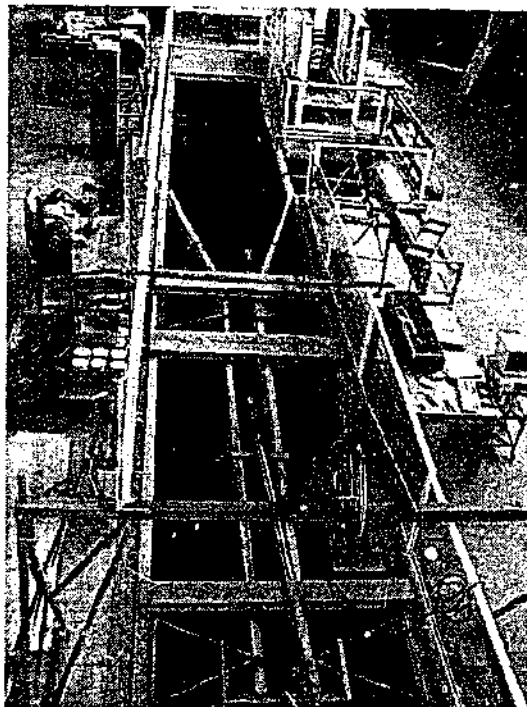
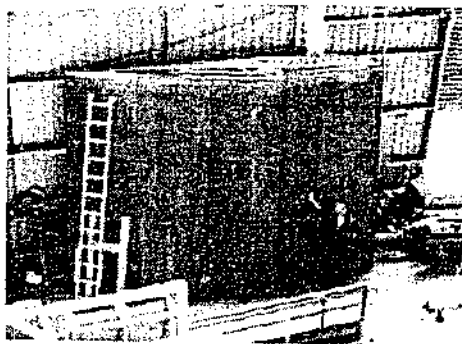


Figure 3-1 Above: One of the six walls forming the constriction prior to installation showing the depth of testing section. Below: A view of the constriction from above. The flow is from top to bottom of photo. The narrowed testing section is 320 mm wide and 4 m deep.

3.1.3. Two-flow Field

The two-flow field experiments were aimed toward categorising the response of a flexible riser in a simple two-flow field. To this end, some small prototype

fluid dynamic tests were conducted in a glass flume to explore the most successful and easiest method of creating the 2-Slab flow. The two-flow field, with each field being uniform, was realised with an adjustable splitter plate that acted to converge and diverge the lower and upper parts of the inlet uniform flow respectively. The final arrangement is depicted in Figure 3-2. A basic mesh type was incorporated into the design with a pressure drop coefficient, $k_p = \Delta p / 0.5\rho U^2 \approx 1$ (where k_p is the pressure drop coefficient, Δp is the pressure drop, ρ the density of water and U the velocity). The mesh type and number used were critical in setting the relative velocities from the respective blockages they provide at the inlet to the diverge/converge sections.

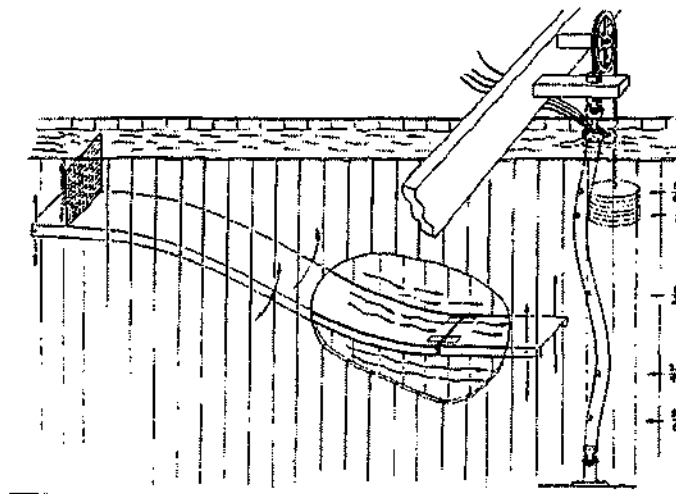


Figure 3-2 A sketch of the experimental set-up in the constriction. Flow is from left to right.

3.1.4. The Riser Model

3.1.4.1 End conditions

The model riser was chosen to have pin-pin end conditions for simplicity in analysis, matching previous experiments more closely and matching the real world application.

An appropriate method of applying tension had to be chosen. If the model riser is made taut at one end with the use of some combination of springs or winches then the end tension is also dependent on the force supplied by the mean drag on the cable. With a relatively stiff spring, the axial force through the riser can vary a great deal while the arc profile of the riser remains relatively the same. If the end tension is applied by means of a pulley and weights then the end tension stays constant (fixed to $m \cdot g$) and the profile of the riser adjusts according to the drag applied. A disadvantage with using end weights is that any vertical oscillation of the weights induces an inertial load in the riser.

Constant end tension was decided upon for the top condition. The deciding factor that influenced the selection of the constant end tension for these series of experiments was the desire to have the natural frequencies of the riser remain the same, despite the flow conditions. Fixed natural frequencies of the model riser make conclusions of the results clearer. For example, with a given spacing between natural frequencies of a riser (hence a given number of possibly excited modes, N_s) the effects of flow alone can be studied for many

varied flow conditions without introducing structural response changing effects. In order to model risers more accurately, the top of the pipe was fitted with a cable leading to a weight via a pulley (the bicycle wheel that acts as a pulley can also be seen in Figure 3-1). The end weight could then be varied so that different tensions and natural frequencies of the riser could be studied. A more subtle effect of a variable end tension is the changing riser properties between cable like (lateral stiffness governed by end tension) and beam like (lateral stiffness governed by bending stiffness) responses, and to observe any effects on the dynamics. Even though risers are generally accepted as being more cable like, the contributions of each decide on the spacings of the natural frequencies.

Vertical translation had to be allowed for with a varying mean drag. An increasing mean drag would shorten the vertical length of the riser as the riser has a different top inclination so that a greater component of its end tension can combat the mean drag. Thus the vertical distance from connecting points of each end of the riser changes and this needed to be accommodated in the design. The top joint consisted of a 15 mm diameter universal joint that was identical to the bottom. Connected to the top joint was a rod free to slide in the vertical direction inside a permanently mounted fixed vertical sleeve. The aforementioned set-up ensured that the top of the riser was free to rotate about the horizontal axes but not the vertical axis.

The b
joint
but fr
enabl
and a
An in
elimin
desig
termin
exten
small
some
small
force
pivot
3.1.4.
The t
vertic
by e
feasib
requi
end t

The bottom connection of the riser to the flume floor consists of a universal joint that acts as the 'pin' so that rotation is constrained around the riser axis, but free in the other two directions. A bayonet type fitting was machined to enable the model to be easily slotted in and out between velocity profiling and also maintain a vertical position while the model was installed.

An important consideration in the design of the model was to minimise or eliminate any part of the model in air. The flexible pipe in this study was thus designed to be terminated before the free surface. Even with the pipe terminating before the free surface, the bundle of instrumentation leads that extend out of it act as a cylinder themselves with a diameter only slightly smaller than the pipe diameter. The instrumentation leads were subject to some fluid drag however since the total global drag was not measured, the small contribution from the leads did not matter. Any fluctuating lift or drag forces that the instrumentation experienced did not affect the results as the pivot of the model was below the freestream exposed leads.

3.1.4.2 Physical properties

The test pipe was designed to model the first three natural frequencies of a vertically tensioned riser. The intent was to have the lateral stiffness governed by end tension rather than bending stiffness as much as possible. The feasibility of designing a model with the very high levels of end tension required to be end tension dominant in stiffness are surmountable. Higher end tensions are accompanied by higher natural frequencies and the ability to

excite these higher frequencies from the Strouhal frequency is limited by the flow capacity of the facility. In this testing program (St is proportional to U/D) U_{max} is limited by the flow facility and D_{min} is limited by the requirement to be fitted internally with instrumentation.

Initially a PVC (Poly Vinyl Chloride) pipe was considered. The pipe required a minimum wall thickness of about 2.5 mm to enable satisfactory installation of tubing connections. The bending stiffness for the selected PVC pipe as a result of the minimum thickness condition was too high to be able to attain the 3rd natural frequency in the 2-Slab flow with the given flow conditions. Achieving the 3rd natural frequency was made possible by a switch in material to HDPE (High Density Polyethylene). HDPE has a Young's Modulus (E) approximately six times less than PVC.

The physical properties of the riser model are shown in Table 3-1. The range of possible vortex shedding frequencies encompasses the first three natural frequencies of the model. It is possible to check the shedding frequency prediction with the use of Equation 2.1 and an added mass correction of $Ca = 1$. Table 3-2 shows the predicted natural frequencies for the HDPE model pipe in the constricted flow with various end tensions.

Tab
E
ter
(
1
1
1
2

A
bo

Table 3-1 The physical properties of the model

Bending Stiffness, EI	74 Nm ²
Length, L	3.58 m
Mass Ratio, m^*	1.08
Mass per unit length, m_L	1.28 kg/m
Outside Diameter, OD	40 mm
End conditions	Pin-Pin

Table 3-2 Predicted nat. frequencies of the model for selected end tensions

End tension (N)	Mode 3		Mode 2		Mode 1		Ratio of Mode 2 : 1 nat. freqs.
	In-air (Hz)	Still water (Hz)	In-air (Hz)	Still water (Hz)	In-air (Hz)	Still water (Hz)	
59	8.53	6.49	4.03	3.07	1.28	0.97	3.15
109	8.89	6.77	4.36	3.32	1.53	1.17	2.85
154	9.21	7.01	4.65	3.54	1.73	1.31	2.69
192	9.47	7.21	4.87	3.71	1.88	1.43	2.60
290	10.10	7.69	5.41	4.12	2.21	1.69	2.44

A picture of the riser model, out of the water, is shown in Figure 3-3. The bottom of the picture shows the top of the riser when in its installed position.

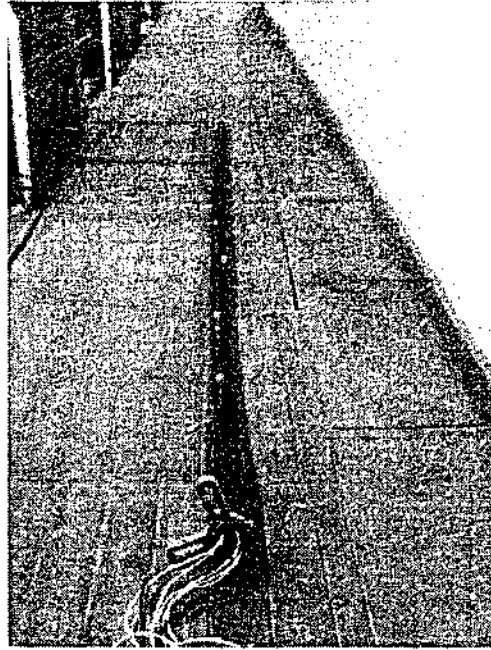


Figure 3-3 The riser model out of the water.

3.1.5. Model Scale and Testing Effects

3.1.5.1 Wall Effects

The peak vibration amplitude remained 2 diameters away from the walls. Data on vortex shedding of stationary cylinders near a wall can be found in Sumer *et al.* (1991). For steady currents, with a cylinder to wall gap of 2 diameters, the Strouhal frequency is within 2 % of the value of that for a cylinder at very large gaps away from a wall. The effects on a stationary cylinder with a fixed gap of 2 diameters are expected to be more pronounced than for an oscillating cylinder with a 2 diameter gap, that is only at the peak amplitude condition, simply due to the mean vortex street distance being further away from the wall.

3.1.5

The

and

amp

wou

3.1.5

The

the

effe

flow

prop

only

mea

also

coef

betw

3.1.

The

the

(Fig

3.1.5.2 Free Surface Effects

The axis of the riser model remained normal to the plane of the free surface and was below the level of the free surface. The largest free surface wave amplitudes noted were $0.5D$, hence any free surface effects on vibration would be insignificant compared to the vortex shedding effects.

3.1.5.3 Blockage Effects

The measurement of freestream velocity was accomplished in the absence of the model with a velocity probe. The presence of the model creates a blockage effect due to the cross-sectional area occupied by the model in the direction of flow. The mean velocity of the flow in the presence of the model will thus be proportionally faster as a ratio of the reduction in cross-sectional area. The only blockage correction applied to the data was to proportionally adjust the mean velocity measurements for the aforementioned effect. Corrections could also be applied to the lift coefficients, however it was decided that the raw coefficients be retained to enable clearer interpretation of the coefficients between the regions of riser, which are both equally affected by blockage.

3.1.5.4 Reynolds number

The uppermost Reynolds number in this study is $Re = 4.8 \cdot 10^4$, which confine the study to the subcritical regime (Figure 2-1). From the literature review (Figure 2-3) it was observed that the St number remains relatively constant for

a stationary cylinder in the subcritical regime, hence varying St number effects are not expected to influence the results.

3.1.6. Instrumentation

The flexible model pipe was fitted with instrumentation to be able to characterise inputs and responses. Inputs are defined by measuring the forces and responses are characterised by the modes of vibration. The input forces are found by deriving the section forces at two axial locations with a ring of pressure tappings. The resulting response is calculated from five accelerometers distributed along the inside of the pipe. The instrumentation was designed in packages that were sequentially installed down the pipe according to their final placement order. As there are no adhesives available that would adhere to the pipe material (HDPE), all the packages were slid a precise distance through the inside of the pipe while maintaining their original orientation and then held in place with a countersunk screw bored from the outside wall through the pipe.

3.1.6.1 Accelerometers

Five accelerometers were designed and fabricated, one of which is shown in Figure 3-4 prior to installation down the inside of the HDPE pipe. The accelerometer axial locations were $L/6$, $L/4$, $L/2$, $3L/4$ and $5L/6$, where L is the length of the riser. The outside ring shown around the accelerometer in Figure 3-4 matches the inside diameter of the model pipe to help stabilise the electronics in the axial direction. The accelerometers are biaxial, sensing in two directions, both in the plane of the outer ring shown. All of the electronics

were potted up with epoxy resin and covered over with a flexible membrane (M-Coat D). The accelerometers were +/- 2 g Dual Axis from ANALOG DEVICES (ADXL202). The circuitry alongside the accelerometers consisted of some amplification and a 30 Hz local analogue low pass filter. Each accelerometer was connected to a larger amplifier out of the water via a 5 m long cable. A space was deliberately maintained within each of the packages to allow for the other instrumentation's leads to pass through.

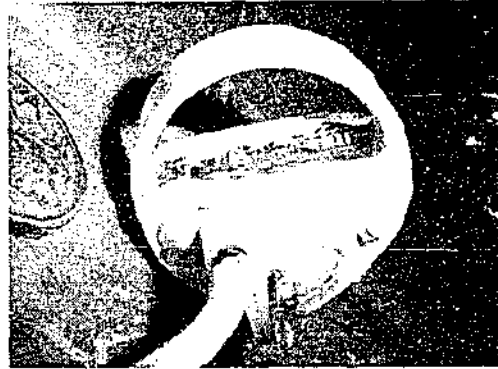


Figure 3-4 One of the accelerometer packages installed inside the model pipe.

The accelerometers selected are of the type that can sense gravity if tilted with a component of their axes in the vertical direction. It was thought that the piezoelectric type accelerometer would not maintain a high enough quality signal at low frequencies if so required during testing. Normal testing sees very little of their measuring axes tilted. Previously, Kaasen (2000) showed that accelerometer position is further optimized when considering the tilt component of the signal in full scale risers. A check was made on the maximum contamination of the signal due to gravity from tilting during the riser vibration. Due to relatively high accelerations, compared to the full scale model, the overall contribution to the total signal from tilting was insignificant. The benefit of the gravity detecting type accelerometer is that a static calibration can be performed with ease to determine a linear calibration relationship between voltage and acceleration.

Dynamic calibration was performed up to frequencies of 3 Hz prior to installation of the accelerometers. It was found that static calibration was

within the experimental accuracy of the dynamic calibration testing, (+/- 2%), after which static calibration was the only method to be employed. A static calibration was performed at the start and end of any substantial testing period, which lasted up to a maximum of 3 months. The calibration factor was found to be within +/- 2% during all of these periods.

3.1.6.2 Pressure Tappings

Two packets of pressure tappings were installed in the pipe at two different axial locations to derive the local lift force in the model riser. The axial location of the pressure packets were as close to $L/4$ and $3L/4$ as possible (each was 50 mm in the axial direction towards the centre of the riser model respectively). Each of the packets forms a 6 point pressure tapping system to derive the local lift force. Figure 3-5 shows the layout of one of these 6 point pressure tapping arrangements prior to installation. There are 3 pressure transducers that span the diameter of the model pipe. The transducers were 0-1 psi. range differential piezoresistive bridge construction from RS (#216-6253). The internals are waterproof where the tubing can be connected, however the externals are not waterproofed and so some potting was required with epoxy resin. The transducers consist of a bridge attached to a membrane at their centre, which senses deflections caused by fluid pressure. Each side of the membrane is exposed to opposite sides of the pipe's external pressure via a small tube. Each tube is bled to ensure there is no air remaining after installation at the testing location. The membrane then senses differential pressure. Three transducers are lined up with their axes in the cross-flow

direction, which then measure lift pressures. The differential pressure from the transducer in the middle is summed with the transducers either side which have a weighting to reduce their importance as a small component of the differential pressure they read will be associated with in-line pressures. The centre transducer provides the differential pressure between the 90 degree and 270 degree points (0 degrees is defined as the upstream point), while the other transducers measure 20 degrees either side of the 90 and 270 degree points. Using a standard sine summation reveals that although pressure information is missing for the majority of angles only half of the integrated lift pressure information is not available.

Intuitively the error involved in using only half of the integrated lift pressure information would seem large. In order to form a valid correction model for the information to determine the actual lift force and estimate the error, data from another facility conducted by another researcher was used. The results of forming a correction model and estimating the error are reported in Section 4.3 of the next chapter.

Figur

b

Stati

tubin

with

Dyna

• D

l

t

t

a

a

•

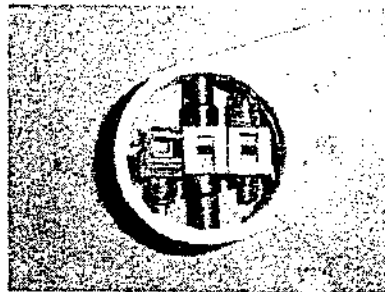


Figure 3-5 The differential pressure sensing ring prior to waterproofing and being placed into the model riser. The 3 transducers provide a 6-point pressure reading system.

Static calibration of the pressure transmitters was performed with a static tubing system on four separate occasions, with the total variation being within $\pm 1\%$.

Dynamic effects of the sensor system can be categorised into two features:

- **Dynamic attenuation effects.** The dynamic attenuation effects of the small length of entrance tube from the outside of the pipe to the centre of the transmitter were investigated. Using a frequency generator and comparing the signals from a system that included the above described length of tube against one without the additional tube showed a negligible effect on amplitude and phase up to the maximum frequency tested of 25 Hz.
- **Dynamic inertial effects.** The bleed pressure transmitter system imparts an inertial effect due to the slug of fluid between the membrane and the outer

pipe wall. This inertial effect needs to be subtracted in order to evaluate the pressures due to the external lift forces. Several steady state oscillations of the whole pipe were conducted in air while with the tube system bled with water. Initially there was no coverage of the tube entrances and the instantaneous acceleration and pressure were recorded as a function of time. A floppy membrane (with very small bending stiffness) was used to cover over the tubing entrances to stop fluid escaping and investigate whether there were any effects due to surface tension that could be adding non-linearities to the signal. There was little difference between the two results. An inertial correction procedure was thus applied to the signal in post-processing based on the results from the steady state oscillations. The procedure made use of the instantaneous cross-flow acceleration, independent of the modal participation factor, applying a correction unique to each transmitter to then calculate the cylinder surface pressure fluctuations. The correction was always relatively very small compared to the total signal.

3.1.6.3 Cabling

To ease handling and installing of the model all instrumentation connections exited the model at the one end (top, as installed). It was anticipated that the extra cabling created a non-uniform mass distribution. A check was made on the mass distribution and found that at the worst case the final 600 mm of each end of the model differed by only 3 % in mass or 1.5 % from the mean value and hence was neglected.

During the construction of the model it was envisaged that collisions between the cabling and tubing with the pipe model wall may create noise. Additionally, any difference in density between the cabling and the inner surrounding mass (water) can lead to lagging or leading inertia effects. The cabling inside the pipe was restrained with the use of silicone sealant injected through the wall of the pipe at the two worst case axial locations to reduce the unrestrained span lengths of the cabling. A previous riser model overcame the noise from the cabling problem by filling the inside of the model with gelatine (Lie *et al.* 1997). Concerns of increasing the bending stiffness too much and not being able to reach desirable natural frequencies in the current facilities drove the decision away from using gelatine for the current model.

3.1.6.4 End Tension

A 225 kg (500 lb) capacity load cell (Interface SSM-500) was used to monitor end tension. Calibration was executed by progressive loading and unloading of a series of 5 weights and then performing a regression analysis. The end tension was recorded as a function of time for all tests. However, only the mean value was used as a quality control check that the correct end weights had been applied in later analyses.

3.1.7. Signal Acquisition

An estimate of the maximum frequency of interest was made at 16 Hz, based on a factor of four applied to the still water natural frequency of the highest mode (Mode 4) that may want to be studied (Factor of 4 = Margin for error (2) x in-line Mode 4 frequency). All analogue instrumentation signals were low pass filtered at 25 Hz and fed into an analogue to digital converter (ADC) (Data Translation DT 3000 64 channel). The ADC was connected to a Pentium I computer wherein the data was recorded at a sampling rate of 100 Hz (Maximum resolvable frequency = 50 Hz). The sampling system operated such that the skew between each channel was $1/\text{channel number}/\text{sampling frequency}$. A check was made on the error introduced from the skew and found to contribute a phase shift of only 10^{-4} radians for the slowest period of interest. Hence there was no correction applied.

The va
curren

- Enc
- Rec
- Pow

In orde
the ris
necess
with th
variabl

- Cha
- Cha
- Cha

3.2. EXPERIMENTAL DESIGN AND VELOCITY PROFILES

3.2.1. Experimental Design

The variables decided to be tested were from the outcomes of the survey of current literature. (Chapter 2). The following list contains the variables:

- End tension, P
- Reduced velocity, U_r
- Power-in length, l^*

In order to achieve the investigate the thesis objectives, investigation into how the riser behaves in a uniform flow, 2-Slab flow and in still water was necessary. As a result, the testing program is broken into three main sections, with their respective results chapters given. Each results chapter adds another variable to the field as shown in the parentheses.

- Chapter 4. Still water and decay tests. (P)
- Chapter 5. Uniform flow conditions. (P, U_r)
- Chapter 6. 2-Slab flow conditions. (P, U_r, l^*)

Five different end tensions were selected ranging from the minimum that would prevent mechanical connection sloppiness, and therefore contamination of the accelerometer signals, to the maximum possible given the velocity achievable. The end tensions were 59 N, 109 N, 154 N, 192 N and 290 N.

Reduced velocity could be varied through the velocity of flow or the value of end tension which alters the natural frequency. Plots of the systematic variation in reduced velocity always originate from the flow velocity being varied. The number of increments tested varied but always contained more than 10.

Three different power-in lengths were selected based on the limits of the facility to be able to generate uniform flow within each section of the flow. The power-in lengths were defined as the percentage of the model length exposed to higher speed flow to the total length. The power-in lengths reported are 30 %, 35 % and 40 %. The uniformity of flow within each slab was lost for power-in lengths above and below the previously stated values for the current facility.

3.2.1.1 Still water and decay tests

The still water tests involved manual excitation of the model riser at its 1st and 2nd natural frequency for the five different levels of end tension. The amplitude of oscillation was kept as small as possible to minimise effects due

to vorticity and shedding so that the values obtained were as close as practicable to irrotational flow conditions.

The decay tests were conducted in air to estimate the structural damping due to model material and end connection damping sources. The model riser was excited and then allowed to decay with the amplitude as a function of time being recorded. The decay tests were conducted for both Mode 1 and Mode 2 at the five different end tension levels.

3.2.1.2 Uniform flow tests

The uniform flow tests involved five sets of tests with the five different end tensions applied to the riser model. For each series of tests, the flow velocity was incremented such that 20 different constant velocity cases were tested up to the maximum that the flume could provide.

In addition, some experiments were conducted to investigate any transient or hysteresis effects. The hysteresis tests involved varying the reduced velocity through altering the end tension over a short time span (order 2 seconds) and recording time histories over a longer time span (order 2 minutes) to see any effects. Three main reduced velocity regions were selected for hysteresis examination, prior to peak response, peak response and after peak response.

3.2.1.3 2-Slab flow tests

The flow field for a vast majority of the tests undertaken in the study program was required to be of type described as '2-Slab'. Each 'Slab' was to be as uniform as practically achievable. The model riser is then tested with the 2-Slabs flowing over its length simultaneously. The intent of conducting the tests in a 2-Slab flow situation was to quantify any interdependency between modes and hence form an improved model of modal response to the current mode-by-mode approach.

The 2-Slab flow tests involved the end tension being varied to the five different levels, flow velocity varied to at least 10 different levels and power-in length varied to the 3 values previously stated.

3.2.2. Flow Profile

The velocity field of the incoming flow was checked before the start of each set of tests for all the conditions requiring testing. An investigation was carried out as to the repeatability of the values of current over the course of a few days. It was found that as long as the water level in the flume remained exactly the same, then for a given pump revolution per minute (RPM) there was no detectable difference in the velocity at each height from day to day. Also, the velocity between selected pump RPM settings could be linearly interpolated with no detectable difference, if so desired. The procedure to

verify the velocity testing conditions involved removal of the model and was by far the most labour intensive part of the whole testing program. The velocity was measured with the use of Acoustic Doppler Velocimetry (ADV) 3 axis probe (from SONTEK). Prior to each set of tests, the riser model was removed and the velocity probe installed so that it tracked the same path as the axis of the model. The probe was raised and lowered to 10 reference heights (spanwise pipe direction) and the velocity recorded along with a general comment on the turbulence intensity levels. After checking the flow the model pipe was brought into position. The mean velocity recorded in the absence of the model was proportionately lower than that when the model was present due to model blockage effects (model width divided by total flow width = 14.3 %). The mean velocity presented in the results had the blockage factor applied to the model-free measurements to reflect the presence of the model.

The turbulence intensity was always in the range 5 - 10 %, generally with a macro length scale, $L_u = 100$ mm. The macro length scale is a result of the mesh used upstream of the testing location to help create a uniform flow. The macro length scale was calculated from

$$L_u = U \int_0^{\infty} R_u(\tau) d\tau , \quad (4.1)$$

where U is the freestream velocity, R_u is the autocorrelation as a function of time lag, τ .

3.2.2.1 Uniform Flow Profile

The uniform flow reported in this section relates to the flow that the riser is exposed to. A boundary layer existed along the bottom surface of the testing facility so the bottom pin joint of the model was raised by 150 mm to ensure that it was entirely in the free stream. The mean velocity of the uniform flow is calculated for each pump setting and subsequently used to calculate the respective reduced velocity dependent on the value of still water natural frequency. In all the uniform flow tests the spatial variation of the flow field from the mean did not exceed $\pm 5\%$. The final range of uniform flow velocities tested is shown in Figure 3-6.

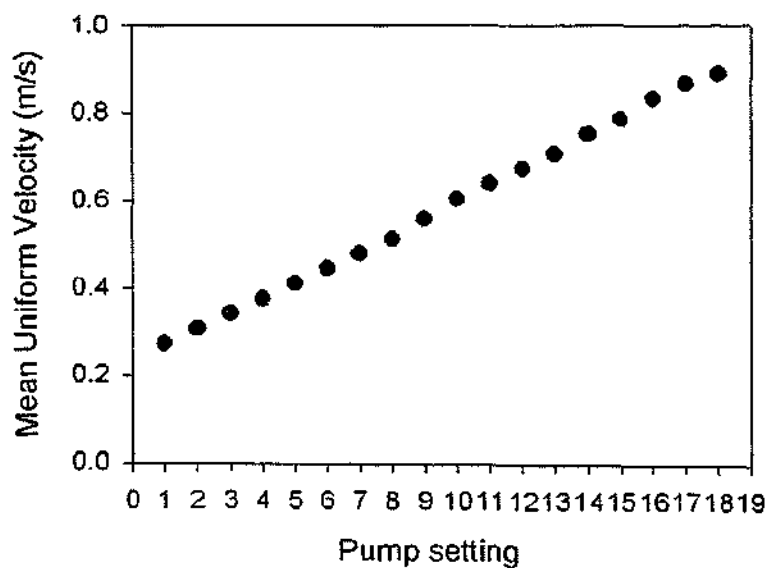


Figure 3-6 The increments of uniform flow velocities tested.

3.2.2.2 2-Slab Flow Profile

To minimize the transition region between the slabs a physical separation was required upstream of the model and terminating as close to the model as

possibl
typica
(Holn
instab
frequ
time s
is see
Figur
VIV f
regio
predi
alway

Fig

possible. An interface between layers of fluid travelling at different velocities typically undergoes a fluid instability of the type Kelvin-Helmholtz (K-H) (Holmes, *et al.* 1996). The 3 axis ADV probe was used to check if the K-H instability provided much of a disturbance to the velocity and at what frequencies it may have been occurring. The autocorrelation of the velocity time series within the interface region and within the centre of the slab region is seen in Figure 3-7. The differences between the autocorrelation of each in Figure 3-7, is the presence of a very low frequency spike (well away from the VIV frequencies under investigation) in the interface region, also the interface region generally contains more noise across all frequencies, as one may have predicted. The region of the riser exposed to the interface *noisy* region was always less than 5 % of its length.

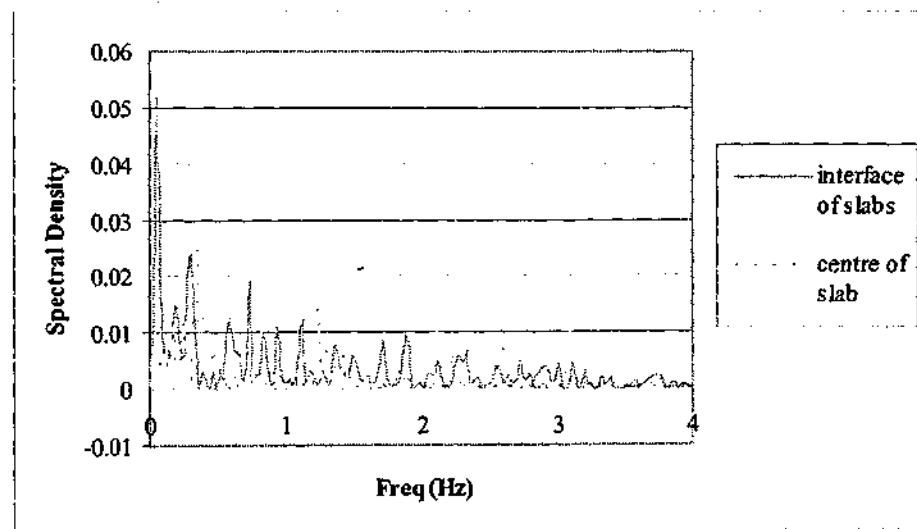


Figure 3-7 Comparison of autocorrelation of interface region and centre of slab region.

Three different length ratios are reported in the tests, these are 40 %, 35 %, and 30 %. A typical velocity flow profile for each is shown graphically in Figure 3-8. Following the graphical representation, Figure 3-9 presents the *mean* velocity of *each slab* for each test. Hence a graph in Figure 3-8 is represented by two points on a graph in Figure 3-9. The reduced velocity has been calculated in the presentation of the results section from the mean velocity value of each slab.

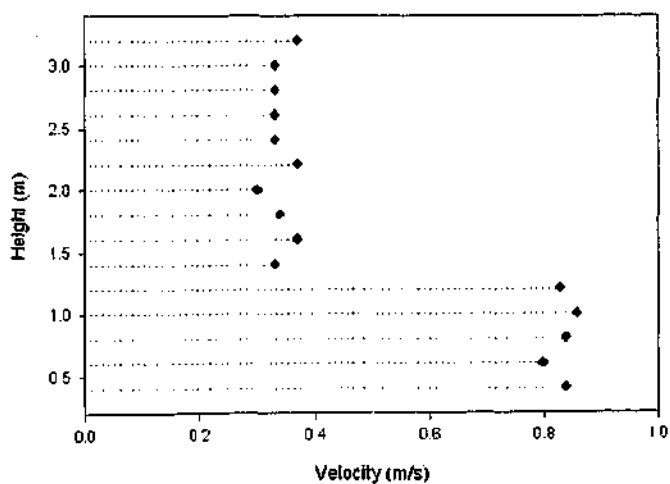
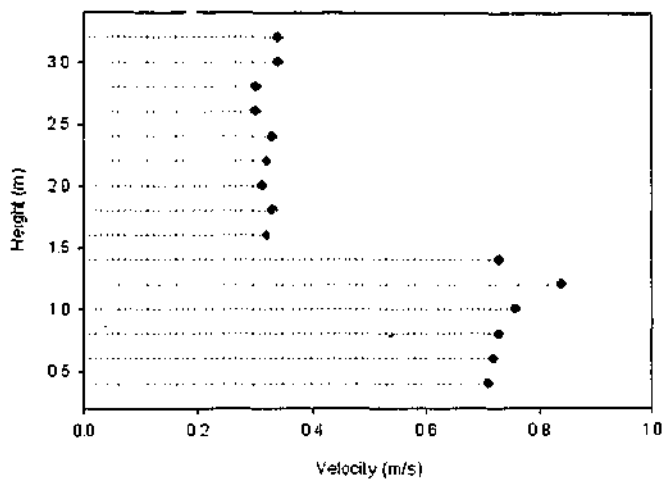
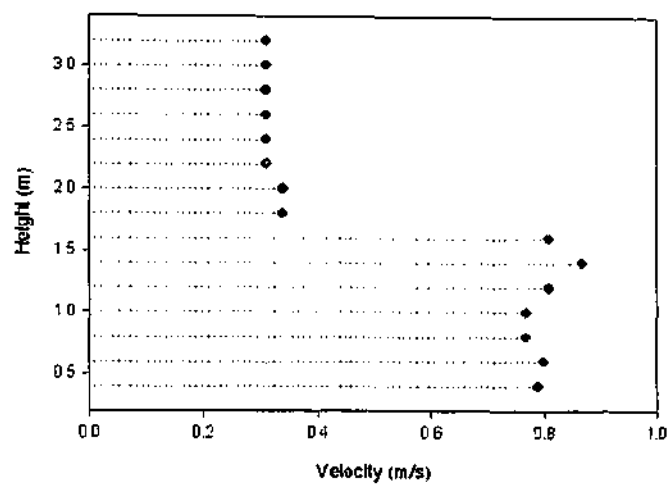


Figure 3-8 Typical example of velocity profile the model is exposed to for power-in lengths of a) 40 % ; b) 35 % ; c) 30 %.

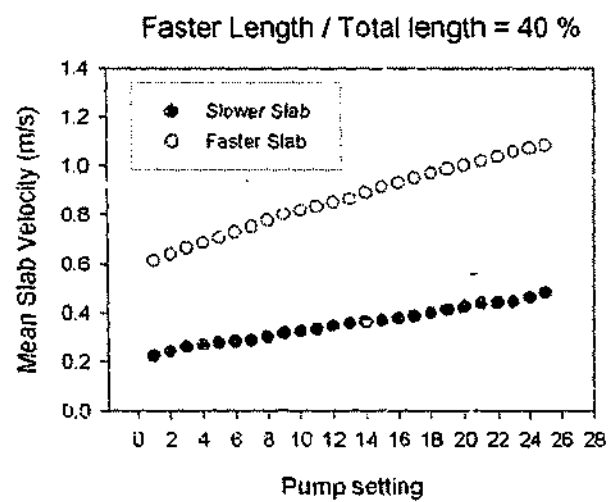
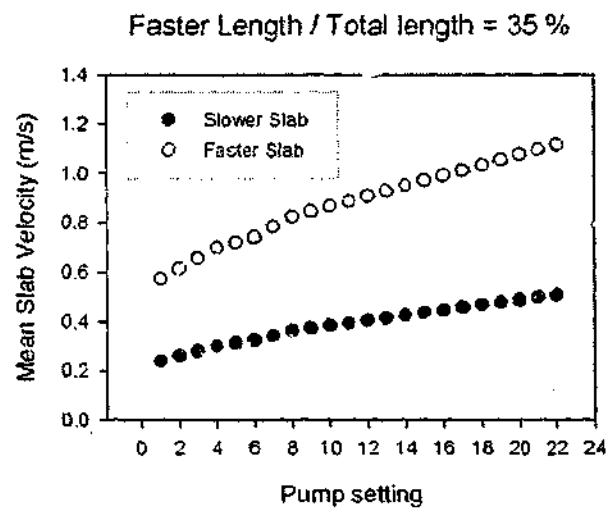
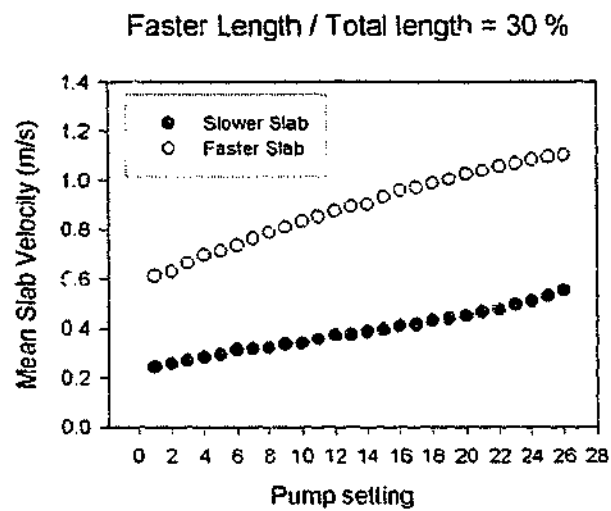


Figure 3-9 Summary of mean velocity in each slab for the three different length ratios tested.

3.3. PROBLEMS ENCOUNTERED

Most experimental programs are not without their disruptions and this program was not an exception. For the most part, the problems were easily overcome and did not delay the testing schedule. The largest unforeseen problem that was not predicted was to do with the lift force measuring system and is detailed below:

The model was initially fitted with a vast pressure tubing system consisting of 28 separate tubes running from the circumferential tapings, through the model, and out the top to 28 separate pressure transmitters on the surface. Construction of the model was eventually completed with the 28 pressure tubes and 10 accelerometer signal cables all fitting through a 33.7 mm ID space. Initially the thought was to have the tubes contain air and provide a seal at the tapping site, so that fluctuating water pressure would be transmitted through a membrane to the tube filled with air. Eventually it was acknowledged that the relatively large static pressure (due to static head of water) compared to the fluctuating component (due to vortex shedding) could not be sealed and still permit the measurement of the fluctuating component. The static head of water was several orders of magnitude greater than the fluctuating component. The tubing system was changed to contain water as the transmission medium, so that the tube was open ended at the tapping site while completely bled of air up to the pressure transmitter. A bleeding procedure was undertaken prior to testing each time. After a few weeks of testing, it was clear that the vibration of the flexible model imparted inertia to

the tubing system. The resulting pressure signal due to inertia was several orders of magnitude greater than the desired fluctuating surface pressure signal. Several inertia subtraction routines in processing of the data were developed, however the inertia originated not only from simple radial movement, but axial displacements as well, occurring at a wide range of frequencies. Thus the whole tubing system was scrapped. The pressure transmitters themselves were then trimmed back to minimum size, waterproofed, and recessed in the model. The resulting space consumed by the pressure transmitters limited the number of possible tapping points and transmitters (as the transmitters were mounted as close to the surface as possible).

Other problems encountered during the experimental program were:

1. The end connection initially consisted of ball joints. It was initially thought that giving the model maximum possible freedom would be of benefit however there was no control of the orientation of the model. The ball joints were changed to universal joints that were rotationally constrained on the *opposite side* to the model. Constraining the model in the rotational sense ensured that the accelerometers axes were always orientated to their intended directions, and then the lift force measurements were always in the cross-flow direction.

2. Viscous dampers were fitted to the top of the model on outrigger arms to be able to model increases in structural damping levels. The dampers were filled with water as with air they just acted as stiffness increasers while the air was compressed in each stroke. Water had to be stroked in and out of throttling valves and the valve openings were varied. During decay testing calibration of the viscous dampers some large non-linear effects were discovered that increased the uncertainty of the estimate of damping provided during the actual tests. Therefore, none of the tests with dampers are reported.
3. Accelerometer number five, the accelerometer at the deepest location, failed early on in the testing program. The fourth accelerometer from time to time experienced a mean offset drift on the in-line direction channel only. It was thought the ingress of water was the cause of the drift. Static calibrations confirmed that the output voltage ranges were not affected, only the mean of the voltage. The effect was only limited to one of the channels of the dual axes of the accelerometer. During experimentation, when this occurred, the in-line channel was subsequently removed from data processing. The riser model was removed from water and allowed to dry out for a few days, whereupon the problem disappeared and once testing began, slowly began to reappear after about 24 hours.

4. Obtaining the resonant response of Mode 3 cross-flow proved impossible even over only a very small part of the model riser. The apparatus was designed with Mode 3 in mind as a possible response to study. However, being limited by the recirculation capacity, it was intended to gain the high velocities required for Mode 3 over only a small section of the riser. The resulting pressure differences from the relatively large velocity differential in the slabs almost caused catastrophic failure of the constriction walls.

The
appa
water
air c
a co

The
of t
the

The
sub
exc
wi
pu
ste
sm

4. STATIONARY FLOW RESULTS AND LIFT FORCE CORRECTION

The following chapter presents the results of the basic investigation into the apparatus. Contained at the start of this chapter is the determination of still water natural frequencies and then structural damping values found from in-air decay tests. The final section of the chapter presents the results of forming a correction model for the lift force from an independent set of data.

4.1. STILL WATER NATURAL FREQUENCIES

The still water tests were performed so as to be able to compare the behaviour of the riser model to that of the in-air motion. The primary result of interest of the still water tests is the measure of the frequency of vibration.

4.1.1. Vibration Technique

The technique used to excite the riser in still water vibration tests was a very subjective one. The riser was touched with a hand on one side and at first excited with large oscillations. The large oscillations were allowed to subside with time and then manual excitation continued, all the time attempting to put as little energy into the system as possible, while still maintaining a steady state small oscillation. The amplitude of oscillation had to be kept very small to enable fluid conditions to be as close to potential flow conditions as

possible. The previous method has also been used by Khalak and Williamson (1999) whereby they found added mass values within +/- 5 % of 1.0.

In all the still water tests the greatest amplitude of oscillation was $0.2D$. The results of the frequencies of vibration for Mode 1 and 2 (cross-flow and in-line are assumed the same as the model has axis-symmetric properties) are presented in Figure 4-1. Included in Figure 4-1 is the theoretical prediction for the frequencies of vibration based on the formula of Rao (Equation 2.9) and using an added mass value of $Ca = 1.0$. Rao's formula provides the in-vacuum values (assumed same as in-air here) and the application of an added mass to the predicted frequency of vibration is done through:

$$f_{sw} = f_{air} / \sqrt{m_L + \rho_f \pi \frac{D^2}{4} Ca}, \quad (4.1)$$

where f_{sw} and f_{air} are the frequencies of vibration in still-water and air respectively and m_L is the mass per unit length of the cylinder.

Figure
th

The resu
that the
frequenc

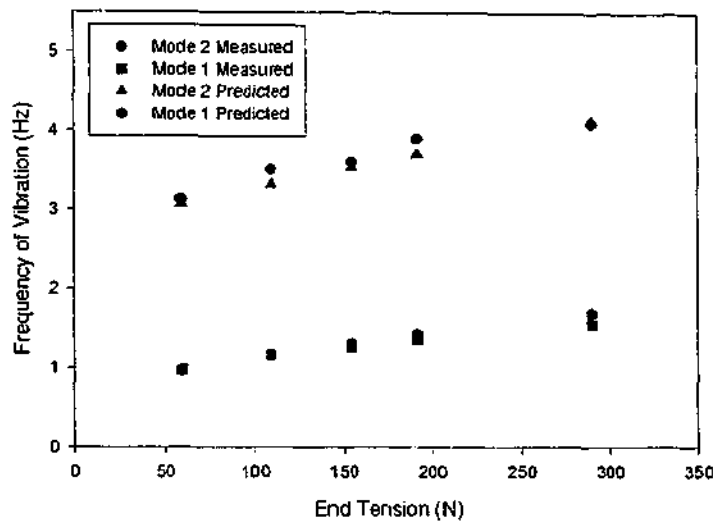


Figure 4-1 The measured and predicted still water natural frequencies for the five different cases of end tension used in the experiments.

The result of the still water vibrations for small amplitudes of oscillation is that the frequencies are found to be within $\pm 5\%$ of the predicted frequencies using the potential flow value of 1.0 for the added mass.

4.2. STRUCTURAL DAMPING VALUES

The decay test is used to determine the damping ratio in the current series of tests. For the purposes of the decay tests, the system can be analysed as an underdamped one-degree of freedom system with viscous damping and free vibration. An underdamped system means that the some harmonic motion can be observed prior to the damping causing the motion to cease. Viscous damping means that the damping is proportional to the velocity. In reality this is an approximation to the main sources of damping which are material (proportional to strain) and end fitting (Coulomb). The equation of motion which can describe the damped, one degree of freedom, free vibration system is:

$$x(t) = x_0 e^{-\zeta \omega t} \sin(\omega_n t), \quad (4.2)$$

where $x(t)$ is the displacement as any time, t , x_0 is the initial amplitude and ω is the natural frequency. By assigning the maximum value of each successive oscillation amplitude as x_i , and disregarding the harmonic component, we reduce the equation to a discrete form:

$$x_{i+1} = x_i e^{-\zeta \omega \Delta t}. \quad (4.3)$$

Δt is the time step between the oscillations and ζ is the damping ratio, which is defined as the ratio of the damping constant to the critical damping constant (Rao 1990) :

$$\zeta = c / c_c. \quad (4.4)$$

Figure 4-2 shows a typical decay test for the 1st mode of vibration.

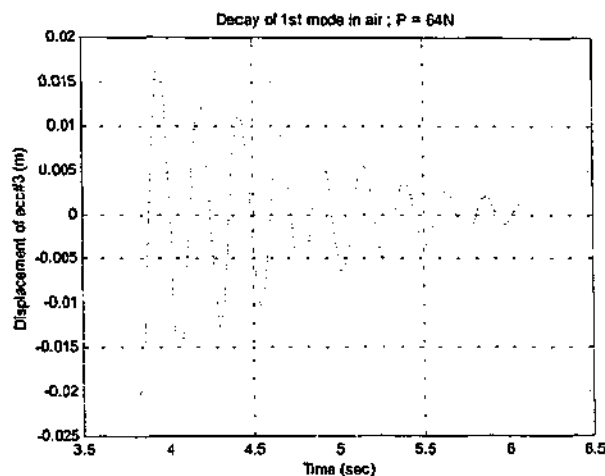


Figure 4-2 Decay of amplitude for 1st mode of vibration in air.

By averaging the values of logarithmic decay for each successive maximum oscillation amplitude an estimate for the damping ratio is obtained. The standard assumption that the in-air damping ratio is approximately equal to the structural damping ratio will be assumed herewith:

$$\zeta_s = \zeta_{in\ air} \quad (4.5)$$

4.2.1. Effect of Mode Number and End Tension

Ten different conditions of decay testing were conducted (each repeated three times) corresponding to the five different end tension values and first two natural modes of the riser model. The results of all the decay testing conditions are shown in Figure 4-3.

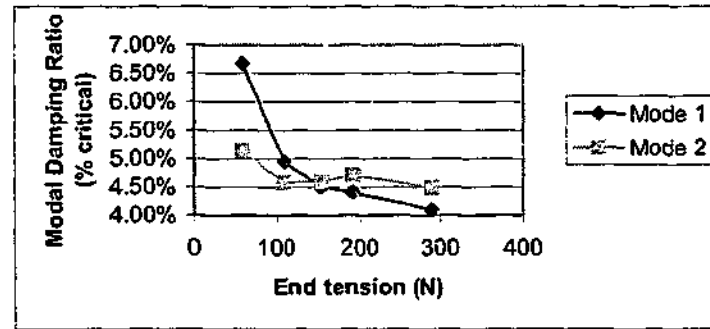


Figure 4-3 Measured modal damping ratios from in-air damping tests.

The modal damping ratios shown in Figure 4-3 that were found for the apparatus are quite high compared to previous VIV experiments, which are typically less than 2 % of critical. Separate experiments were performed, but not reported, on a cantilever piece of HDPE in a clamped joint. The level of structural damping found from the cantilevered piece of HDPE was similar to that found for high end tensions in Figure 4-3 (order 4.5 %). The likely cause of the higher modal damping ratio was then attributed to the HDPE material itself and not the mechanical joints.

The behaviour of Mode 1 follows the same trend as predicted by Fang and Lyons (1996) in that the modal damping ratio decreases with increasing end tension, if the damping is due to material damping sources. The Mode 2 modal damping ratio does not exhibit a clear downward trend with increasing end tension, thus the contribution of damping from mechanical effects (Coloumb type) may be greater for Mode 2.

4.3. LIFT FORCE CORRECTION MODEL

The following section presents the results of an analysis of an independent researcher's set of pressure distribution data. A correction model is formulated to apply to the current data to determine the lift force. The following approach was taken:

1. Determine a suitable correction from data taken on another cylinder with significantly higher pressure distribution resolution.
2. Apply the correction to the current model to determine instantaneous local lift force.

4.3.1. Correction Model from Stationary Cylinder

Available data to form a correction model comes from a stationary cylinder. Although no detailed pressure distribution data was available from an oscillating cylinder, it is the intent to compare the results of the correction model with sets of independent data from oscillating cylinders later (Section 5.3.2).

The stationary cylinder experiments were conducted in the small wind tunnel at the Department of Mechanical Engineering, Monash University by Eaddy (2002). Eaddy's experiments were conducted on a smooth stationary brass cylinder 38 mm in diameter for a range of Re number starting at 36,000 to 80,000 (similar Re to the current flexible riser model). A set of data was selected with similar turbulence intensity levels, 5%, to the riser model

conditions. The length macro scale of the turbulence in the wind tunnel tests was of the order of 130 mm. Eaddy's cylinder contained 18 circumferential pressure tapings, evenly spaced at 20 degree increments, so as to be able to gain detailed instantaneous pressure distribution information. Data was recorded at a sampling rate of 1 kHz and then processed to obtain fluctuating sectional lift and drag forces on the cylinder.

Of the 18 circumferential tapings on Eaddy's cylinder, 6 were at exactly the same orientation as the current riser model tapings, namely 70, 90, 110, 250, 270 and 290 degrees (0 degrees is the upstream front stagnation point).

The correction model was formulated by creating a lift force time series integrated from the 18 point pressure information and comparing it to a lift force integrated from only 6 points, both on Eaddy's cylinder. The 6 points chosen were at the same orientation as the 6 points on the current riser model. A correlation of the two different lift force values at each time step was then conducted to establish an error estimate for the stationary cylinder case. Figure 4-4 presents a short sample of time series from Eaddy's data (from his experiment 'G1P510') with the 18-point deduced lift force versus the 6 point deduced lift force. Figure 4-5 presents the correlation of the whole time series of the 6 point lift force versus the 18 point lift force.

F
Fig
lift
wi
pro
is a

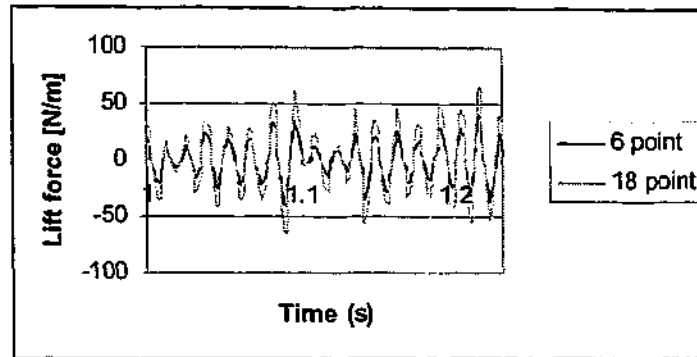


Figure 4-4 A time series sample of the fluctuating 6-point (dotted) and fluctuating 18-point (solid) lift force per unit length values.

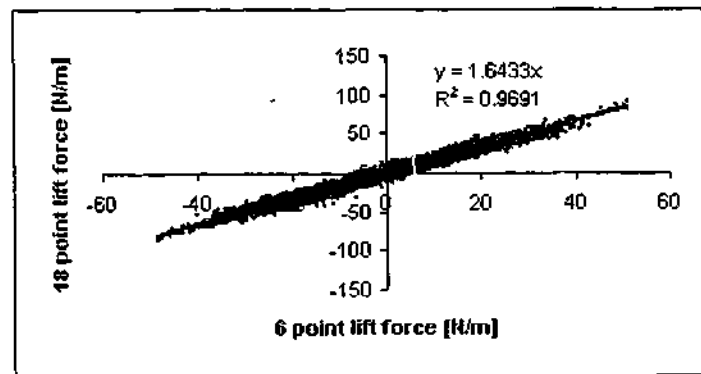


Figure 4-5 The correlation of the 6 point lift force versus the 18 point lift force for the entire time series along with a line of best fit.

Figure 4-5 demonstrates that by applying a linear factor of 1.643 to the 6 point lift force value will equate to the lift force found from the 18 pressure points with a coefficient of determination of $R^2 = 0.97$. Hence the 6 point lift force provides a highly accurate determination of the lift force once the linear factor is applied. A correction model has been formulated from stationary cylinder

data. In the next two chapters the correction model was applied to the current testing data in post-processing.

4.4. CONCLUDING THE CHAPTER

The current chapter has presented the results of a basic investigation into some of the model properties. The still-water natural frequencies were found for the first two natural modes and five different selected end tension values. Decay tests conducted in-air found the structural damping properties of model for the first two modes and five selected end tension values. Finally the chapter finished by presenting a lift force model formed from a previous researcher's stationary cylinder data that can be applied to the current 6 point data to more accurately determine the lift force.

5. UNIFORM FLOW RESULTS

The following chapter has two purposes:

- The first purpose is to verify the experimental set-up by comparing the results to other researcher's experiments previously conducted.
- The second purpose is to gather new data which will investigate the thesis objectives and with which later chapter results can be compared against.

The chapter is broken into subsections. The basic equation tools used to describe the experimental results are firstly introduced. The chapter then presents the results of the different sets of uniform flow VIV experiments. The behaviour of the cross-flow fluid force is scrutinized and then in-line and cross-flow coupling effects are examined.

5.1. LIFT FORCE COEFFICIENTS

In the case of these current reported model riser experiments, displacements at various lengths can be well approximated by the use of sinusoid shapes. The system can then be classified as moving as whole in one shape (or *mode*) or a combination of several shapes. Once the motion is modelled in this way the methods of oscillator systems can be utilised. When the riser is primarily moving in the form of only one shape then the methods of single degree of freedom systems become very useful. The equation for a single degree of freedom linear oscillator valid for small displacements is

$$m \ddot{x} + c \dot{x} + kx = F(t), \quad (5.1)$$

where x is the displacement, m the mass, c the damping, k the stiffness and $F(t)$ is an arbitrary forcing function. In the case of VIV phenomena, one way of describing the system is to group all the structural effects initially on the left hand side (LHS) of the equation and all the fluid dynamic effects on the Right Hand Side (RHS). The equation for cross-flow VIV motion, where y is the cross-flow displacement, can then be stated as

$$m \ddot{y} + c \dot{y} + ky = F_L(t). \quad (5.2)$$

The lift force, $F_L(t)$, is the force in the cross-flow direction and can be modelled as a sum of harmonic components. For the purposes of defining coefficients, we shall drop all harmonic components with the exception of the first. Later, we will re-visit the third harmonic component of the lift force in some phase-plane plots (Figure 5-8).

The motion, $y(t)$, of the oscillator is harmonic and we assume that it is well approximated by the 1st harmonic, $y(t) = y_0 \sin \omega t$, where y_0 is the peak amplitude of oscillation at ω rad/s. The lift force can also be represented as the sum of a sine and cosine component and then the force can be split into components in phase with body velocity and in phase with body displacement. Also note that the component in-phase with displacement will be 180 degrees out-of-phase with acceleration, $\ddot{y}(t)$. It follows from the

previous assumptions that by representing the lift force as $F_L(t) = F_o \sin(\omega t + \varphi)$, where φ is the phase angle and F_o is the peak force in the cycle one may then use the expansion of the sum of sines and write:

$$m \ddot{y} + c \dot{y} + ky = F_o \cos \varphi \sin \omega t + F_o \sin \varphi \cos \omega t, \quad (5.3)$$

which can be manipulated to:

$$\left\{ m - \frac{F_o \cos \varphi}{\omega^2 y_o} \right\} \ddot{y} + \left\{ c - \frac{F_o \sin \varphi}{\omega y_o} \right\} \dot{y} + ky = 0. \quad (5.4)$$

The lift force has now been split into two individual and much more useful components, an *added mass* term contained within the first bracket and an *excitation or damping* term contained within the second bracket.

Just as the total lift force can be non-dimensionalised in the normal manner to form an associated lift coefficient, the components too can have lift coefficients assigned to them. Thus the coefficients are defined as the total lift coefficient,

$$C_L = \frac{F_o}{\frac{1}{2} \rho D L U^2}, \quad (5.5)$$

the lift coefficient in phase with body velocity,

$$C_{L_V} = C_L \sin \varphi, \quad (5.6)$$

and the lift coefficient in phase with body acceleration,

$$C_{L_A} = C_L (-\cos \varphi) . \quad (5.7)$$

ρ is the fluid density, U is the fluid velocity, L and D the length and diameter of the body respectively and φ the phase difference between the total lift force and the body displacement.

The coefficients have been defined similarly to the work of Gopalkrishnan (1993) and Vikestad (1998). The previous definitions of lift coefficients use explicitly the total force of the fluid on the body. Previously, researchers have partitioned the force by making an estimate of the inertial added mass effects. Here, the total fluid force, along with fluid inertial effects, remains and any changing inertial effects can be observed through the component in phase with body acceleration.

Added mass coefficients can be deduced from the coefficient of lift in phase with body acceleration, making use of the following equation:

$$Ca = -\frac{2U^2}{\gamma D^2 \gamma_0} C_{L_A}, \quad (5.8)$$

where \ddot{y}_0 is the peak acceleration of the body. C_{L_A} is a *force* based coefficient to determine Ca , which is a *mass* based coefficient.

While the lift coefficient in phase with body acceleration reveals the inertial effects and their involvement on the frequency of body vibration, the lift coefficient in phase with body velocity plays a vital role in determining the extent of VIV. For continued steady state VIV all damping sources in the riser system have to be overcome.

The average value of the amount of power transfer, \bar{P} , can be expressed as

$$\bar{P} = \frac{1}{T} \int_0^T F_{L_V}(t) \dot{x}(t) dt, \quad (5.9)$$

where F_{L_V} is the lift force in phase with body velocity, and \dot{y} is the body velocity. Equation 5.9 is evaluated over an integer number of oscillations. By substituting Equation 5.9 into Equation 5.8 it can be shown to be reduced to:

$$\bar{P} = \frac{1}{4} \omega y_0 \rho L D U^2 C_{L_V}. \quad (5.10)$$

Hence, the amount of power transfer depends directly on the lift coefficient of force in phase with body velocity. Furthermore, positive values of C_{L_V} arise from the lift force phase lying in the range $0^\circ < \phi < 180^\circ$ and indicate energy

transfer from the *fluid to the body*, while negative values of the coefficient arise from the phase condition $180^\circ < \phi < 360^\circ$ and indicate energy transfer from the *body to the fluid*.

The difference between local and global lift coefficients must be emphasized. An example of the difference is easily realised in the case of a long flexible cylinder undergoing VIV. Here the net power provided by the fluid to overcome damping due to structural and hydrodynamic sources can be calculated in terms of a modal force in phase with modal velocity. The modal lift force is a spatial average contribution from all the local lift forces along the structure which may or may not be correlated. A modal lift coefficient can then be assigned as a measure of the modal lift force originating from the fluid velocity. Just as the modal lift force is a spatial average contribution of all the local lift forces, so too is the global lift coefficient. The local lift coefficients may vary considerably along the structure having dependence on the amplitude.

5.2. UNIFORM FLOW RESPONSE

Five sets of experiments were undertaken to study the response of the riser when subjected to an incoming uniform flow field. The five sets of experiments involved five different end tensions applied to the riser and described in Section 3.2.1. During the experiments the end tension was shown

to oscillate
varied

Due to

the axial

The low

vibrations

range

ultimately

in that

frequencies

the test

where

In the

second

so small

Through

flow

vibrations

arising

new

velocity

to oscillate about these initial values. For the largest variation case the tension varied $\pm 6\%$ of the mean value.

Due to the in-air natural frequencies of the riser being directly dependent on the axial tension, a range of fluid-structure conditions was able to be tested. The lowest tension case of 59 N was able to be excited to the onset of Mode 2 vibration, while the highest tension case of 290 N covered only the Mode 1 range but with better reduced velocity resolution than the others. The ultimate pumping capacity of the facility of 850 Litres/second was restrictive in that a flow generating a Strouhal frequency matching the Mode 2 resonant frequency could not be tested over the entire length of the riser. However in the tests reported in Chapter 6, Mode 2 was excited over fractions of the riser where the flow was sectioned into faster and slower regions.

In the current chapter the response for cross-flow modes higher than the second ($n > 2$) are not reported due to their amplitude of response levels being so small they are practically insignificant.

Throughout the following sections the reduced velocity was used to define flow speeds. Reduced velocity is usually defined with a frequency of vibration in the denominator. In cases dealing with the combined effects arising from two natural frequencies, there is the logical thought to define a new combined parameter. Rather than invent a new combined reduced velocity or non-dimensional frequency term however, two separate reduced

velocities were maintained where possible, so that the reader can easily establish the expected response if one of the frequencies were isolated. The two reduced velocities are therefore Mode 1 reduced velocity ($U_{r_{n=1}}$) and Mode 2 reduced velocity ($U_{r_{n=2}}$) as follows:

$$U_{r_{n=1}} = \frac{U}{f_{n=1}D}; \quad U_{r_{n=2}} = \frac{U}{f_{n=2}D}; \quad (5.11)$$

where $f_{n=1}$ and $f_{n=2}$ are the natural frequencies of Mode 1 and 2 respectively for the riser in *still water*.

5.2.1. Modal Displacement

5.2.1.2 Modal data reduction

As stated in the description of the experiments section, the response of the riser is known from accelerometer time series histories. The first step in processing the accelerometer time series was to determine a representative displacement time history for each of the accelerometer locations in both the cross-flow and in-line directions. The procedure to determine local displacement from local acceleration involved the following steps:

1. Acquire the acceleration data through analogue/digital converter and a 25 Hz low pass analogue filter.

2. Apply a 2% cosine taper window to each accelerometer time series in preparation for Fourier transforming. Amplify the time series proportionally to make up for the 2% cosine taper so that power estimations and standard deviations are representative.
3. Fourier transform the time series with an 8192 point FFT.
4. Transform the acceleration Fourier series to a displacement Fourier series by multiplying each Fourier component by the frequency squared value of its respective ordinate.
5. Apply a bandpass digital filter to the data to eliminate D.C., any low frequency drift and high frequency noise. The bandpass lower and upper limits were set at 0.3 Hz and 20 Hz respectively.
6. Inverse Fourier transform the displacement Fourier series to create a displacement time series, which has a 2% cosine taper at the beginning and end.

The response of the riser has been expressed in terms of a modal participation factor $q_i(t)$, for Mode i . The modal participation factor is determined by assuming that the various displacements at a given time consist of the sum of the first four orthogonal modes (each operating harmonically). Each individual mode shape time series (modal participation factor) is then back calculated from:

$$y(z,t) = \sum_{i=1}^n \phi_i(z) q_i(t), \quad (5.12)$$

where $y(z,t)$ is the displacement of the riser at height z , and $\phi_i(z)$ is the mode shape factor for Mode i at height z . The sensitivity of Equation 5.12 to the total number of modeshapes, n , fitted was investigated. Values of n were varied from $n = 2, 3$ & 4 . The difference in estimation of Mode 1 and Mode 2 response (in the tests where Mode 1 and 2 were both resonantly responding) was less than 2 % between all the trials and so $n = 4$ was used thereafter.

A typical accelerometer time series and modal participation time series along with their associated power spectra are shown in Figure 5-1. Each test duration contained a total of 8192 data points sampled at 100 Hz, thus lasting about 1 minute 20 seconds. The total number of cycles of oscillation in each was of course dependent on the frequency of oscillation. The test with the minimum number of oscillations (lowest frequency of oscillation) still provided 57 complete oscillations thus ensuring the power spectrum provided a reliable average estimate.

The accelerometer spectra typically show higher harmonics than the first harmonic. These are shown later to be due to the higher harmonics present in the fluid force. As characteristic of all harmonic systems the displacement has smaller contributions from higher frequencies when compared to the acceleration due to the relationship for single frequency phenomena being

$$y = -\frac{\ddot{y}}{\omega^2}, \text{ where } \ddot{y} \text{ is the acceleration.}$$

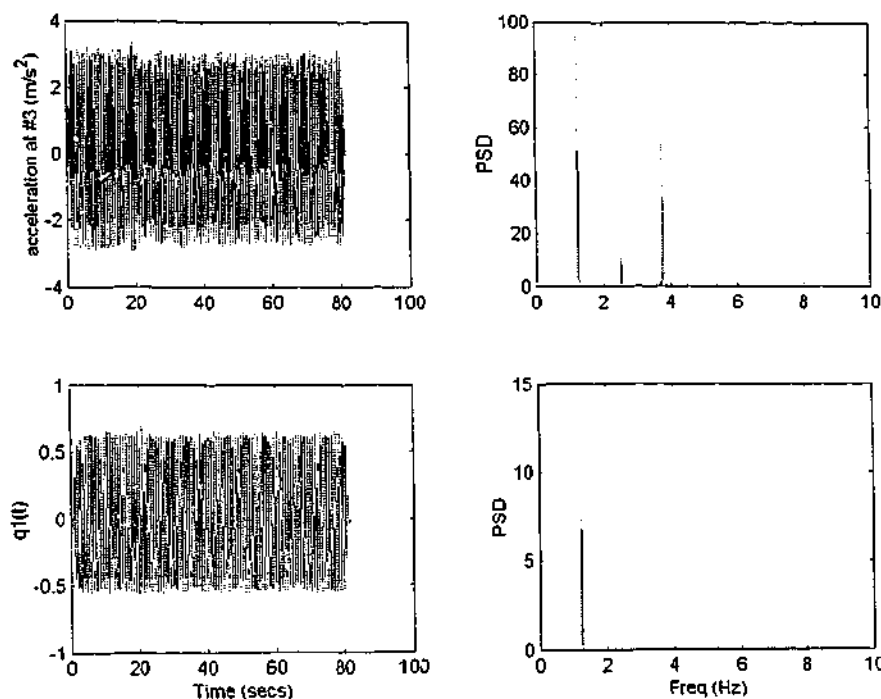


Figure 5-1 Typical acceleration time series and modal participation time series along with their respective spectra.

Examination of Figure 5-1 reveals that the response is not a steady state monochromatic one. Beating to a minor degree is present. However, for the purposes of analysis, it was felt that by using the standard deviation of each modal participation's entire time series provided as good an approximation as any of the response, this technique has also been used by other researchers (Lie *et al.* 1997). The modal participation time series is then:

$$q_n(t) = q_{no} \sin(\omega t), \quad (5.13)$$

where q_{no} is the peak modal displacement defined as follows:

$$q_{no} = \sqrt{2} \times \text{std}\{q_n(t)\}. \quad (5.14)$$

The peak modal displacement is then normalised by the diameter of the riser, D , such that the normalised peak modal amplitude, response be easily compared to that of rigid cylinder results where A/D is a common measure of response (A being the amplitude).

Use of the normalised peak modal amplitude indicates that for a value of $A_{o,n} = 1.0$, the shape of the mode is such that at its antinodes it has a local amplitude of $1.0 A/D$.

5.3. CROSS-FLOW DYNAMICS

The cross-flow direction dynamics is reported in the following sequence:

- Amplitude of Response
- Frequency of Vibration and Added Mass
- Lift Force measurements
- Effects of spacing of natural frequencies
- Hysteresis

The r
veloc
tensio
right
Koch
data
based
comp
value
value

Peak A/D

Fig
en

5.3.1. Amplitude of Response

The normalised peak modal amplitude response of Mode 1 at 18 different velocities is shown in Figure 5-2 for the sets of test involving the highest tension, 290 N. These tests cover completely the response of Mode 1 including right through its lock-in range. The results are compared against those of Koch which were introduced in Section 2.5.8. The reduced velocity in Koch's data was based on the in-air natural frequency ($Ca = 0$) and is modified to be based on the still water natural frequency (assuming $Ca = 1$) for the comparison in Figure 5-2. Additionally, the amplitude in Koch's data are *rms* values and have been modified per Equation 5.14 to form comparable peak values.

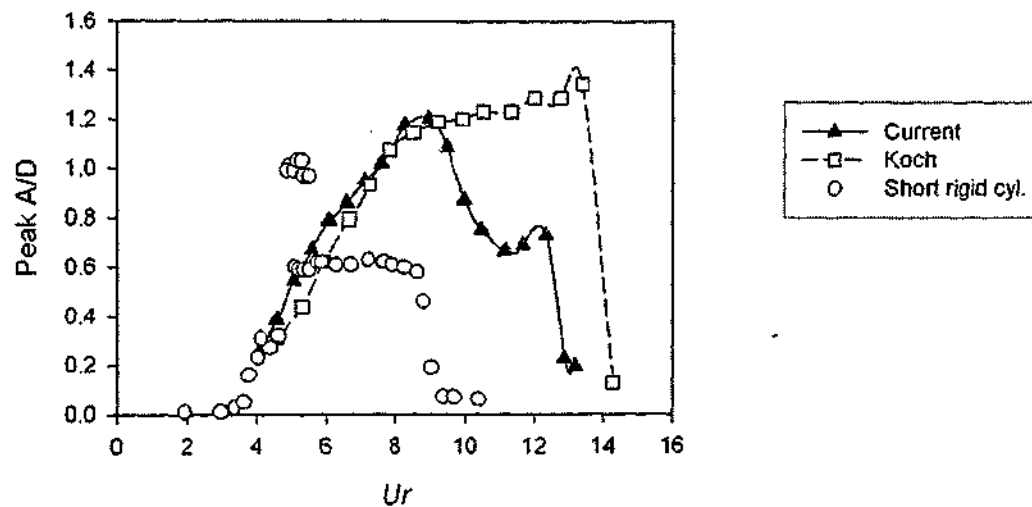


Figure 5-2 Peak A/D response of Mode 1 as a function of Ur for the highest end tension case (290 N) compared with other researcher's data against reduced velocity.

Figure 5-2 shows that the response peaks for the current data peaks at about $Ur_{n=1} = 8.5$. Unlike a single spring short rigid circular cylinder setup, the riser has a second mode of response beginning to become active at $Ur > 11$. There is good agreement between the current data and Koch's data up to the peak at $Ur_{n=1} = 8.5$. However the location in Koch's tests of the second natural frequency (and the Mode 2 peak) is unknown.

The maximum peak resonant amplitude of VIV has been shown to be a function of the structural damping (Griffin 1985). Koch's Aluminium cylinder has a much smaller value of structural damping, $\zeta = 0.019$, compared to the current $\zeta = 0.041$. Even though the structural damping values are so different the amplitudes agree well as a function of Ur until $Ur = 8.5$. Further comparison to Koch's data is made in Section 5.3.4., investigating the differences to the current data in the range $Ur > 8.5$.

When compared to the results of a typical elastically mounted short rigid cylinder (Khalak and Williamson 1999) as is done in Figure 5-2, the peak amplitude of response is observed to occur at a much higher value of Ur . However, for the region $Ur < 5$ all three sets of data follow the same trend.

5.3.2. Frequency of Vibration and Added Mass

5.3.2.1 Mode 1 Only

The frequency of vibration of the riser tells us a lot about the fundamental characteristics. As discussed in Section 2.5.7 one of the characteristics of lock-in, especially in high mass ratio cases, is the departure of the body oscillation frequency from the Strouhal frequency. For low mass ratio bodies, with the possibility of multiple modes excited, the frequency of oscillation becomes a fundamental indicator of the mode of the bodies' response.

Since the oscillation frequency varies throughout the lock-in region in cases of low mass ratio, then we attribute this variation to a changing added mass coefficient. The added mass described herein is then the fluid force in phase with body acceleration, different to that described by Leonard and Roshko (2001) and Khalak and Williamson (1999) which is the added mass solved completely by potential flow methods.

Using the present method, the added mass then becomes a convenient descriptor of the fluid dynamics of the system and we can back calculate the added mass from the body oscillation frequency and the still water natural frequency through Equation 4.1.

The frequency of response for each mode for each test was determined by batch processing of the spectra. With the aid of a MATLAB routine, the centre of energy for each spectrum was found. The centre of energy has been found

with a 'first moment of area' type calculation, where the value of the spectrum at each point is weighted with its distance along the abscissa.

The Mode 1 oscillation frequency divided by the still water natural frequency is shown for uniform flow conditions and the case of highest end tension in Figure 5-3. The added mass for Mode 1 vibration from the same tests is shown in Figure 5-4 and compared to previous short rigid cylinder results (Vikestad (1998) and Gopalkrishnan (1993)). The short rigid cylinder data have both been read from Vikestad's Figure 5.5.

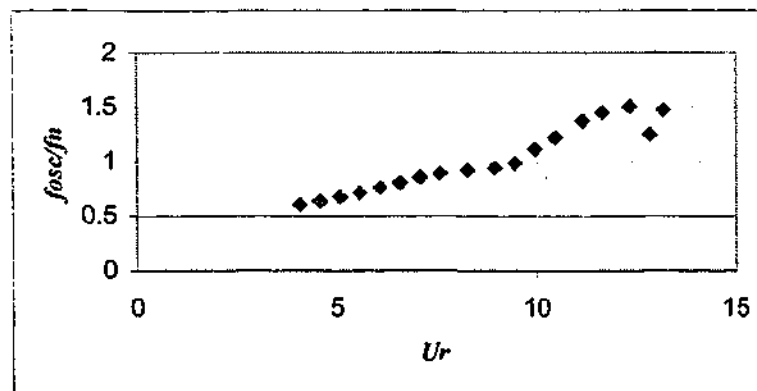


Figure 5-3 Oscillation frequency, f_{osc} divided by still water natural frequency, f_n against reduced velocity.

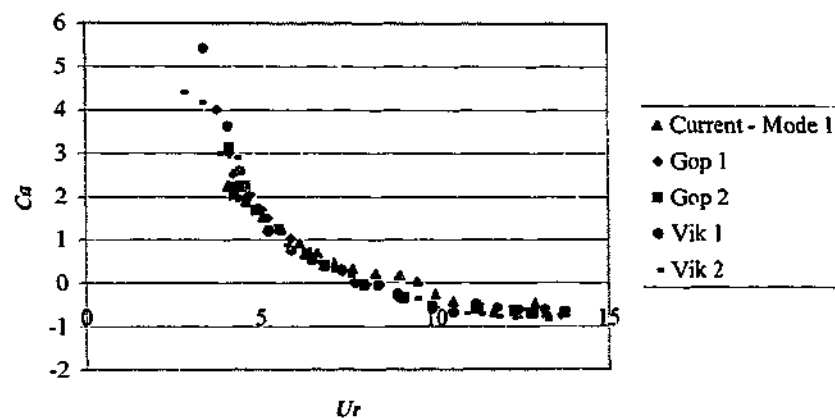


Figure 5-4 Added mass, Ca , versus reduced velocity for the current uniform flow tests and previous researcher's short rigid cylinder results.

In the literature review (Section 2.7.3), it was previously shown that the added mass was dependent on A/D for forced oscillation tests. Forced oscillation tests represent a large matrix and the added mass is shown to behave such that $Ca = f(A/D, Ur)$. Ur may also be substituted for a non-dimensional frequency term, \hat{f} . The particular case of free vibration tests represent a subset of the forced vibration tests as for each value of Ur the system converges to one A/D value, such that $Ca = f(Ur)$ only. The current results of free vibration of a long flexible cylinder in uniform flow conditions show that the results of Vikestad (1998) with $Ca = f(Ur)$ only is more widely applicable.

5.3.2.2 Mode 1 and Mode 2

The set of tests involving the least end tension provides the greatest Mode 2 response in the uniform flow testing series. As mentioned previously, the peak Mode 2 response was unable to be reached to due facility limitations for

the uniform cases. The frequency of response of both Mode 1 and Mode 2 are compared for identical tests in Figure 5-5.

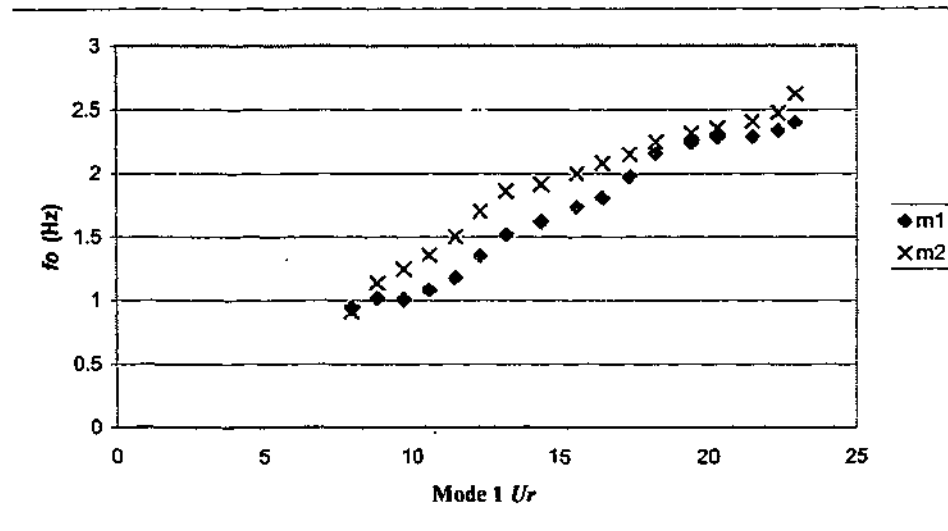


Figure 5-5 Mode 1 and Mode 2 response frequencies for identical tests.

Figure 5-6 shows the back calculated added mass coefficients based on the observed vibration frequencies, still water natural frequencies and uniform flow speed. This time identical tests, but collapsed according to their respective reduced velocities.

One interesting feature of the cross-flow response frequencies in Figure 5-5 is that Mode 1 and Mode 2 appear to be active at close to the same frequencies. Based on intuition from in-air structural vibration, one would expect Mode 2 to be active at a much higher frequency, a value that would be predicted by Equation 2.9.

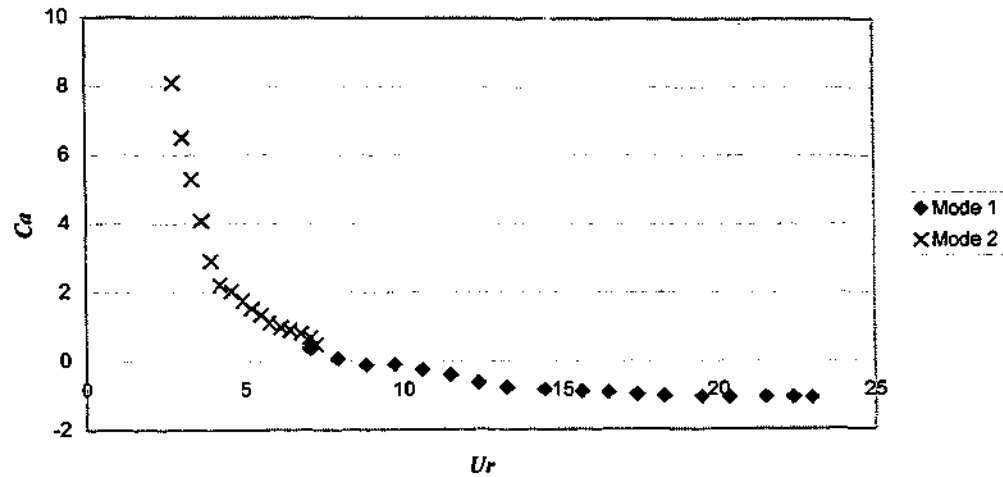


Figure 5-6 Individual added masses for Mode 1 and Mode 2 from the same set of tests.

However, plotting the modes as a function of their respective reduced velocity (based on their natural frequencies) they respond as would be predicted, as demonstrated by the curve in Figure 5-6 following the same path as in Figure 5-4. Even in the situation where one mode is dominating the response.

5.3.3. Lift Force

The set of tests involving uniform flow for the highest end tension are presented in the current section. Ring 1 is the upper half of the riser, while Ring 2 is in the lower half of the riser. For completeness, the total lift force and all associated coefficients are presented.

Firstly, example time series are shown for the riser in its peak Mode 1 lock-in region. Figure 5-7 shows the local lift force (per unit length), the lift force multiplied by local velocity and the lift force multiplied by local acceleration at the upper ring location.

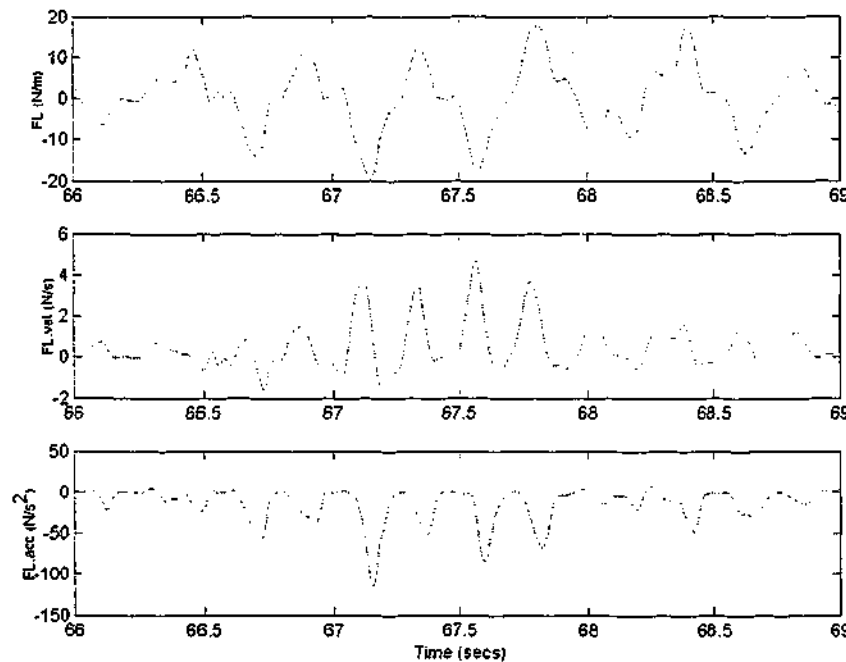


Figure 5-7 Typical times series of local lift force, lift force multiplied by local velocity and lift force multiplied by local acceleration.

The cycle averaged lift coefficients are deduced from the *rms* or mean values of these times series according to the respective procedures outlined at the beginning of the current chapter and similarly to the methods of Vikestad (1998).

The phase relationship of the lift force can be examined with a phase-plane plot as done in Figure 5-8. Several different Ur cases are presented down the figure with the lift force measured on the upper ('R1') and lower ('R2') rings on the LHS and RHS respectively. The axis scales are different for clarity of the shapes.

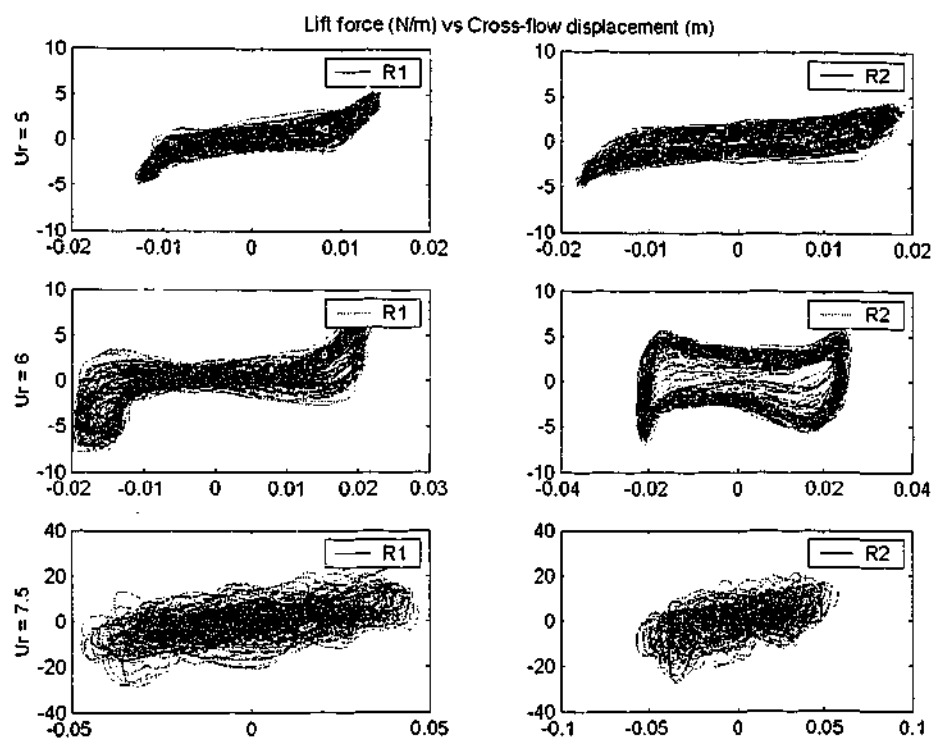


Figure 5-8 Phase-plane plot of total lift force against cross-flow displacement for a) $Ur = 5$; b) $Ur = 6$; c) $Ur = 7.5$.

An intriguing result from Figure 5-8 is that the lift force has a strong 3rd harmonic component especially noticeable in the lower Ur cases. Note also the magnitude of the lift force generally increasing with Ur . Blackburn *et al.* (2000) also presents a phase plane plot for a short rigid circular cylinder similar to

that of Figure 5-8 b) R2. Blackburn quite rightly states that the area enclosed by the average trajectory is representative of the average work transfer per motion cycle between the fluid and the cylinder. The trajectory just mentioned has the largest area enclosed of the above plots and, as will be shown in Figure 5-11, can also be determined from a maximum in C_{L_r} .

The *rms* lift force (per unit length) for both rings are shown in Figure 5-9.

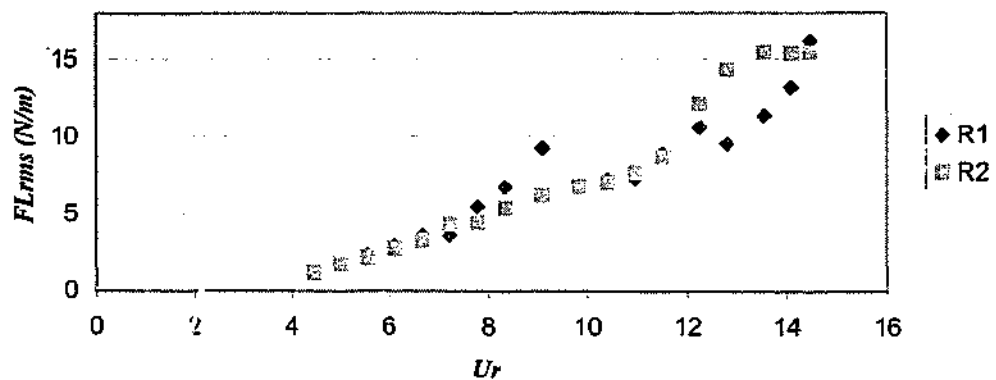


Figure 5-9 Rms lift force per unit length at both the upper and lower rings for uniform flow conditions against Mode 1 reduced velocity.

The *rms* lift force shown in Figure 5-9 covers the identical set of tests as reported in Figure 5-2, that being the entire Mode 1 lock-in region and the very beginning of Mode 2 excitation.

The total lift force coefficient, C_L , for the same tests as in Figure 5-9, is reported in

Figure 5-10. Equation 5.5 has been used to determine C_L , which makes use of the peak force, rather than the *rms* value.

As discussed at the commencement of the current chapter, the total lift force coefficient is of little use for an oscillating cylinder. Much more information is to be gained by examining the coefficients in phase with velocity and acceleration. The lift coefficients in phase with riser local cross-flow velocity and in phase with riser local cross-flow acceleration are presented for both rings in uniform flow conditions in Figure 5-11 and Figure 5-12 respectively.

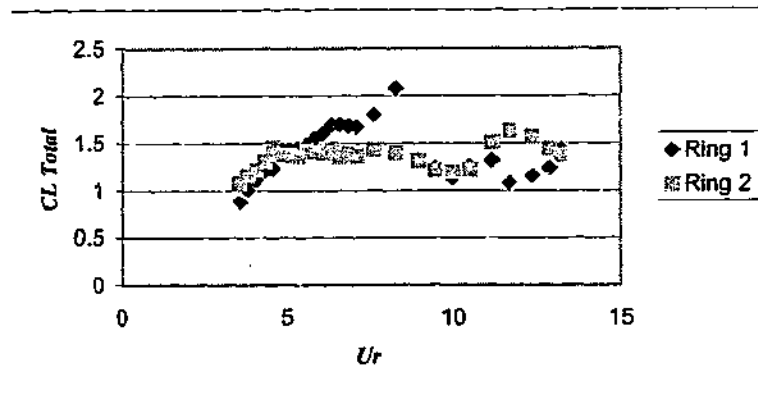


Figure 5-10 Total local lift force coefficient, C_L , against reduced velocity.

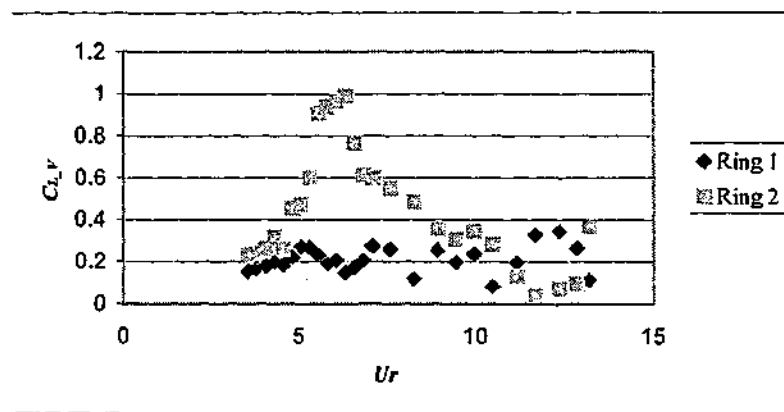


Figure 5-11 The local lift coefficients in phase with riser cross-flow velocity, C_{L_v} , against reduced velocity.

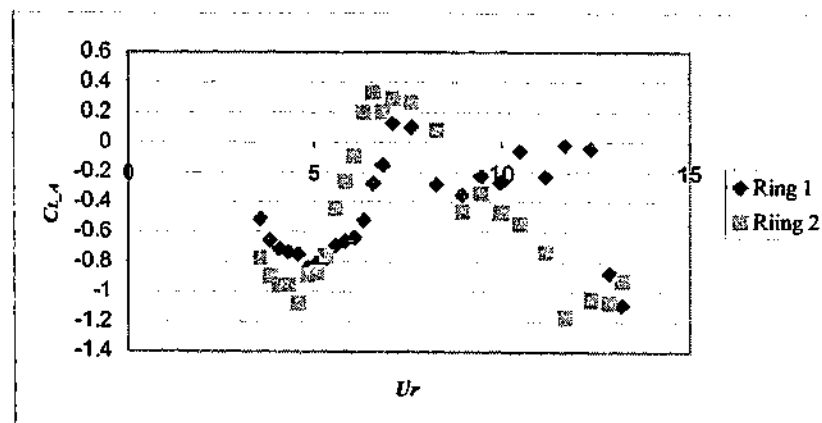


Figure 5-12 The local lift coefficients in phase with riser cross-flow acceleration, C_{L_A} , against reduced velocity.

An alternative way of presenting the lift coefficient in phase with acceleration data is as added mass coefficients. The lift coefficient data of Figure 5-12 was converted to added mass coefficients via Equation 5.8 and is shown in Figure 5-13.

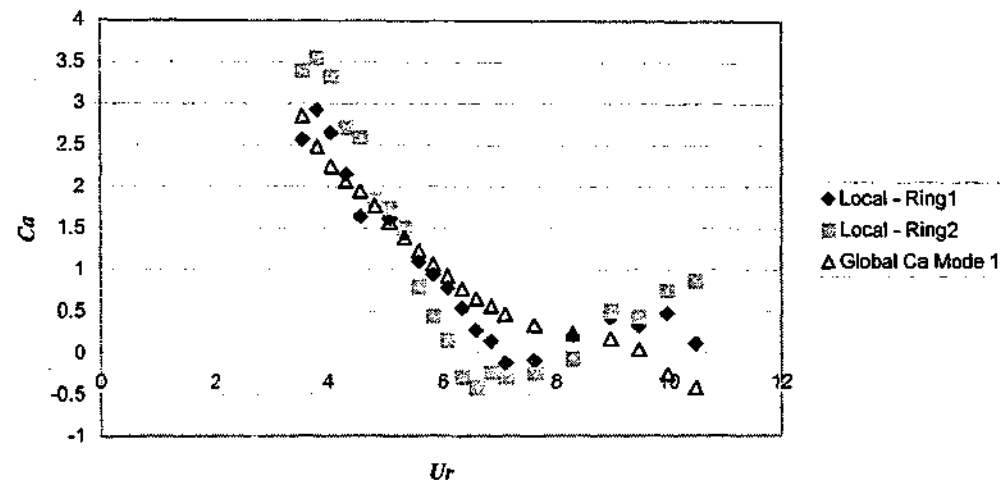


Figure 5-13 Added mass coefficients for uniform flow conditions from the local lift force measurements and the global modal response against reduced velocity.

Looking at the $Ur < 6$ Mode 1 region initially, in Figure 5-11 and Figure 5-13, the local added mass terms from the two different regions follow similar trends as a function of Ur , while the local lift coefficients in phase with velocity do not exhibit a similar trend as a function of Ur . In the range $Ur > 6$, the absence of displacement symmetry between the different regions of the riser due to the in-line motion (discussed later in this chapter) and the

beginning of Mode 2 response means there will be a loss of symmetry between the characteristics of the local coefficients from the different regions.

Figure 5-11 shows a maximum $C_{L_V} = 0.9$ recorded in the lower region. As shown by Equation 5.10 at the start of the chapter, C_{L_V} represents the power transfer *from the fluid to the riser*. The absence of any negative values of C_{L_V} in Figure 5-11 indicates for the two instrumented regions the power transfer is *from the fluid to the riser* (in these uniform flow conditions). In uniform and resonant flow conditions the power is historically assumed to be working against the action of structural damping (Section 2.7.3). The peak C_{L_V} does not coincide with the peak amplitude probably due to hydrodynamic sources of damping associated with non-resonant conditions being larger than the structural sources of damping at resonance.

The local added mass coefficients in the high Mode 1 Ur region of Figure 5-13 are shown to be increasing as a function of Ur , with Ring 1 suddenly increasing for the highest values of Ur to match that of Ring 2. The global added mass result shown in Figure 5-13 has been filtered so that it pertains only to Mode 1 while the local added mass term relates to the total local motion and can be associated with whichever mode is dominant or with a combination. For the previous reason it becomes clear as to why the local added mass rises at high Mode 1 Ur ; it has to be caused by the onset of Mode 2 vibration. The high Mode 1 Ur values in Figure 5-13 are also low Mode 2 Ur values.

5.3.4. Effects of Spacing of Natural Frequencies

The five different sets of end tension provide a different spacing of natural frequencies, as shown in Table 3-2. In Figure 5-14 the Mode 1 responses of the different cases (all in uniform flow) are collapsed onto the Mode 1 reduced velocity scale, so that we can observe any effects caused by the different spacings of the Mode 2 to Mode 1 natural frequencies. The ratios of the Mode 2 to Mode 1 natural frequencies, w_2/w_1 , are given in the key of Figure 5-14. These ratios will be the same for either in-air or still-water conditions.

Estimation of the location of the peak in Mode 2 response in Figure 5-14 can be made by multiplying the Mode 1 reduced velocity peak value by the given ratio (as the reduced velocity scales linearly with natural frequency).

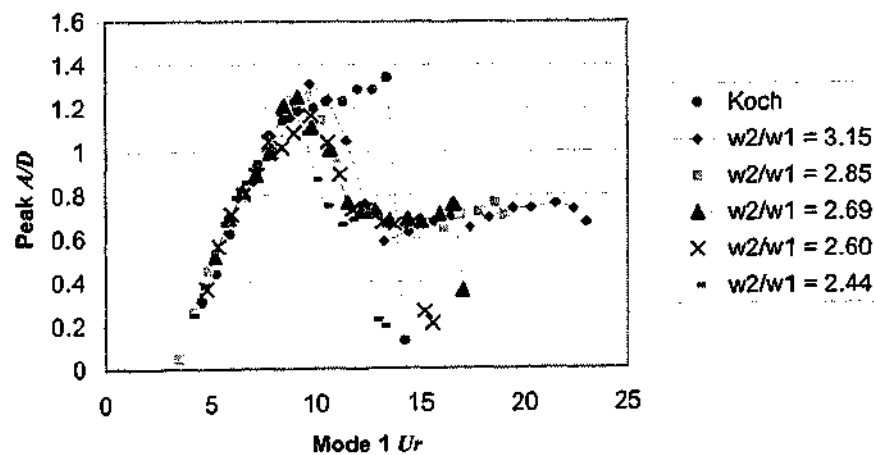


Figure 5-14 Mode 1 response as a function of reduced velocity for various Mode 2/Mode 1 natural frequency ratios.

Figure 5-14 shows that the effect of different spacing of natural frequencies is most apparent at and after the peak in Mode 1 response. A trend is observed, as a function of U_r , that the peak response and then the immediate drop off occur at higher U_r values for greater spacing to the next natural frequency. There may also be a higher maximum of the peak value in Mode 1 for a greater spacing, although this is not as conclusive as the previous trend. Also shown in Figure 5-14 is Koch's data (from Figure 5-2). Unfortunately Koch's Mode 2 to Mode 1 ratio of natural frequencies was not reported. However if one were to speculate that Koch's tests did not include any end tensioning mechanisms then the Mode 2 to Mode 1 frequency ratio would be equal to 4 (the Mode 2 to Mode 1 natural frequency ratio for a beam with no end tension is always equal to 4). If Koch's ratio was 4 then it supports the hypothesis that the spacing of natural frequencies is crucial to the location of peak response.

5.3.5. Hysteresis

During preliminary testing a hysteresis in the response was discovered. The response, consisting of both Mode 1 and Mode 2 time series, was observed to have two distinct levels dependent on the order in which the tests were conducted and the greatest variation between these levels occurred in the non-resonant reduced velocity region between Mode 1 and Mode 2. Upon further examination it was found that greater Mode 2 response was obtained if the model riser had previously been closer to the Mode 2 peak response. In the region showing the greatest response differences (the non-resonant

reduced
attribu
for the
test is
at lea
secon
a sud
decre
comm
tensio

Fig

reduced velocity region between Mode 1 and Mode 2) the hysteresis is mainly attributed to the Mode 2 response. In Figure 5-15 the hysteresis is highlighted for three different cases of $Ur_{n=2} = 3$. The history prior to commencement of test is the only difference. In Figure 5-15 a) the riser remains at the same Ur for at least 3 minutes prior to testing. In Figure 5-15 b) the riser is at $Ur \gg 3$, 2 seconds prior to commencement of test; the Ur change was obtained through a sudden increase in end tension, which shifts f_n to a higher value and thus decreases Ur . In Figure 5-15 c) the riser is at $Ur \ll 3$, 2 seconds prior to commencement of test; the Ur change was obtained through a decreased end tension.

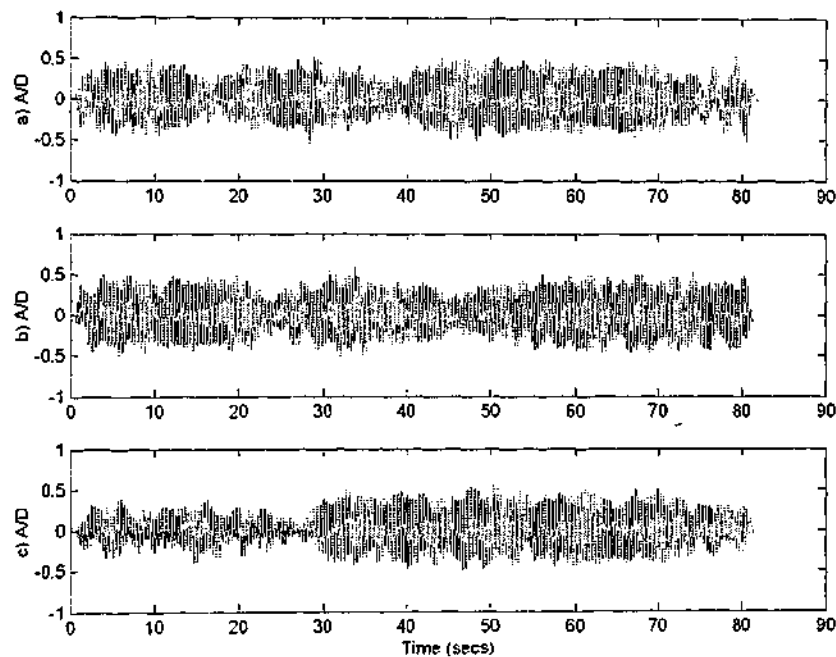


Figure 5-15 Mode 2 time series at $Ur_{n=2} = 3$ for previous Ur value of a) $Ur = 3$;

b) $Ur \gg 3$, c) $Ur \ll 3$.

The time series in Figure 5-15 show that for the selected $Ur_{n=2} = 3$ case, the energy in Mode 2 takes approximately 30 seconds to build up (graph c) to the level it experiences in a steady state situation (at least 3 minutes as shown in graph a). While Figure 5-15 b) shows that if the Mode 2 energy was already present in the riser, as it had previously been closer to its peak Mode 2 Ur value, then there is no apparent time lag in it reaching its longer term equilibrium value.

The time it takes the riser to distribute energy into its Mode 2, or any other Mode for that matter, could be a function of the number of oscillations. No conclusive results have been drawn, however after discovery of the hysteresis effect, a longer time window prior to commencement of data logging was introduced into the experimental method (approximately 2 minutes).

5.4. IN-LINE RESPONSE

In this section a detailed examination is made of the in-line response of the flexible cylinder throughout the band of cross-flow response covering all of Mode 1 and the onset of Mode 2. The response of the riser in the in-line direction is best examined in the uniform flow cases with only one Strouhal frequency. A varying spatial velocity profile may contribute more than one Strouhal frequency and complicate the analysis.

5.4.1. Mode 1 In-line

The initial in-line instability reported in the literature (Figure 2-13) occurred in the range $1.5 < Ur < 3.5$. Figure 5-16 shows the results of a separate set of uniform flow tests conducted with the aim exploring the in-line Mode 1 response in detail. Mode 1 in-line response is the only in-line response that is uncontaminated by higher cross-flow harmonics. Unfortunately, due to the very low levels of model scale acceleration the fluctuating voltage signals were very weak, even with a gain of 1,000. For instance, the accelerometer with the largest fluctuating signal from the lowest flow speed tests consisted of only three voltage steps. For the previously stated reason, the low flow speed tests reported contain large errors and should be used as a guide to the qualitative trends rather than as an accurate quantification of response. The figure shows Mode 1 in-line and Mode 1 cross-flow response as a function of reduced velocity.

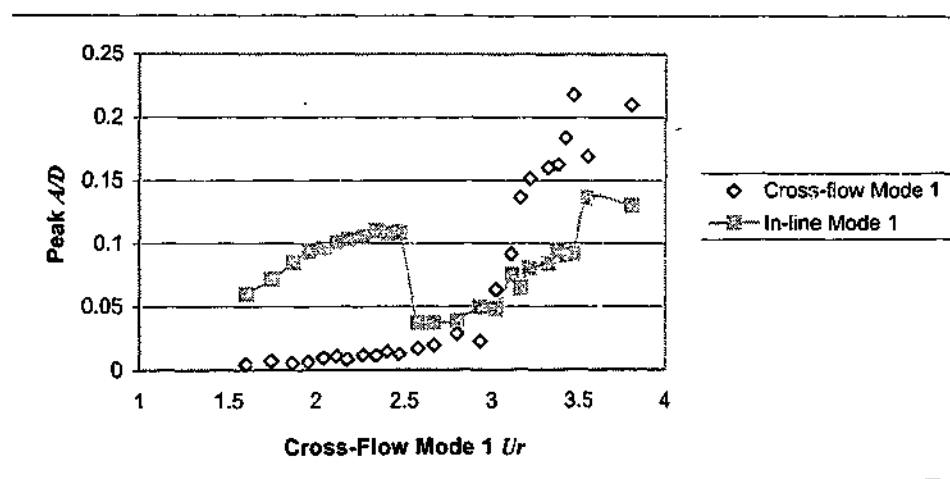


Figure 5-16 Qualitative low Ur Mode 1 in-line response shown as a function of Mode 1 cross-flow reduced velocity.

The in-line response of Mode 1 shown in Figure 5-16 confirms the existence of in-line only response for a riser model with sinusoidal mode shapes at low Ur prior to the dominant cross-flow response at higher Ur .

5.4.2. Higher In-line Modes

Of the present tests, the set of uniform flow with the highest tension allows examination of both the in-line and cross-flow responses and their coupling in the greatest detail. The response amplitude of Mode 1 cross-flow is plotted together with Mode 1 and Mode 2 in-line in Figure 5-17.

An obvious result of Figure 5-17 is that the in-line response takes the form of Mode 1, while the Mode 1 cross-flow response is dominant.

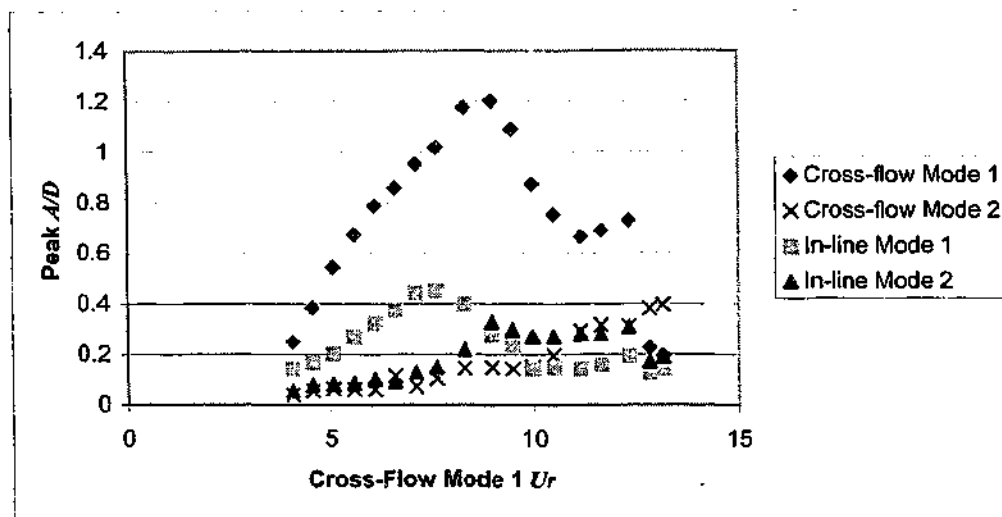


Figure 5-17 Mode 1 and Mode 2 in-line response together with Mode 1 cross-flow response.

Figure 5-18 shows the modal time series and modal power spectra for Mode 1 Cross-flow and In-line and Mode 2 Cross-flow and In-line for a case of $Ur = 6$.

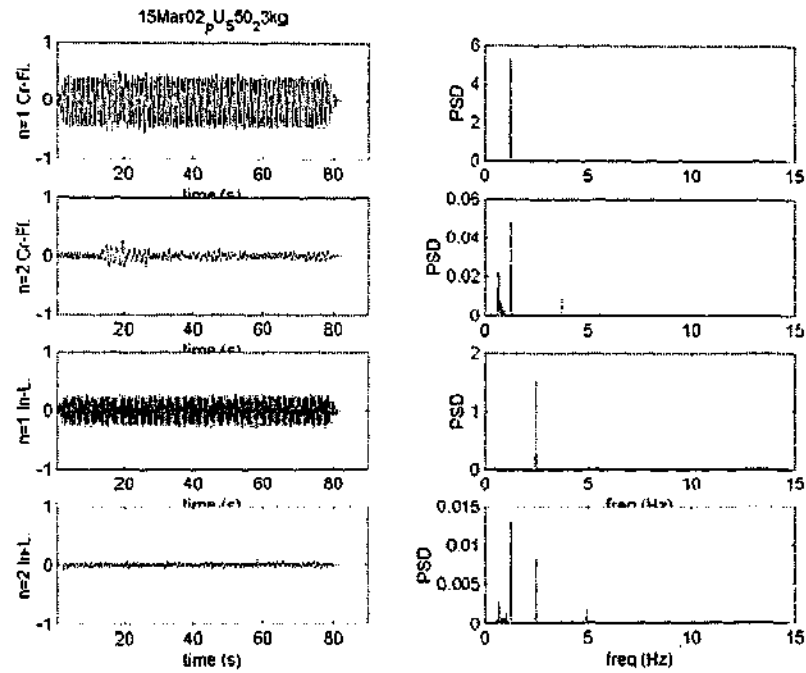


Figure 5-18 Modal participation time series and power spectra for cross-flow Mode 1 and 2 and in-line Mode 1 and 2.

In general, in-line response is expected to occur at twice the cross-flow Strouhal frequency and examination of the power spectra presented in Figure 5-18 certainly reveals the same here. For a rigid cylinder the vortex shedding process alternates vortices on opposite cross-flow sides while the vortices

only ever fluctuate about the downstream side of the cylinder, thus imposing two in-line force fluctuations for every one full transverse force fluctuation. Hereafter the frequency of twice Mode 1 cross-flow will be referred to as the in-line 'driving frequency'. The intriguing result of Figure 5-17 is the persistence of Mode 1 in-line response while the frequency of excitation would favour Mode 2 in-line. After $Ur_{n=1} = 7.5$ there is a switching of in-line response such that Mode 2 in-line becomes active rather than Mode 1 in-line. The switch in in-line Modal response coincides with the cross-flow response beginning to decline after its maximum amplitude.

Investigation of the respective frequency of Mode 1 in-line and Mode 2 in-line response can be done globally. Figure 5-19 has the centre of energy of oscillation frequency for Mode 1 in-line, Mode 2 in-line and a comparison against the 'driving frequency' of twice Mode 1 cross-flow.

Collection of Experiments (U.S.)
Fig
Fig
exa
of
Th
am
Th
na
exc
exc

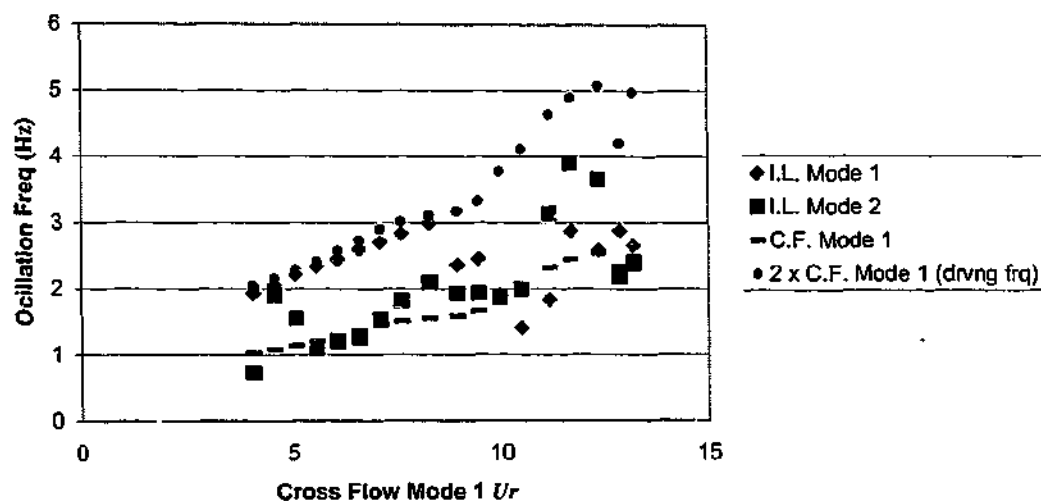


Figure 5-19 Oscillation frequencies of in-line Mode 1 and 2 as well as the driving frequency.

Figure 5-19 shows that the previous examination of one of the spectra in Figure 5-18 correctly identifies that Mode 1 in-line oscillation frequency is exactly the *driving frequency* (twice Mode 1 cross-flow frequency) in the region of $U_{r_{n=1}} < 8$. Mode 2 in-line response frequency steadily rises after $U_{r_{n=1}} = 6.5$. The region where Mode 2 in-line frequency rises is also where Mode 2 in-line amplitude increases above a previous straight line trend (Figure 5-17).

The persistence of Mode 1 in-line response at frequency values far above its natural frequency is contrary to what one would expect. The cross-flow excitation must be responsible for this effect. For the in-line modal shape to be excited at such high frequency values requires negative added mass values

(simply meaning the inertia of the vortices add to the acceleration direction). Figure 5-20 shows the back calculated in-line added mass values based on the in-line response frequencies and the Mode 1 natural frequency (according to Equation 4.1) corresponding to the lower Ur region of Figure 5-19. The added mass values are found to be well below that which would be predicted for standard cross-flow motion.

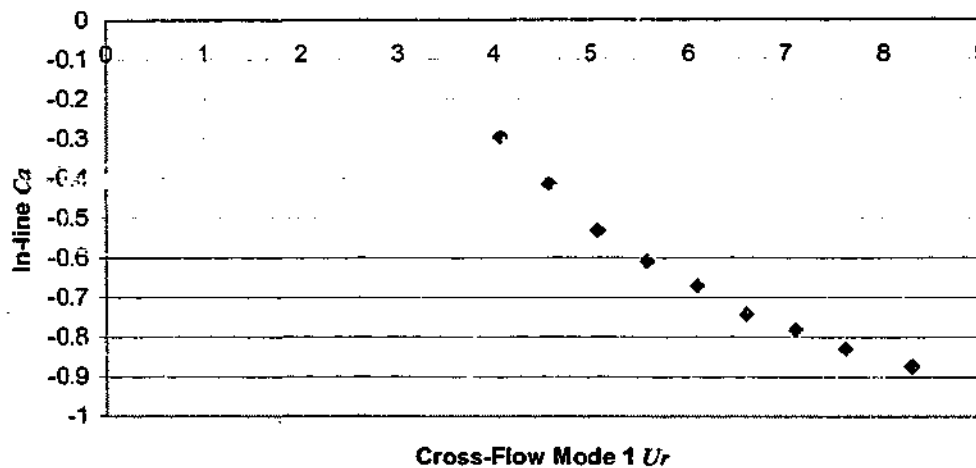


Figure 5-20 In-line added mass value for the persistence of Mode 1.

The Mode 1 cross-flow response requires its largest amplitude to be at halfway along the riser length. Previously Toebes (1969) found that the axial correlation length of vortex shedding is a function of the amplitude of motion (Figure 2-12). Toebes found that the greater the amplitude of motion, the longer the correlation length of the vortex shedding. Applying Toebes findings here it could be said that at the anti-node of the Mode 1 cross-flow response there is the strongest vortex correlation due to the largest amplitude

of motion. An in-line Mode 2 response would require that the half way point of the riser be a node and therefore the vortices have a different phase of shedding on one half of the riser compared to the other half due to the asymmetric motion. The strong vortex correlation in the halfway region due to Mode 1 cross-flow must therefore override any tendency for the riser structural forces to adopt a Mode 2 in-line vibration and hence it persists with Mode 1 in-line response.

The trajectories of the riser reveal some of the behavior. Figure 5-21 shows the trajectory of the riser at the midpoint along its axis for three different reduced velocity cases. Case a) is $Ur_{n=1} = 4$; case b) is $Ur_{n=1} = 6$ and case c) is $Ur_{n=1} = 9$. Note that the scales between the cases are different.

e 1.

to be at
the axial
of motion
tion, the
Toebes
cross-flow
amplitude

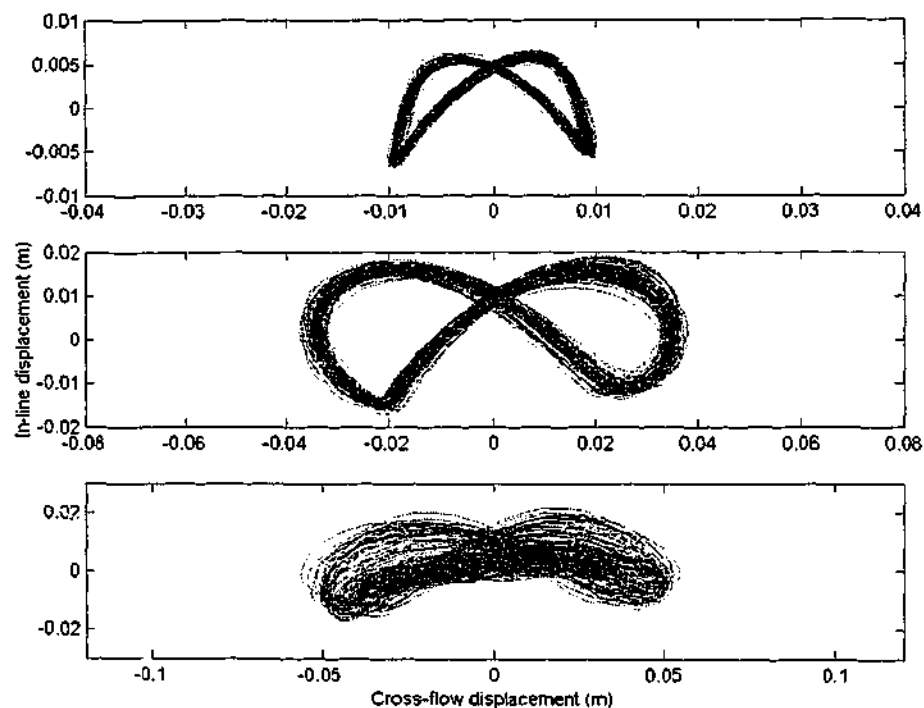


Figure 5-21 Uniform flow riser trajectories for a) $Ur = 4$; b) $Ur = 6$; c) $Ur = 9$.

The first two cases in Figure 5-21 indicate a 2:1 in-line to transverse vibration pattern while the final case is not conclusive but is approximately the same. Note that the phase of in-line response to cross-flow response changes with Ur . Examination using modal analysis of the separate contributions to the response in Figure 5-21 c) show that the trajectories become less defined due to the equal presence of both Mode 1 and Mode 2 in-line response.

5.5. SUMMARY OF CHAPTER

The derivations of the coefficients that are fundamental to VIV were presented firstly. The response amplitude and added mass as a function of reduced velocity for uniform flow conditions was next presented. Results showed while the added mass has excellent agreement with short rigid cylinder cases, the location of peak amplitude does not agree well. The effects of in-line response were also examined. In-line response was re-affirmed to occur in its own right and in-line response was also seen to be affected by cross-flow response.

= 9.

tion

me.

with

the

due

6. 2-SLAB FLOW RESULTS

The following chapter presents results of experiments where competition effects between different modes were examined. The chapter starts with a brief introduction then explains the variables examined. The results of the different cases are next presented. Finally VIV prediction methods are discussed in light of the new results.

6.1. VARIABLE EXAMINED

Figure 6-1 shows a conceptual sketch of the types of flow profiles considered in the current chapter, where Mode 1 is favoured to respond over one region of the riser, while Mode 2 is favoured to response over the rest of the riser. l^* is the percentage of length of riser exposed to Mode 2 favoured region,

$$l^* = \frac{l_2}{l_{total}}, \quad (6.1)$$

where l_2 is the actual length of riser exposed to Mode 2 favoured region (the faster region) and l_{total} is the total length of riser.

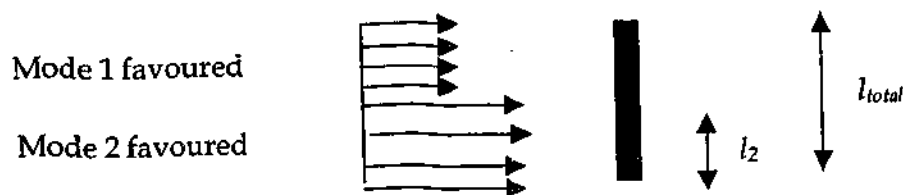


Figure 6-1 Conceptual sketch of a typical profile considered in Chapter 6.

The experiments reported in the current chapter were previously described in Section 3.2.1. The variables under examination are;

- I^* , the power in length ratio of Mode 1 to Mode 2
- $Ur_{n=2}$, Mode 2 reduced velocity.
- $w2/w1$, the ratio of still water natural frequencies.

6.2. AMPLITUDE OF RESPONSE

A typical time series of Mode 1 and Mode 2 response, along with their respective spectra, for a competing modes test (both modes resonant) is shown in Figure 6-2.

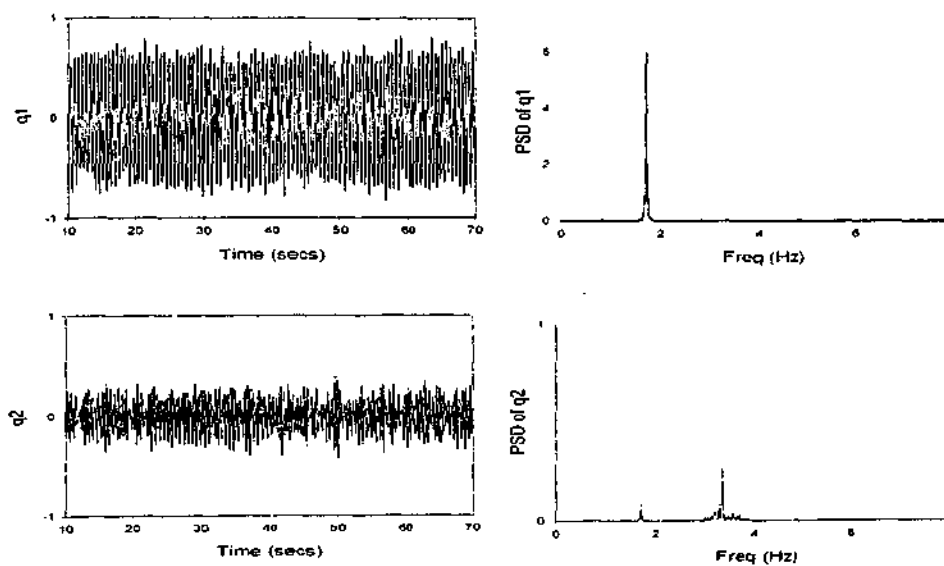


Figure 6-2 Time series of Mode 1 and 2 for a typical competing modes test.

Each mode's time series was briefly examined for each individual test. Intermittency or switching between the modes was found to be very regular (when it occurred) such that the standard deviation of each respective mode's time series formed a suitably accurate quantification of the response. In Figure 6-2 Mode 1 amplitude is shown to be greater than Mode 2, while its frequency of response is similar to what one would expect in-air; Mode 2 being substantially higher than Mode 1. Qualitatively, the results previously mentioned are reflective of an approximately zero added mass effect on each mode. The added mass is typically zero at $Ur = 8$ for simple VIV cases as shown in Figure 5-4. The multimodal case shown in Figure 6-2 is very different to the measurements one would make of modal responses in uniform flow conditions (e.g. Figure 5-5). In a uniform flow case two separate modes cannot be experiencing lock-in at the same time (for low mode numbers) and thus their added masses are very different (based on their respective Ur values from Figure 5-4). The very different added masses will cause their actual response frequencies to be closer to each other than in the simultaneously resonant case of Figure 6-2. The previously mentioned effect is the main difference between a uniform flow and a 2-Slab flow.

Thre

1 an

• F

• F

All

Mod

Fig

of 4

is s

Three sets of tests are first presented to show the amplitude response of Mode 1 and 2 together with the ratio of Mode 2 divided by Mode 1 as a function of:

- Power-in length and
- Reduced velocity.

All results presented, unless otherwise specified, arbitrarily reference the Mode 2 reduced velocity for the faster region.

Figure 6-3 shows the one set of tests pertaining to a Mode 2 power-in length of 40 %. Mode 1 response, Mode 2 response and (Mode 2 / Mode 1) response is shown as a function of Mode 2 reduced velocity for the faster region.

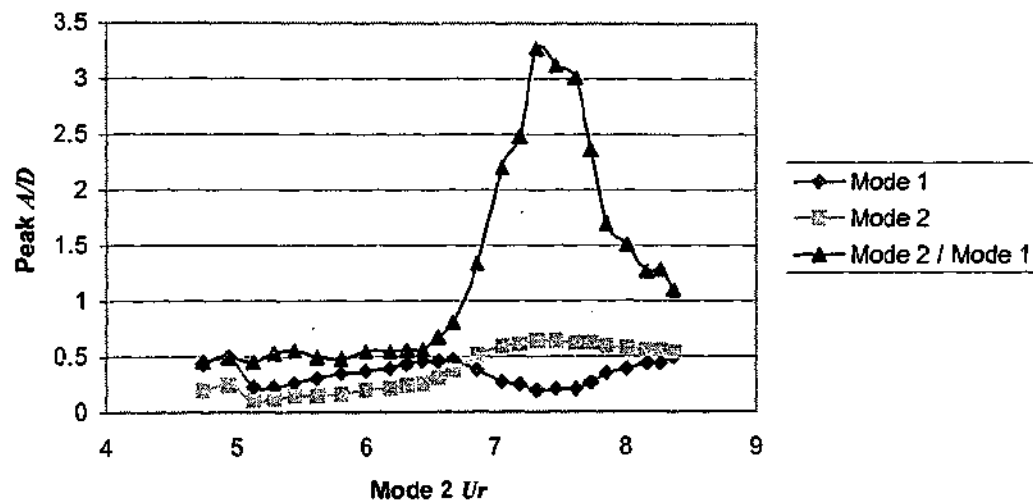


Figure 6-3 Modal response vs reduced velocity for a power-in length of 40 % shown as a) Mode 1; b) Mode 2; c) Mode 2 divided by Mode 1 for each individual test.

Figure 6-4 and Figure 6-5 show the Modal amplitude results of tests with power-in lengths of 35% and 30% respectively. In all these initial figures, the end tension value is equal to 192 N. The dependence of the ratio of natural frequencies are examined later in Section 6.5. For the immediate results, the ratios of flow velocities and still water natural frequencies remain fixed both at 2.4 respectively. In Section 6.5 the ratio of natural frequencies is different to the flow velocity ratio.

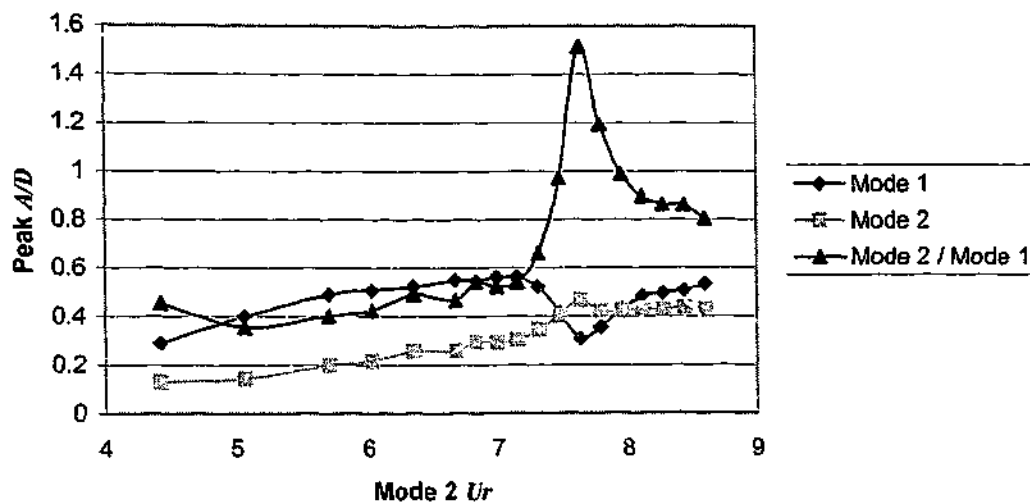


Figure 6-4 Modal response vs reduced velocity for a power-in length of 35 % shown as a) Mode 1; b) Mode 2; c) Mode 2 divided by Mode 1 for each individual test.

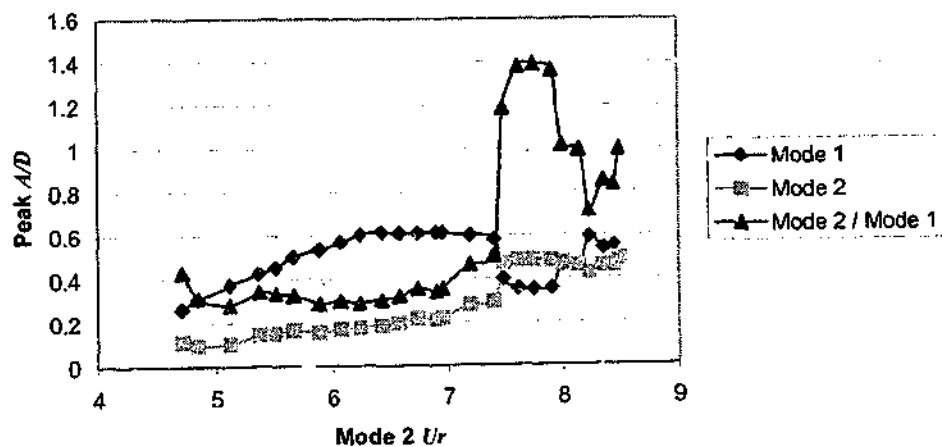


Figure 6-5 Modal response vs reduced velocity for a power-in length of 30 % shown as a) Mode 1; b) Mode 2; c) Mode 2 divided by Mode 1 for each individual test.

From the previous figures (Figure 6-3 to Figure 6-5), the following general observations can be made:

1. Mode 1 is observed to dominate the response for reduced velocities less than the simultaneous resonant condition ($Ur < 7$).
2. The amplitude of Mode 2 response increases as a function of Ur in the range $7 < Ur < 8$ while simultaneously Mode 1 response decreases.
3. The ratio of Mode 2 to Mode 1 provides an estimate of the dominance of Mode 2 in the range of Ur where Mode 2 peak amplitude occurs. It is observed that with greater Mode 2 power-in length, there is greater Mode 2 dominance in the response.

The standard deviation that was used to quantify the response in Figure 6-3 to Figure 6-5, provides a normalised measure of the variance of a modal amplitude from the zero mean. The kurtosis, as shown in Section 2.7.2, classifies the response more clearly as either a multimode mixture or single mode lock-in. Mode 1 and Mode 2 kurtosis are shown in Figure 6-6. The set of tests shown in Figure 6-6 are the same as that shown in Figure 6-3 to Figure 6-5. Each kurtosis value has been calculated by finding the mean values of the statistical parameters from the whole of the given test.

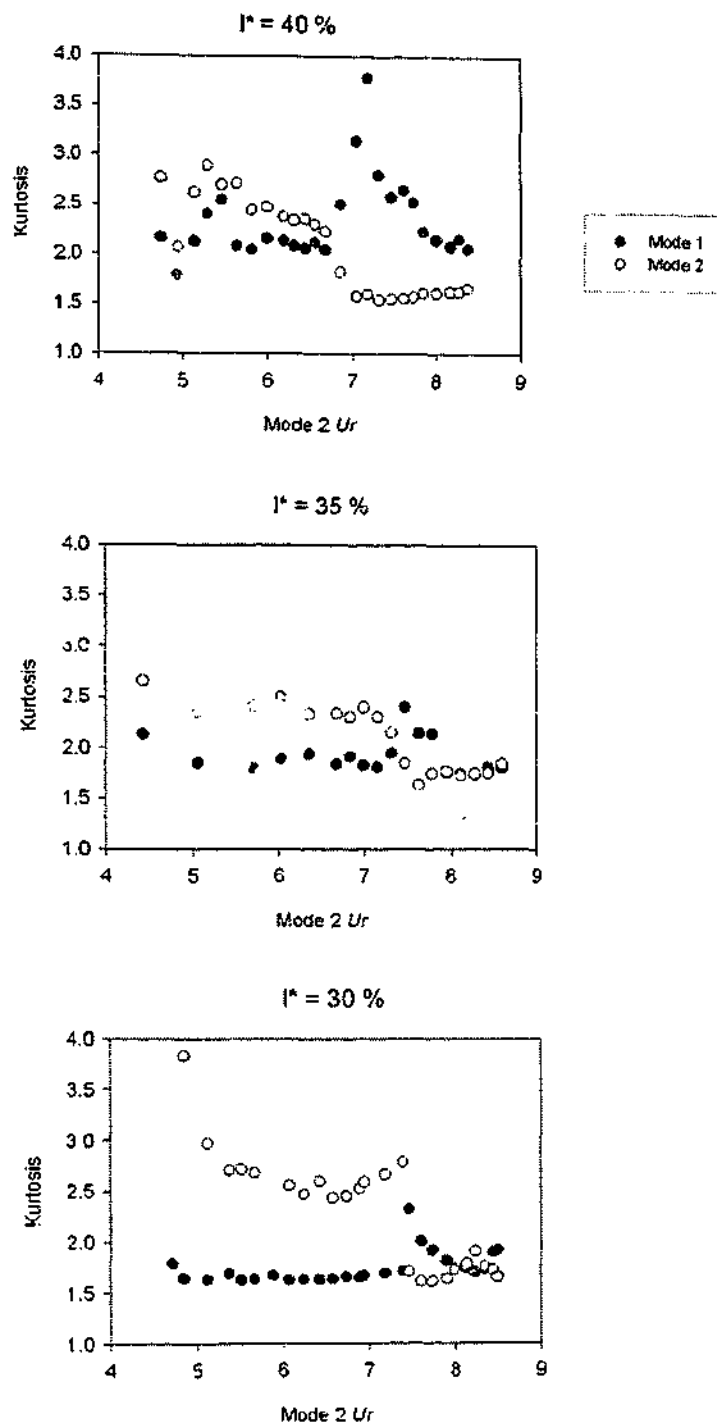


Figure 6-6 Kurtosis of Mode 1 and Mode 2 amplitude response as a function of Mode 2 reduced velocity for different I^* .

In all cases of Mode 2 in Figure 6-6 the kurtosis falls to the *lock-in* value ($K_i \approx 1.5$) at the same value of Ur that the Mode 2 amplitude begins to dominate the response. Whereas Mode 1 exhibits a lock-in type response in the Ur range lower than the Mode 2 dominance range. Interestingly, the K value of Mode 1 in the lower Ur region, has higher values for the cases with greater Mode 2 power-in length. The Mode 1 amplitude is therefore more *noisy* (Gaussian) with cases of greater Mode 2 power-in length. Another feature of Mode 1 that can be observed is the large peaks that coincide with Mode 2 dominating response. The cases of large values of K in Mode 1 indicate the modal amplitude has lost its steady sinusoidal response form.

To explore the effect of power-in length on each mode's amplitude, the various modes were plotted individually in Figure 6-7. The amplitude response has been calculated for the first four normal modes in both the in-line and cross-flow direction, however, only the first two cross-flow modes and the first three in-line modes and are shown in Figure 6-7 due to very small amplitude response of the others over the entire testing range.

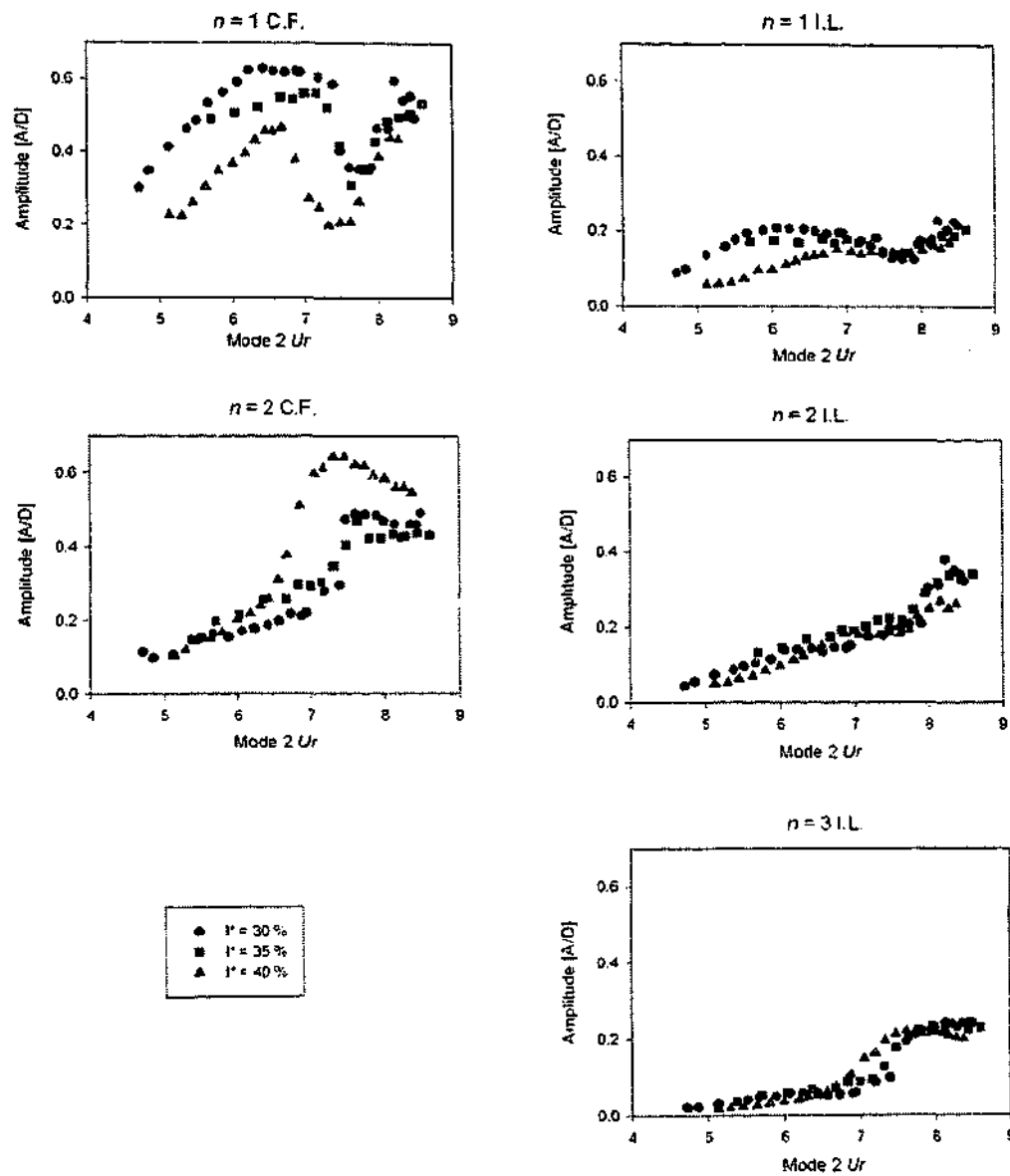


Figure 6-7 Amplitude of response against Mode 2 reduced velocity for each individual mode and each power in length (shown in legend). Cross-flow Mode 1 and 2 are on the L.H.S. while in-line Mode 1, 2 and 3 are on the R.H.S.

Figure 6-7 shows that both the cross-flow responses are affected most in the peak regions by power-in length, with increases in the Mode 2 power-in length causing both a higher Mode 2 amplitude and smaller Mode 1 amplitude. In-line response is commented on in later sections.

6.3. FREQUENCY OF RESPONSE

The frequency of response of each mode is shown in Figure 6-8 for the set of tests with lowest power-in value, $I^* = 30\%$. The values of center of energy for the response of each mode are calculated as previously described in Section 5.3.2 and are plotted all on the one plot as a function of Mode 2 Ur in Figure 6-8. As done previously, only the first two cross-flow and the first three in-line modes are shown due to the minimal response of the others.

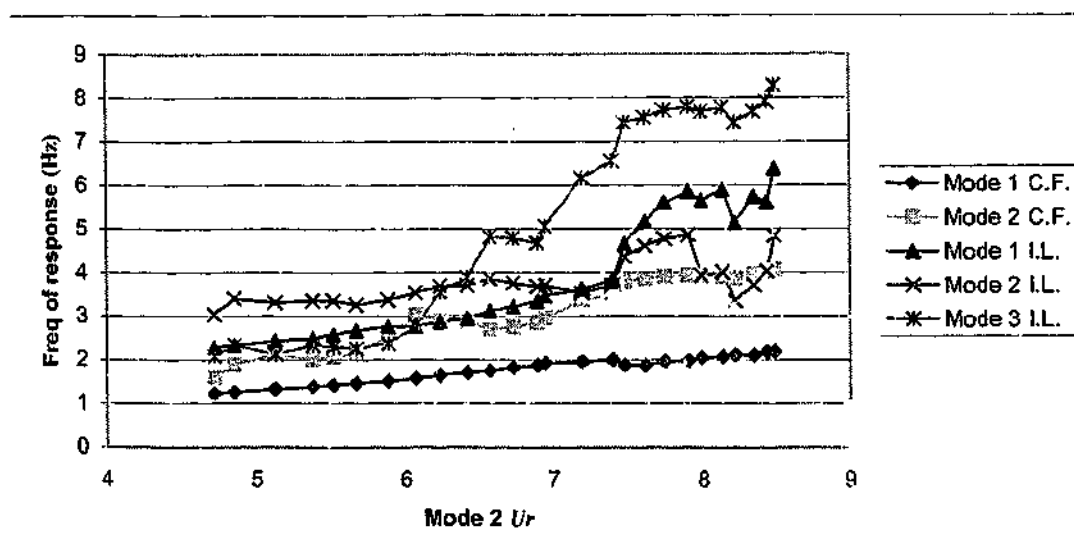


Figure 6-8 Central response frequency for each mode as a function of reduced velocity.

The Mode 3 in-line response frequency, as shown in Figure 6-8, undergoes a substantial increase as a function of reduced velocity in the region just prior to Mode 2 amplitude dominance (previously shown to be $Ur = 7.5$). The frequency rises to a value of exactly double the Mode 2 cross-flow vibration frequency. Also, Mode 2 cross-flow frequency can be seen to actually fall to a value less than Mode 2 in-line.

To investigate any power-in length effects on the frequency of response, all the individual modes are plotted with each power-in length case in Figure 6-9.

de 1 C.F.
de 2 C.F.
de 1 I.L.
de 2 I.L.
de 3 I.L.

of

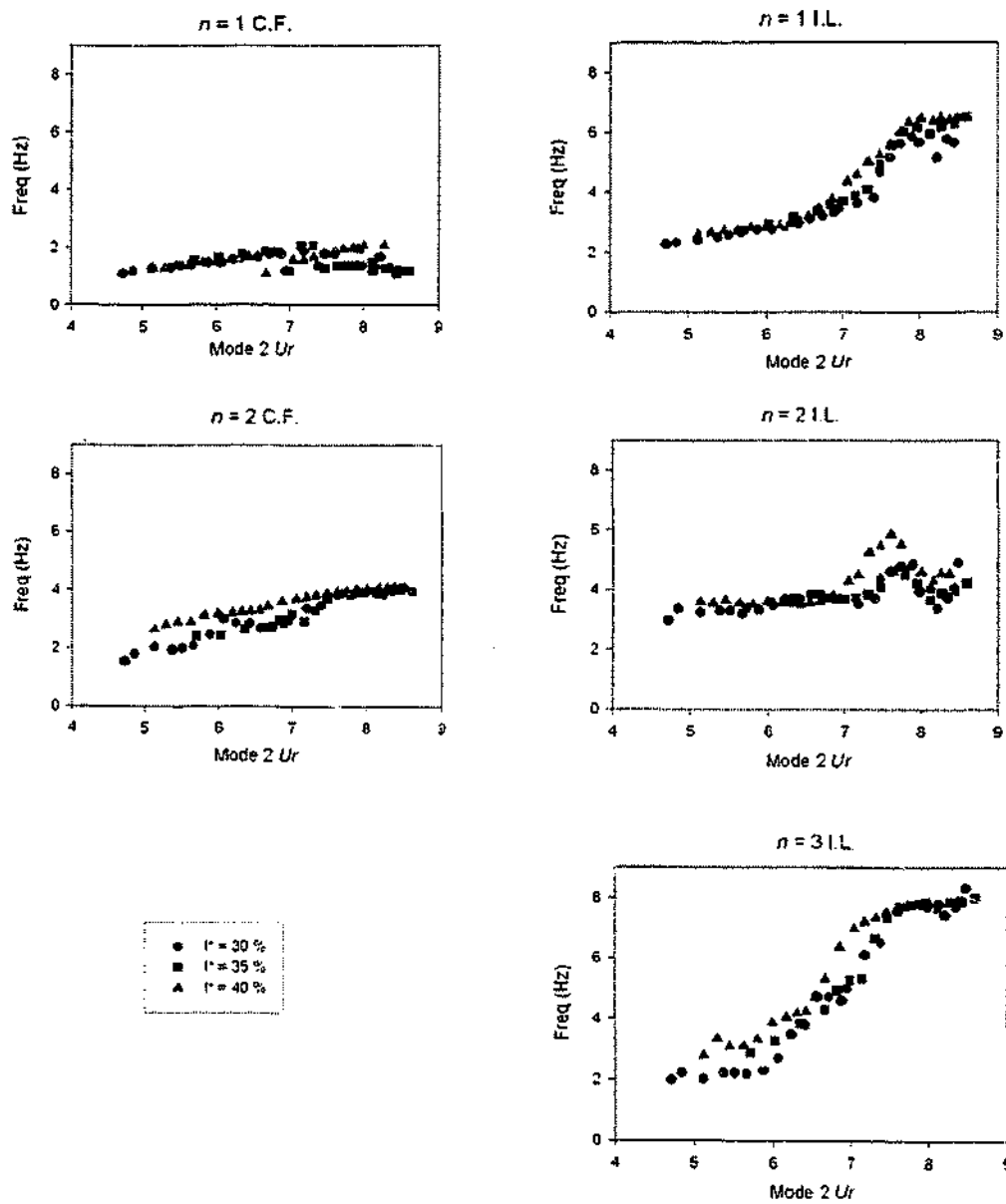


Figure 6-9 Frequency of response against Mode 2 reduced velocity for each individual mode and each power in length (shown in legend). Cross-flow Mode 1 and 2 are on the L.H.S. while in-line Mode 1, 2 and 3 are on the R.H.S.

The frequencies reported in Figure 6-9 show a tendency for the highest power-in length too cause an increase in the cross-flow modal vibration frequency. Also a general comment can be made on the behaviour of Mode 2 in-line response being different to Mode 1 and 3 in-line. Just as the amplitudes are different, so to are the frequencies of response. Mode 2 in-line seems to be almost independent of reduced velocity except for $Ur > 7.5$. While Mode 1 in-line frequency rises as a function of Ur and Mode 3 in-line rises many multiples in the range shown.

The global frequency of response can also be interpreted as an added mass. Equation 4.1 is again used to calculate the global added mass of each mode based on the individual modes oscillation frequency. The vibration frequency of each mode is calculated from the center of energy of the power spectra (as described in Section 5.3.2). The results presented in Figure 6-10 are produced from the power spectra of the modal participation time series for each mode individually.

Figure 6-10 shows the global added mass of the cross-flow modes only as a function of their respective reduced velocity and power-in length. The results are collapsed onto the one plot in Figure 6-10 by determining the reduced velocity for each mode.

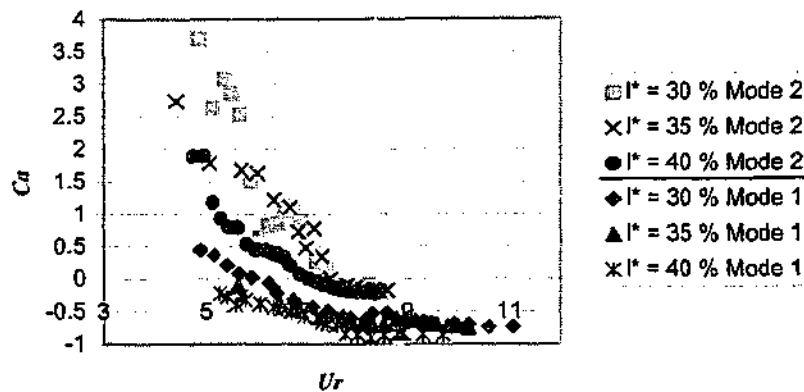


Figure 6-10 Global cross-flow added mass (based purely on response frequency) of each mode as a function of each mode's reduced velocity for various values of l^* .

The global added mass values for each mode in Figure 6-10 show a clear separation based on being either Mode 1 or Mode 2. In the middle to higher U_r region shown, the Mode 1 added mass values compared to the Mode 2 values, are about 0.5 less. Also apparent is large scatter in the Mode 2 values at low U_r . The accuracy of determining the Mode 2 values decreases in the low U_r region as the response (as obvious from Figure 6-3 to Figure 6-5) is very small and the Mode 2 spectrum becomes more susceptible to contamination from harmonics of the Mode 1 response. The dependency on l^* is also apparent, with a lower added mass for a higher power-in length. The previous comment directly compares to the higher vibration frequencies shown in Figure 6-9, higher actual vibration frequencies correspond to a smaller added mass. If the differences between the two curves are assumed small enough then it may be more generally said that each mode's added

mass can be approximated by using its *resonant region* reduced velocity value such that application of the basic curve in Figure 5-4 is valid.

6.4. CROSS-FLOW FORCE

Measurements of the cross-flow force were made and processed as described in Section 5.3.3 for two locations on the riser; one in the slower flow region corresponding to Mode 1 and one in the faster flow region corresponding to Mode 2. The cross-flow force at each location is split into two much more useful components, the force in phase with velocity and the force in phase with acceleration. Cycle averaged coefficients are deduced and presented in this section.

Due to the multi-frequency forcing and multi-modal response nature of the riser, there exist many different components of both the force and the motion for a single test. Due to the previously mentioned reason, another section in the results has been included which involves filtering to examine the effect of the two different Strouhal frequencies (from slower flow and faster flow regions).

Low pass (lp) and high pass (hp) filtered results at each pressure reading ring for each test were obtained with an automatic procedure developed in MATLAB and described below for a typical single test:

- The power spectra of the modal participation time series under investigation were determined.
- The center of power of the Mode 1 and Mode 2 cross-flow spectra were evaluated.
- The frequency value midway between the Mode 1 and Mode 2 centre's of power was calculated and called the *splitting frequency*.
- All the original time series variables (F_L , \ddot{y} , \dot{y} , y) were split into two separate time series at the *splitting frequency* by high pass filtering (hp) and low pass (lp) filtering. The filtering was realized with the aid of a 3 pole IIR Butterworth filter that was phase invariant with frequency.
- Cycle averaged coefficients were determined at each pressure transducer ring by the various combinations of only the lp time series or only the hp time series.

The characteristics pertaining to Mode 1 and Mode 2 response can be uniquely identified for the model riser at each pressure transducer ring (one of which is in the slower region, the other in the faster). The lower frequency characteristics pertain to Mode 1 and the higher frequency characteristics pertain to Mode 2.

In summary, the information from the cross-flow force is combined with the riser response to determine lift coefficients in phase with velocity and in phase with acceleration. Added masses are deducted from the previous

information as well. The various coefficients are then presented in a manner comparable to Vikestad (1998) with the results plotted as follows:

1. Average coefficients from unfiltered time series
2. Filtered coefficients producing Mode 1 and Mode 2 coefficients for both the slower and faster flow regions.

The validity of the average coefficients in (1, above) deteriorates as the time series from which they are formed becomes multi-frequency based. The multi-frequency behaviour is best examined using the filtered coefficients approach in (2, above). The filtering section is carried out differently to Vikestad (1998) who bandpass filtered narrowly on the Strouhal frequency to present 'VIV frequency results' and the remaining time series was presented as values 'for the excitation frequency'. The division through low pass and high pass filtering for the current results is carried out as there are two 'VIV frequencies'.

6.4.1. Forces and Coefficients from Original Time Series

The first set of data shows the typical behaviour of the lift coefficient (average) in phase with cross-flow cylinder velocity, C_{L_V} . Recall from Equation 5.10 that C_{L_V} represents a coefficient of power transfer and provides a simplistic way to reveal the fluid-structure interaction. Figure 6-11 presents

values of C_{L_V} found from the tests previously shown in Figure 6-7 and Figure 6-9. The two values of C_{L_V} correspond to one from the region where Mode 1 is favoured (Ring 1 in the slower region) and the other from the region where Mode 2 is favoured (Ring 2 in the faster region). Each C_{L_V} value is plotted against the Mode 2 reduced velocity to form a basis of comparison.

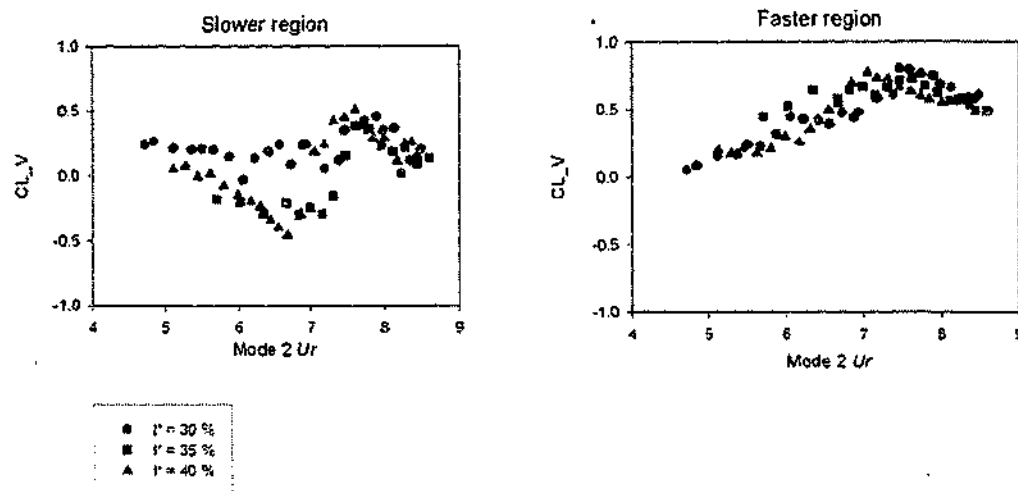


Figure 6-11 C_{L_V} , the average lift coefficient in phase with cylinder velocity from the faster and slower regions as a function of Mode 2 reduced velocity.

Figure 6-11 shows that C_{L_V} (based on the original unfiltered time series) is always positive in the faster Mode 2 favoured region while in the slower Mode 1 favoured region there are negative values of C_{L_V} in the range $Ur < 7.5$.

The Mode 2 power-in length, l^* , has the most effect in the slower region around $5 < Ur < 7.5$ where for larger values of l^* , C_{L_V} is more negative, indicating greater damping type behaviour.

As in the cases of uniform flow, the highest value of C_{L_V} measured is around 0.8, also agreeing with previous research on multi-frequency cylinder studies: "...the lift force coefficient in phase with velocity is always less than 1.0" (Vikestad 1998).

Next, the two coefficients C_{L_A} and Ca are presented for each region and for each mode. Previously, in the current chapter, the global added mass was evaluated based on the response frequency of each mode. Here, the added masses are local added masses and result from the fluid force in the region of interest. Both the lift coefficient in phase with acceleration, C_{L_A} , and the added mass, Ca , are presented. The local lift coefficient in phase with acceleration, C_{L_A} , for the slower Mode 1 favoured region and for the faster Mode 2 favoured region are shown in Figure 6-12. The corresponding local added masses are shown in Figure 6-13. The set of tests shown in both figures is the same set as previously investigated (Figure 6-5 through Figure 6-11).

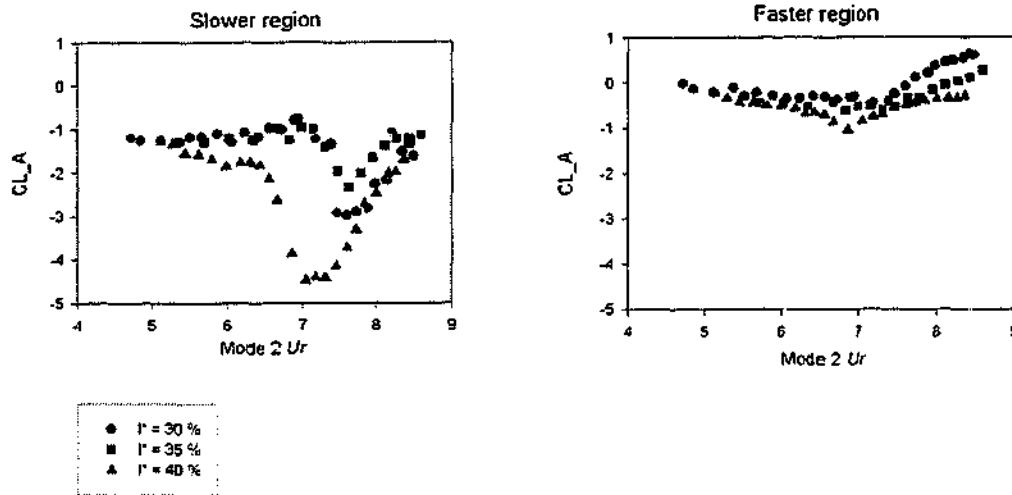


Figure 6-12 C_{L_A} , the local lift coefficient in phase with acceleration in the faster and slower regions as a function of Mode 2 reduced velocity.

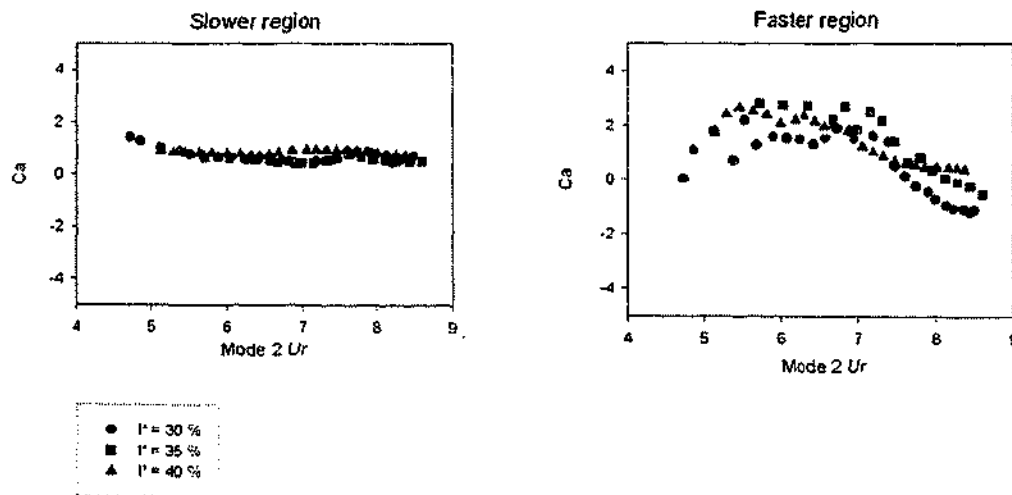


Figure 6-13 C_a , the local added mass for the faster and slower regions as a function of Mode 2 reduced velocity.

C_{L_A} in the slower region, as seen in Figure 6-12, is always negative while for the faster region, it has both negative and positive values. When comparing the two coefficients that both originate from the same force measurements in Figure 6-12 and Figure 6-13 it is startling to see how well Ca collapses the data compared to C_{L_A} . The success of Ca in collapsing the data is due to source of the measured force being from a well behaved added mass effect. In calculating Ca compared to C_{L_A} there is an additional step that requires normalising by the average peak acceleration, thus making Ca a purely inertia representative coefficient rather than a force related coefficient.

The local added masses in Figure 6-13 display quite different behaviour. Recall the basic behaviour of the global added mass in uniform flow from Figure 5-6, where Ca tends to minus 1 for high Ur and Ca increases to large values at low Ur for a given Mode.

In Figure 6-13 the local added mass in the faster region can be seen to decrease to around -1 at the Mode 2 resonant condition (peak amplitude response shown in Figure 6-5) while in the region $5.5 < Ur < 7.5$ Ca remains relatively constant. For small Ur the faster region Ca is seen to be very small. The reason that Ca doesn't increase as Ur decreases in the low Ur region can be explained by the fact that very low Ur values in the faster region represent high Ur values of Mode 1 within the same region (i.e. the lowest Ur test point shown in the faster Mode 2 favoured region ($Ur_{n=2} = 4.7$) can similarly be denoted as $Ur_{n=1} = 12.3$). At lower Ur values than those shown here Mode 1

dominates the whole response. The local added mass presented herein is found from the total local acceleration, which is the sum of several modes thus if one mode is dominant then the added mass calculation will be dominated by that mode. The local added mass can then be used as an identifier to distinguish if a mode is dominating the vortex shedding in the region by comparing the local Ca and Ur values to that predicted from the basic behaviour in uniform flow of the global added mass (Figure 5-6).

The local Ca for the slower Mode 1 favoured region in Figure 6-13 appears to follow the uniform flow behaviour at low Ur but then stays relatively flat at a value of 0.5, except for a peak of 1.0 around $Ur = 7.5$. Once again the local added mass is representing the summation of several modes of dominance. In the range of $7.5 < Ur < 8.0$ for the slower Mode 1 region, Mode 2 is dominating the whole riser response (Figure 6-5) and thus a high vibration frequency in a relatively slower region of flow would correspond to a higher predicted value of Ca from the basic behaviour curve of global added mass in uniform flow (Figure 5-6).

6.4.2. Forces and Coefficients from Filtered Time Series

The filtered coefficients found through the technique previously described in Section 6.4 are presented in this section. The coefficients represent Mode 1 (lp filtered) and Mode 2 (hp filtered) characteristics for both the Mode 1 and Mode 2 favoured flow regions.

The slower region's (Mode 1 favoured flow region) characteristics are shown on the L.H.S. of Figure 6-14. The Mode 1 and Mode 2 curves combine (in the sum of the squares sense) to form the total original results of the single slower region curve in Figure 6-11.

The faster region's (Mode 2 favoured flow region) characteristics are shown on the R.H.S. of Figure 6-14. Likewise, the sum of the squares combination of the two curves form the single faster region curve previously seen in Figure 6-11.

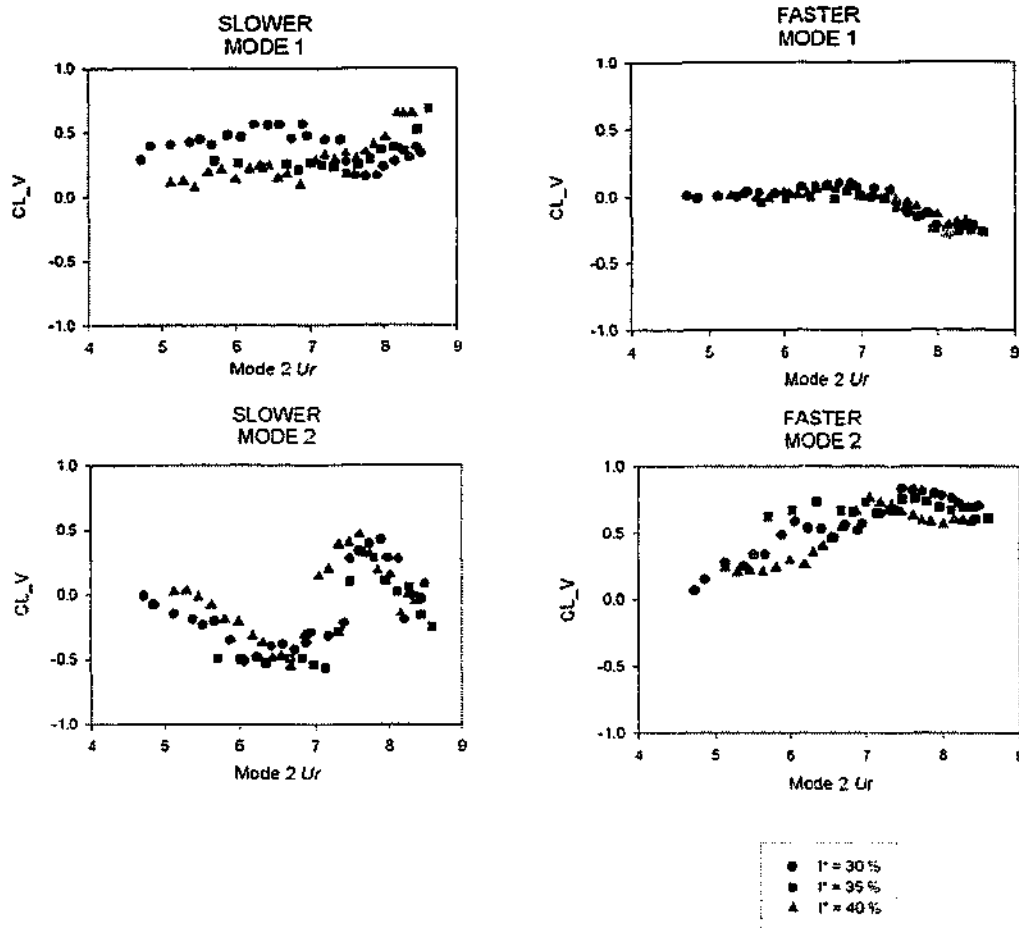


Figure 6-14 Slower and faster flow region's C_{L_V} Mode 1 and C_{L_V} Mode 2 characteristics.

The behaviour of C_{L_V} in the slower flow region shows two distinct and different paths when filtered in Figure 6-14. Attributing the sign of C_{L_V} to an indication of the power transfer direction, then it is observed that Mode 1 vibration continually has some power-in in the slower region, while Mode 2 is being damped everywhere except between $7.5 < U_r < 8.5$. Coincidentally, the U_r range where Mode 2 has power-in in the slower region is also where Mode 2 amplitude dominates the whole response (Figure 6-5). The slower Mode 1

region shows that for the smallest l^* , C_{L_v} is the highest. Therefore for the greatest Mode 1 power-in length (smallest Mode 2 power-in length = l^*), C_{L_v} is also the greatest.

C_{L_v} shown for the faster flow region in Figure 6-14 exhibits a power-in behaviour for Mode 2. The actual power-in is a function of several parameters (Equation 5.10) and most importantly it is dependent on the vibration frequency. Hence, even though the trend is for the slower region Mode 1 (Mode 1 power-in) to have an increasing power-in for $Ur > 7.5$, the actual power is considerably smaller than that of the Mode 2 power-in due to the very different vibration frequencies. In the faster Mode 2 region for the range $7.5 < Ur < 8.0$ (where Mode 2 is very dominant (Figure 6-7)), C_{L_v} is smaller for greater l^* , indicating a limiting behaviour in this region. In other words, in this dominant region, when the power-in length is greater, the power per unit length extracted is less.

The filtered lift coefficients in phase with local acceleration are shown in Figure 6-15. The corresponding filtered local added masses are shown in Figure 6-16. Both figures correspond to the set of tests previously presented in Figure 6-7 through to Figure 6-14.

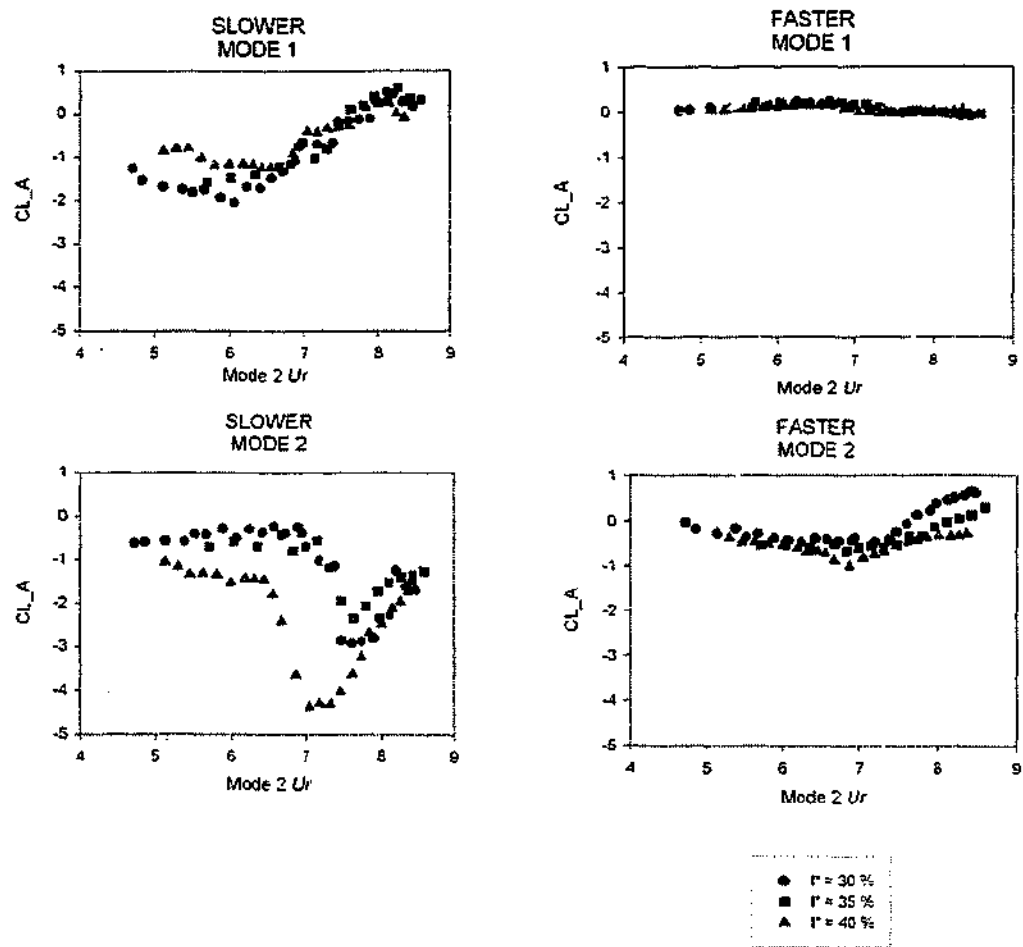


Figure 6-15 Slower and faster flow regions' $C_{L,A}$ Mode 1 and $C_{L,A}$ Mode 2 characteristics.

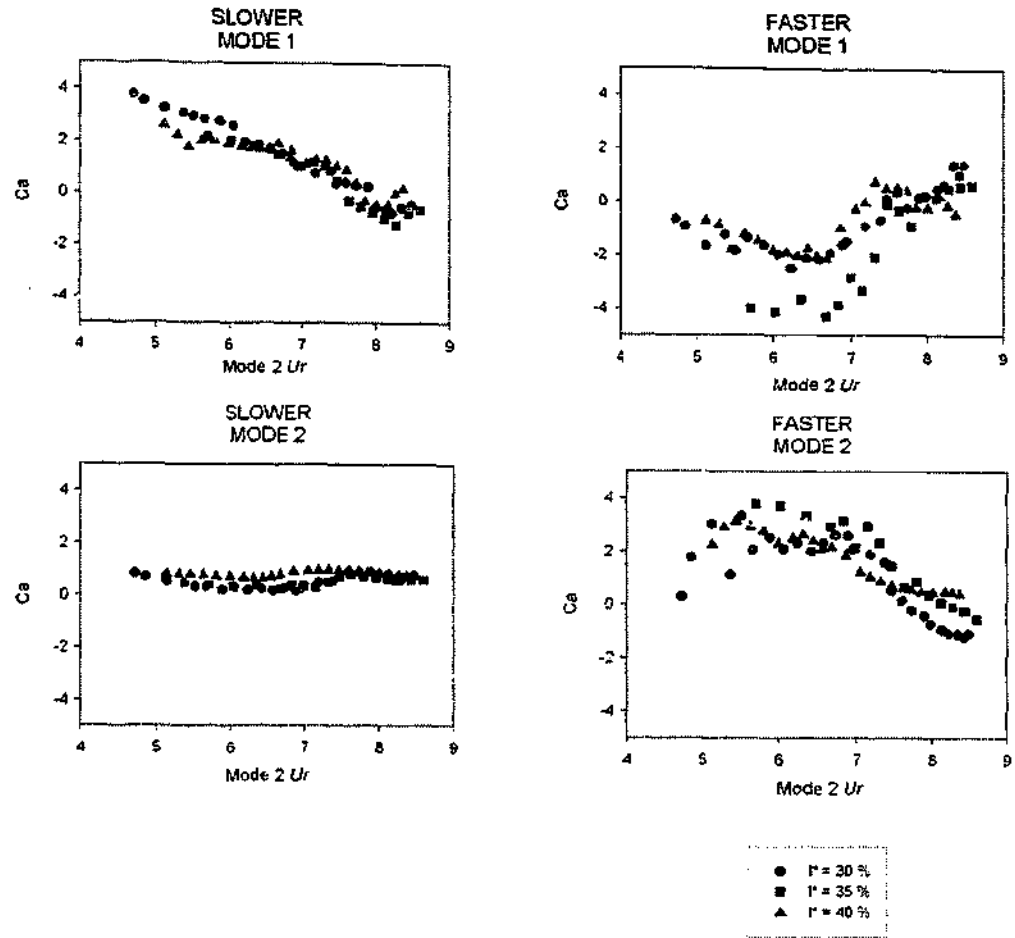


Figure 6-16 Slower and faster flow regions' Ca Mode 1 and Ca Mode 2 characteristics

Several comments can be made about the behaviour of the local added masses in Figure 6-16. The faster flow region values in Figure 6-16 show that the Mode 1 characteristic is what would be predicted from the uniform cases, that is, around the value of $Ca = -1.0$ for high Mode 1 Ur (shown as low Mode 2 Ur in the top right figure). For $I^* = 35\%$ an even more negative Ca is found. In the range of higher Ur in the faster flow, Mode 1 Ca rises steadily from $Ur = 6.5$ to $Ur = 8.5$. The variation of faster Mode 1 Ca compared to relatively constant $C_{L,A}$ in Figure 6-15 shows that it is not an inertia effect. $C_{L,A}$ remaining

relatively constant and near zero indicates that the size of the force is small and displays little variation, whereas the variation in Ca is not typical of a constant inertia and is caused by small force changes accompanied by varying small acceleration changes. The Ca attributed to Mode 2 shows a decline as Ur increases, displaying the same type resonant behaviour as the global Ca in uniform flow, but in a much narrower band (which matches the region of Mode 2 resonance shown by the amplitude response).

The variation of $C_{L,A}$ in the slower region is much the same as in the unfiltered case. The slower zone Mode 1 Ca takes on the shape of the behaviour of the global Ca in uniform flow, decreasing as Ur is increasing. The slower zone Mode 2 $C_{L,A}$ when compared to Ca shows that while there is a large variation in force, the inertia remains relatively constant.

6.5. EFFECT OF DIFFERENT SPACING OF NATURAL FREQUENCIES

The effect of spacing of natural frequencies was examined for the uniform flow cases in Section 5.3.4. The conclusion of the uniform flow tests was that the position of the peak uniform flow response occurs at lower Ur for a smaller gap to the next natural frequency.

In the current section, the effects of spacing of natural frequencies will be examined for the 2-Slab flow condition, using the same five values of end tension used in the uniform flow tests. The five different values cover the largest range possible within the design limits of the apparatus.

The ratio of natural frequencies examined to date in the current chapter provide the closest match to simultaneous resonant conditions in both slabs of flow. The different ratios of natural frequencies presented in this section can still be classified as both 'simultaneously resonant' when the broad lock-in range that was shown from the results of the uniform flow tests is considered. The different ratios of natural frequencies are then exploring the effect which the ratio of natural frequencies causes within the two regions.

With the riser simultaneously exposed to two flow fields there are two reference reduced velocities to choose from. The Mode 2 reduced velocity was chosen to enable any comparisons the reader may wish to make with results

presented earlier in this chapter, which are all in terms of Mode 2 U_r . The span of reduced velocities reported in this section is shown in Figure 6-17.

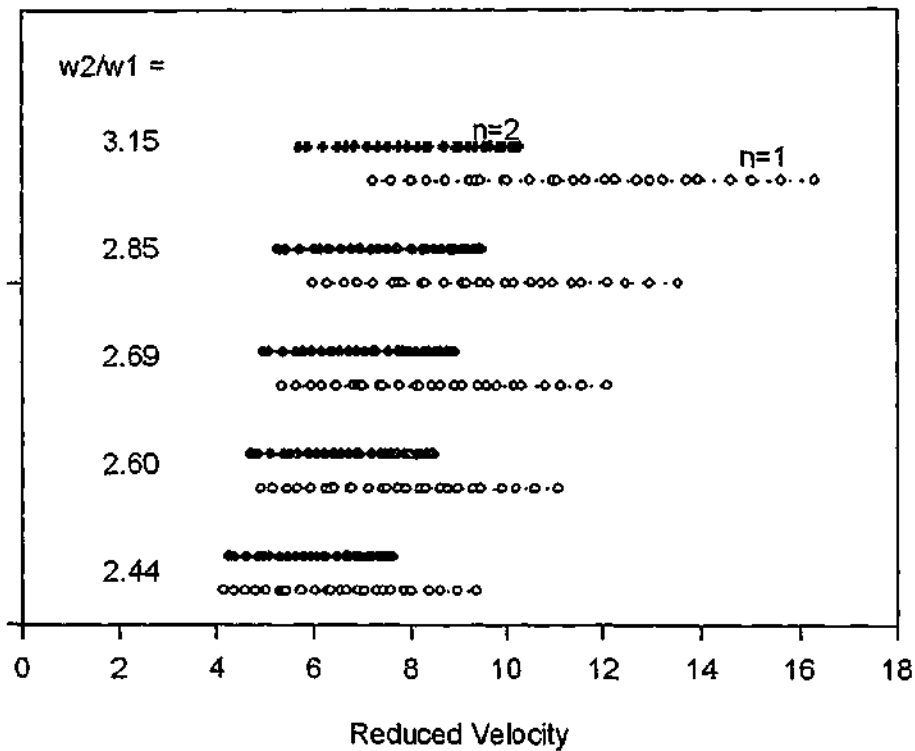


Figure 6-17 The range coverage of Mode 1 (hollow circles) and Mode 2 (solid circles) reduced velocities. Each pair of lines represents a test series for the ratio of natural frequencies given (w_2/w_1), with each circle representing a test.

Figure 6-17 shows the span of reduced velocities in the different test series. One set of tests corresponds to a pair of lines with each individual test being the same number of circles along the line in a given pair.

The peak modal amplitude response for all the tests identified in Figure 6-17 is shown in Figure 6-18 for Mode 2 as a function of $Ur_{n=2}$, in Figure 6-19 for Mode 1 as a function of $Ur_{n=1}$ and in Figure 6-20 for Mode 1 as a function of $Ur_{n=2}$. The different values of w_2/w_1 indicate the different ratios of still water natural frequencies.

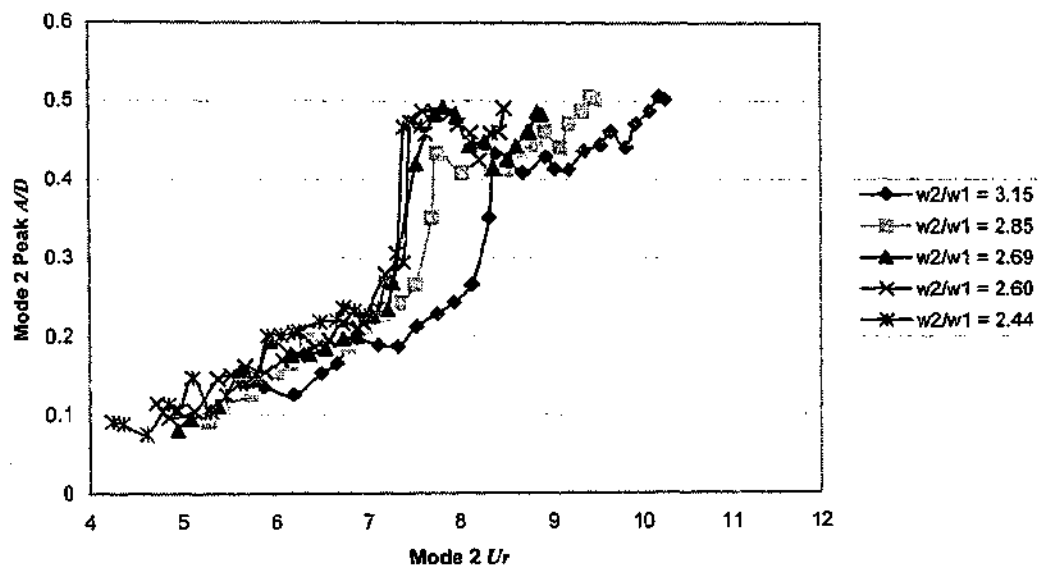


Figure 6-18 Mode 2 Peak A/D response as a function of the Mode 2 reduced velocity.

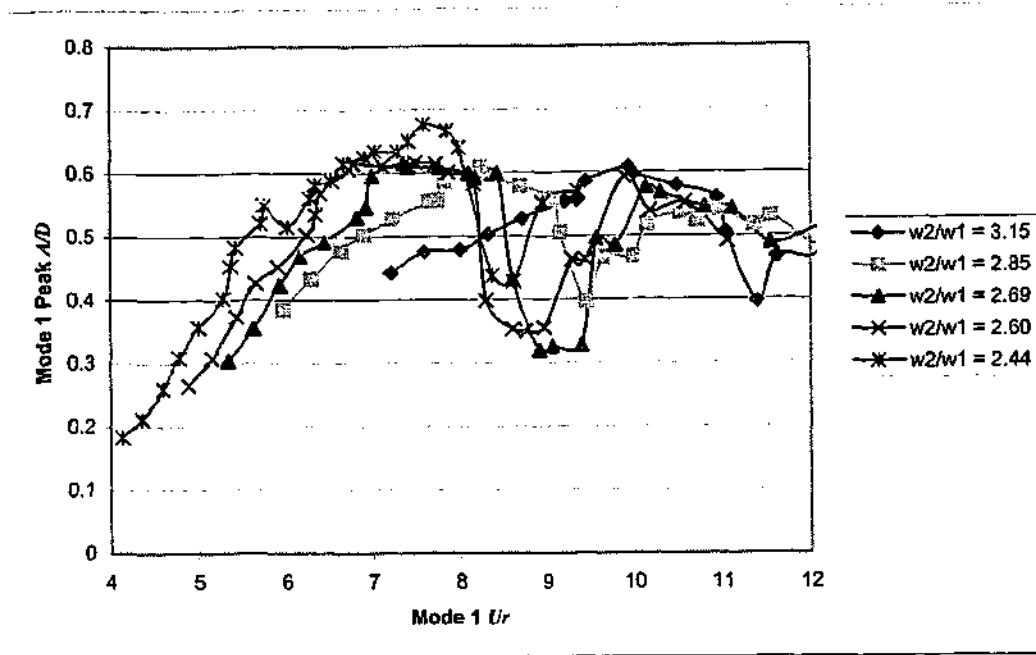


Figure 6-19 Mode 1 Peak A/D response as a function of the Mode 1 reduced velocity.

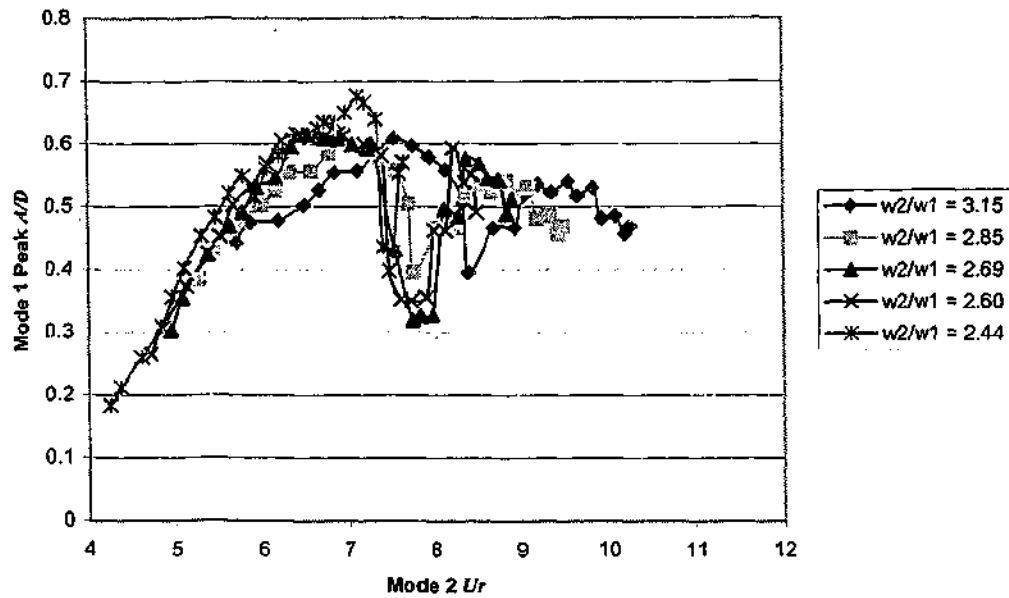


Figure 6-20 Mode 1 Peak A/D response as a function of the Mode 2 reduced velocity.

The difference in behaviour of Mode 2 in its dominating region between the tests can be observed in Figure 6-18. The Mode 2 peak response location as a function of Ur appears quite unaffected by the location of the peak response of Mode 1 (as shown in Figure 6-19). The differences of Mode 2 response can be then be said to not be a function of any of the effects of Mode 1, but can merely be attributed to the same differences that caused the shift in the peak response in the uniform flow tests.

It can be clearly seen in Figure 6-19 that the Mode 1 peak (and trough) response varies substantially to allow Mode 2 to govern the total response location. The variation is most clearly observed with the resulting collapse of Mode 1 response when shown as a function of Mode 2 reduced velocity in Figure 6-20. Mode 2 is setting the forcing conditions for Mode 1 and varying the location of peak Mode 1 response. This aforementioned effect shows that considering Mode 1 on its own, as would be done in a typical mode-by-mode analysis would be inaccurate in predicting the location of its peak response.

6.6. PREDICTION OF RESPONSE

One of the major results of reviewing of the literature (Chapter 2) was that modal response is found in a mode-by-mode fashion. Each mode is considered independently and regions of the riser are denoted power-in or power-out dependent on the relative reduced velocity with respect to the mode. All regions of the riser that fall outside the lock-in reduced velocity band are denoted as damping regions and in the literature the damping regions are identified as the most important to quantify for determination of overall modal response. Here, to examine modal competition issues and relate them to existing prediction programs, the hypothesis that regions not within the lock-in reduced velocity range (now termed non-favoured regions) are *all* damping is examined.

6.6.1. Contributions from the Non-favoured Regions

The power transfer has already been considered and shown for each mode previously (Figure 6-14) in the form of the lift coefficient in phase with riser velocity $C_{L,V}$. Perhaps easier interpretation of the transfer of power in the non-favoured regions is through examination of the power itself. The actual power transfer per unit length into each respective mode from the non-favoured region is plotted in Figure 6-21 for the Mode 1 power-out (M1 P.O.) and Mode 2 power-out condition (M2 P.O.). Also in Figure 6-21 is the response of Mode 2 divided by Mode 1, q_2/q_1 . The series of tests shown is typical of all test series.

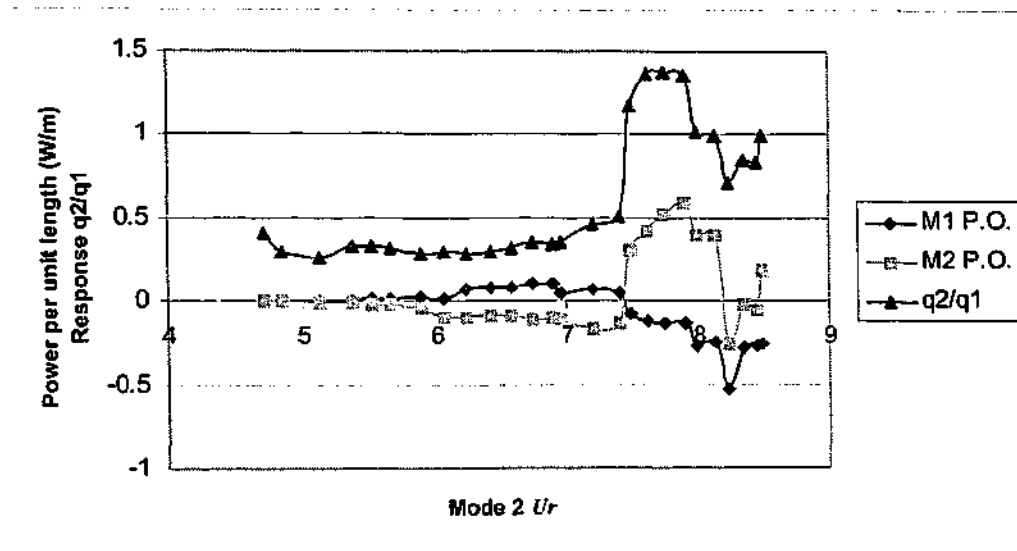


Figure 6-21 The power transfer in the 'non-favoured' regions for Mode 1 (M1 P.O.) and Mode 2 (M2 P.O.), along with response (q_2/q_1) as a function of reduced velocity.

In the lower reduced velocity ranges, the non-favoured Mode 1 region is shown to be actually exciting Mode 1. It has been previously shown (Figure 6-16) that in the faster flow region, for low flow values Mode 1 is excited. While the higher reduced velocity range shows that the non-favoured Mode 2 region contributes to exciting Mode 2 which is not at all intuitive. When comparing both the non-favoured regions to the overall response it is observed that the non-favoured Mode 2 region (slower region) is key to determining overall response. The power into Mode 2 from its non-favoured region follows the overall response trend.

The unexpected results of Mode 2 power-in from the slower flow region was examined further by plotting the path taken by the riser through the fluid for

different flow speeds. Figure 6-22 shows the motion of the model riser relative to ambient fluid through the slower flow region of fluid for a) slower than Mode 2 resonant condition, b) Mode 2 resonant condition and c) faster than Mode 2 resonant condition.

ative
that
than

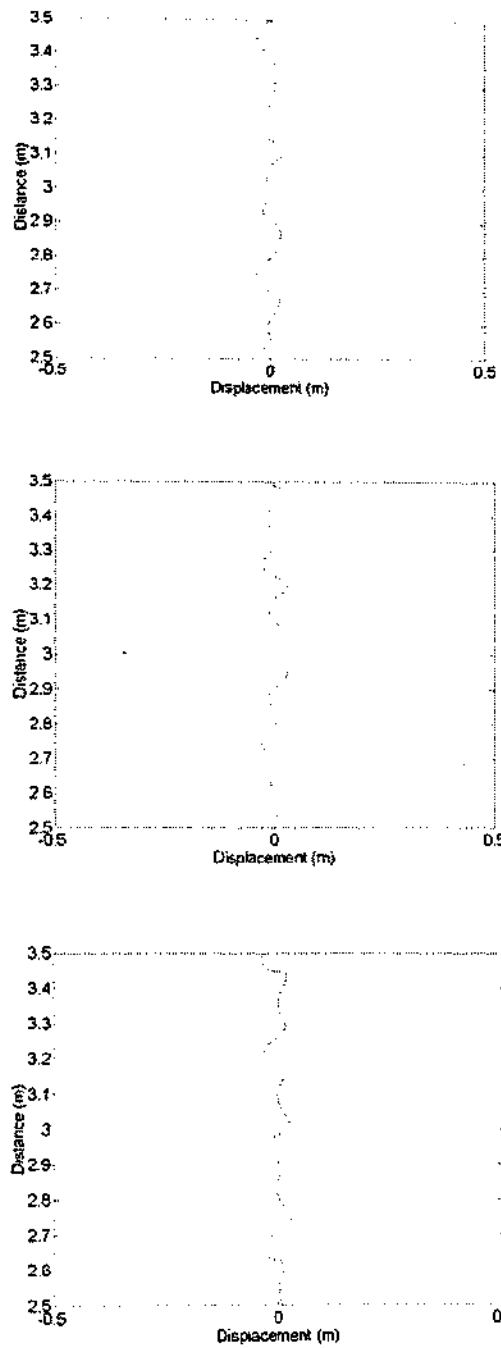


Figure 6-22 Motion of the model relative to ambient fluid through the slower flow region of fluid for a) less than Mode 2 lock-in ($Ur_{n=2} = 6.8$ for faster region) ; b) Mode 2 lock-in ($Ur_{n=2} = 7.63$); c) greater than Mode 2 lock-in ($Ur_{n=2} = 8.44$).

Figure 6-22 reveals that in the resonant region, the path taken by the riser exhibits a very regular pattern and compared to the non-resonant cases is very nearly symmetrical in nature for each cycle. The local flow pattern and vorticity distribution left behind in the wake of the resonant case are likely to be symmetrical thus imposing equal and alternating fluid forcing on the cylinder. Such a symmetrical flow pattern would typically result in a regular forcing and as the region has been shown to be a power-in one then a regular excitation is being provided. The source of the excitation is investigated in the next section.

We have seen a cross-flow Mode 2 power-in effect occurring in the slower region. The reduced velocity (calculated from the slower region velocity and Mode 2 natural frequency) for the power-in effect is in the range $2.5 < Ur_{n=2} < 3.5$. Either the cross-flow vibration or the in-line direction vibration must be driving the power-in effect. In light of the last statement, a generalised summary of the literature (from Chapter 2) and results from the uniform tests follows:

- Cross-flow excitation occurs on its own only after about $Ur = 4.0$.
- In-line excitation occurs over a wide range of Ur , and on its own in the range $1.5 < Ur < 3.5$.

As in-line excitation is possible at such low values of Ur , the effect must be due to an in-line lock-in motion. What is unknown is why the riser model

decides to switch from the Mode 1 natural frequency cross-flow response and choose an in-line lock-in response mode that supports Mode 2 cross-flow. The two most likely reasons for the switch occurring are:

- The local vortex shedding instability prefers to take the form of a single frequency phenomenon than exist in a multi-frequency environment.
- The local vortex shedding instability for a single frequency phenomenon has opposite shear layers rolling equally in magnitude, rather than what would occur in the case of competing multi-frequency events that would lead to non-zero mean lift forces lasting greater than one cycle of the dominant higher frequency mode.

In order to determine which mode was causing the lock-in and providing power-in effects, a cross-correlation analysis was performed. The analysis was conducted on all the in-line and cross-flow modal participation factors with the exciting cross-flow fluid force in the slower region. A peak cross correlation was calculated as

$$\rho_{xy}(\tau) = \frac{C_{xy}(\tau)}{\sqrt{C_{xx}(0)C_{yy}(0)}}, \quad (6.2)$$

where ρ_{xy} is the peak cross correlation and is the maximum value across the range of τ . Figure 6-23 shows ρ_{xy} for:

- The first three cross-flow and in-line modal participation factors all correlated with the exciting cross-flow fluid force in the slower region.

Also shown as a reference is the ratio of response of Mode 2 / Mode 1, q_2/q_1 .

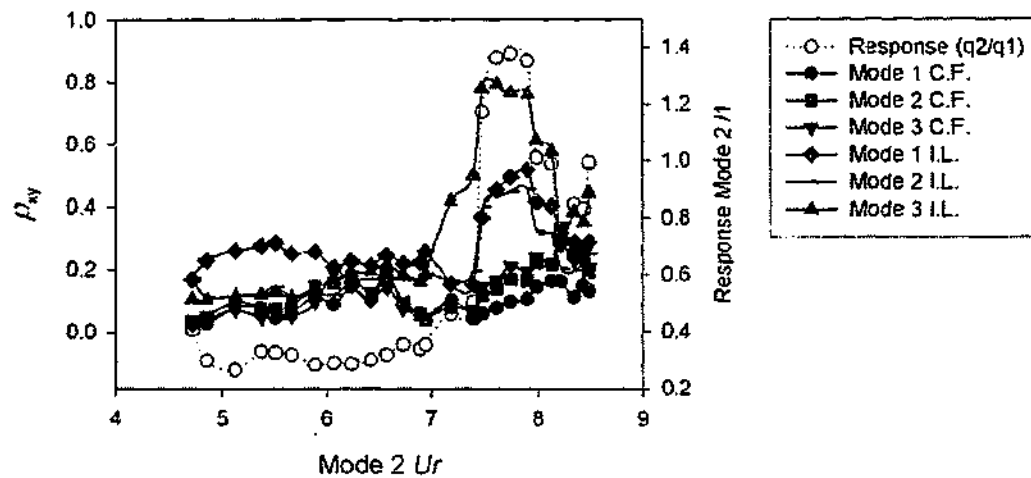


Figure 6-23 Peak cross-correlation values as a function of Mode 2 reduced velocity for a) all modes correlated with the higher frequency force in the slower region b) Mode 1 and Mode 2 correlated with their respective excitation and damping forces. Also shown is Mode 2/ Mode 1 response.

Figure 6-23 shows that around the range of peak Mode 2 divided by Mode 1 response, there is strong correlation (0.8) between that part of the filtered exciting force causing Mode 2 power-in (in the slower favoured flow region) with Mode 3 in-line. Mode 3 is therefore the in-line response responsible for the cross-flow Mode 2 power-in effect in the non-favoured region. As an indication of just how strong the previous correlation is, the next largest correlation between *any* mode and *any* fluid forcing (all combinations were tried although not all are shown graphically) was 0.5.

The frequency of Mode 3 in-line is observed in Figure 6-8 to increase prior to the resonant Mode 2 cross-flow condition, so that it is exactly double the Mode 2 cross-flow frequency. The in-line oscillation frequency is twice that which would be measured from an in-line uniform flow lock-in test.

The current results of Mode 3 in-line response in the 2-Slab flow conditions are plotted against Mode 2 cross-flow reduced velocity in Figure 6-24. Mode 2 reduced velocity is chosen on the abscissa as the frequency of in-line response was previously shown to be more unpredictable (Figure 5-19) than the cross-flow response frequency. The in-line VIV shown in Figure 6-24 is coupled to the Mode 2 cross-flow vibration (providing the power-in), therefore Mode 2 reduced velocity is the logical reference reduced velocity to choose. Also shown in Figure 6-24 are the results of in-line VIV cylinder experiments reported in the literature (Figure 2-13) and the results from the in-line uniform flow tests obtained in this research (Figure 5-16).

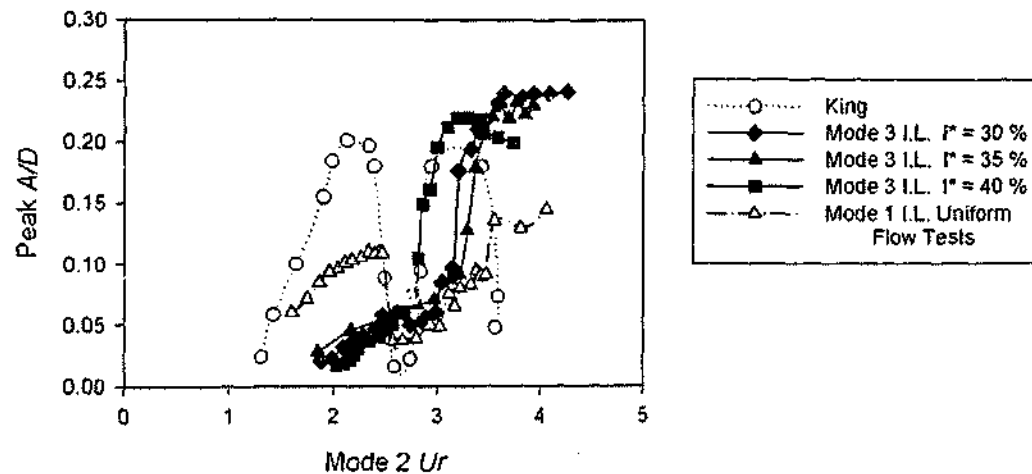


Figure 6-24 In-line VIV in the slower flow region against reduced velocity.

Figure 6-24 shows that the in-line movement of the riser model in the slower flow region undergoes a large increase in response around $Ur = 2.5$ to 3.0 . There are differences in the point at which the response increases. Compared to the second instability region in King's data, the location of the increase of in-line responses ($Ur \approx 2.8$) matches well for the case $l^* = 40\%$. While the peaks of $l^* = 30\%$ and 35% match a peak in the results of uniform flow tests. Other observations are that the first instability region (identified by King (1977) as *symmetric vortex shedding*) doesn't exist for the 2-Slab flow conditions where there is also significant Mode 2 cross-flow response. It is observed that only the in-line instability caused by *asymmetric vortex shedding* remains. It may be that symmetric vortex shedding does not occur when there is significant cross-flow movement present. The amplitude levels reported by King (for the tip of a cantilever) are similar to the in-line instability for the 2-Slab flow conditions. Recall from section 5.4, the amplitude levels from the in-line uniform flow tests are only a qualitative guide due to the accelerometers operating at the lower end of their range of sensitivity.

In summary from the current section:

Mode 2 peak amplitude response has been shown to be a function of Mode 2 power-in length. The supposed Mode 1 power-in region actually helps the Mode 2 peak (for a narrow range of reduced velocity) by an in-line lock-in

(Mode 3) effect. The power-in from the in-line Mode 3 lock-in effect region is obviously not as large as that from the faster region as increasing the power-in length of the Mode 2 favoured region has a positive increasing effect on amplitude. The results shown in Figure 6-14 also support the aforementioned statement as the peak $C_{L,V}$ from the in-line effect is about 0.5, while the peak $C_{L,V}$ from the Mode 2 power-in zone is about 0.8.

6.6.2. Applicability of coefficients

The current study involving a 2-Slab flow condition has idealised the realistic ocean current profiles that risers are subjected to. Obviously there are few situations that involve 2 uniform slabs of flow. However one may use the $C_{L,V}$ coefficients from the figures presented in the current chapter to form trends and apply these trends in modal superposition techniques for more complicated flow problems. For instance when one mode is largely dominating others the trend of $C_{L,V}$ may be used as a qualitative guide to determine how this mode will compete against all the others, treating all the others like they were 'one slab'. The plots of Ca may also be used to determine frequency response behaviour of dominating modes of less significant response modes in a competing modes environment.

The spacings of natural frequencies data in Figure 6-18 can be extrapolated to predict the exact Ur that a mode's peak response will occur at, given a riser's spacing of natural frequencies. Likewise some minor extrapolation of the

results of the power-in lengths can be performed for a dominant mode to predict the dominant modal amplitude.

6.6.3. Deviations from Previous Mode-by-Mode Approach

Regions of a riser that can be subject to the in-line instability need to be checked when performing a mode-by-mode analyses. At a minimum the regions must be removed from the calculation of the hydrodynamic damping component of the modal response. More accurate prediction would involve adding the in-line regions to the calculation of power-in with a reduced lift coefficient ($C_{L_y} = 0.5$ shown here) as compared to cross-flow power-in regions ($C_{L_y} = 0.8$ shown here).

7. CONCLUSIONS AND RECOMMENDATIONS FOR FUTURE WORK

A summary of contributions is outlined and then the conclusions follow. Future research possibilities are presented at the end of the chapter.

7.1. SUMMARY OF CONTRIBUTIONS

This thesis has investigated the fundamentals of a long flexible cylinder undergoing VIV in large scale laboratory conditions under both uniform and 2-Slab flow conditions. The most significant intent behind the work has been to improve predictions of multimode VIV effects on large scale offshore structures, which currently has limited understanding.

The main contributions from the thesis are categorised under the thesis objective headings (from Section 2.10) :

The accuracy of short rigid cylinder results for long flexible cylinder cases.

The added mass from short rigid cylinder results has excellent agreement to long flexible cylinder cases. The peak amplitude of response from short rigid cylinder experiments is not accurate at predicting the reduced velocity of peak response for a long flexible cylinder.

In-line motion and its effect on cross-flow response.

In-line motion is shown to be of vital importance in predicting single mode cross-flow lock-in events in a shear flow. In a shear flow an in-line VIV can occur at low Ur (as in uniform flow tests) dominating over lower frequency cross-flow response alternatives and supporting the higher frequency cross-flow resonant response.

Modal competition and dominant response behaviour.

Mode-by-mode prediction methods of long flexible cylinders in shear flow need to consider possible in-line responses of other modes. The magnitude of modal response under competing conditions is shown to be a function of spacing of natural frequencies and power-in lengths.

7.2. CONCLUSIONS

The following conclusions address the thesis objectives in the order the objectives are presented above. Each conclusion is referenced to the section of the main text from where the conclusion was drawn.

The accuracy of short rigid cylinder results for long flexible cylinder cases:

- i. The peak amplitude of VIV on a long flexible cylinder in Mode 1 response is confirmed to occur at much higher values of reduced

velocity than the peak response of a short rigid cylinder case (Section 5.3.1).

- ii. The reduced velocity at which the peak amplitude of VIV on a long flexible cylinder occurs at is a function of the spacings of natural frequencies. A closer spacing to the next natural frequency causes the peak to occur at smaller reduced velocity values (Section 5.3.4), an effect that cannot be predicted from short rigid cylinder results.
- iii. The added mass as a function of reduced velocity for a long flexible cylinder in uniform flow conditions shows remarkable agreement with the results from both free and forced short rigid cylinder experiments (Figure 5-4). The clear agreement between the results shows that the use of the modal amplitude is a valid method of averaging the conditions along the cylinder and that the short cylinder added mass data may be applied for prediction of long flexible cylinder behaviour.
- iv. The magnitude of the lift coefficient, $C_{L,V}$, does not exceed 1.0 for any uniform or 2-Slab flow cases of long flexible cylinders thus showing agreement with multi-frequency short rigid cylinder experimental results (Section 6.4). The local values of $C_{L,V}$ in non-uniform flow cases can be used to determine the presence of any global effects that would exclude the use of applying short rigid cylinder results.

In-line motion and its effect on cross-flow response:

- v. In-line response in uniform flow conditions cannot be predicted using the basis for cross-flow response. For the first mode, in-line response occurs on its own in the range $1.5 < Ur < 3.5$ at lower Ur values than cross-flow. Once the cross-flow response range has been entered, in-line response persists longer as a function of Ur (Section 5.4).
- vi. When dominant cross-flow response of a long flexible cylinder occurs in uniform and 2-Slab flow conditions an increased in-line response can occur. (Section 5.4.2 and Section 6.6).
- vii. In-line lock-in can occur in a region to reinforce cross-flow response throughout the whole structure. The in-line lock-in frequency will be twice the cross-flow response frequency (Section 6.3).

Modal competition and dominant response behaviour:

- viii. Modal frequency can be calculated from the basic added mass and hence is a function of reduced velocity (Figure 5-4). In a spatially varying flow, each mode's added mass can be approximated by using the closest flow velocity to the *resonant* reduced velocity value.

- ix. Increasing the power-in length of a mode associated with a faster flow in a competing mode environment increases that mode's overall response domination of the whole riser (Figure 6-7).
- x. The trends of $C_{L,y}$ from Figure 6-14 can be used to predict the response in competing mode environments.
- xi. By reducing the spacing of natural frequencies of a riser in a multi layer flow, the location of peak response of the dominant cross-flow mode as a function of U_r will be reduced (Section 6.5).
- xii. Non resonant regions of a riser are critical to prediction of modal response. The hydrodynamic power exchange in the non resonant regions follows the same trend as modal dominance as a function of U_r (Section 6.6.1).
- xiii. The locally measured motion of a long flexible cylinder relative to ambient fluid can reveal whether lock-in behaviour is occurring in that region in a competing mode environment (Figure 6-22).
- xiv. When two modes, well separated in frequency, are each individually predicted to have large cross-flow amplitude responses, the power-in region of the lower frequency mode may switch over to an in-line lock-

in response. The in-line response supports the higher frequency dominant cross-flow mode (Section 6.6.1).

7.3. RECOMMENDATIONS FOR FUTURE WORK

The following list identifies the key experimental areas of importance that are in the author's opinion in most need of attention:

- The importance of in-line lock-in effects need to be more fully investigated both in simple short rigid cylinder tests and more complicated cases. In particular for a given flow speed all the modes have a different reduced velocity associated with them and quantifying when the structure selects to lock-in in the in-line direction (low Ur values) over the cross-flow (high Ur values) is of vital importance to shear flow response prediction.
- More testing with local pressure distribution measurements on field or laboratory experiments is highly desirable. One is then be able to determine how the local vortex shedding behaves.
- Simultaneous flow visualisation of the multimodal situation can be conducted in a laboratory. Visualisation will help understand the vortex shedding patterns that cause the response.
- Higher mode number interaction can be investigated with more compact and expensive instrumentation using the current facility. Increasing m^* of the current model would also enable the effects of both m^* and higher mode numbers to be studied. Smaller diameter models in the laboratory (due to size constraints, smaller models would probably require an alternative to accelerometers to measure response) would also enable a greater understanding of higher mode numbers.

- Tests involving greater variations of power-in length would be extremely valuable. Both in 2-Slab and other shear flow conditions, these tests can reveal more about the boundaries of modal dominance as a function of power-in length.
- The effects of different structural damping on riser response could be investigated in the current facility to determine if material selection issues are a large factor in VIV response.

8. REFERENCES

Achenback, E., Heinechen, E. 1981 On vortex shedding from smooth and rough cylinders in the range of Reynolds numbers 6×10^3 to 5×10^6 . *Journal of Fluid Mechanics*.

Bearman, P. 1984 Oscillating Bluff Bodies. *Annual Review of Fluid Mechanics*.

Blackburn, H.M., Govardhan, R.N., Williamson, C.H.K. 2000 A complementary numerical and physical investigation of Vortex-Induced Vibration. *Journal of Fluids and Structures* 15, 481-488.

Blevins, R.D. 1977. *Flow Induced Vibration*. Robert E. Krieger Publishing Company.

Chaplin, J.R. 1999 History forces and the unsteady wake of a cylinder. *Journal of Fluid Mechanics* 393, 99-122.

Cheung, J. C.K., Melbourne, W. 1983 Turbulence effects on some aerodynamic parameters of circular cylinders at supercritical Reynolds numbers. *Journal of Wind Engineering and Industrial Dynamics* 14, 399-410.

Eaddy, M. 2002 *Personal Communication*, Monash University, Australia.

Fang, J., Lyons, G. J. 1996 Structural damping of tensioned pipes with reference to cables. *Journal of Sound and Vibration* 193(4), 891-907

Gerrard, J.H. The mechanics of the formation region of vortices behind bluff bodies. *Journal of Fluid Mechanics* 25, 401-413.

Gharib, M.R., 1998 *Vortex-Induced Vibration, Absence of Lock-in, and Fluid Force Deduction*. Ph.D. thesis, California Institute of Technology, USA.

Gopalkrishnan, R. 1993 *Vortex-Induced Forces on Oscillating Bluff Cylinders*. PhD Thesis. M.I.T., USA.

Griffin, O.M., Skop, R.A., Ramberg, S.E. 1975 The resonant vortex-excited vibrations of structures and cable systems. 7th *Offshore Technology Conference*, OTC Paper 2319, Houston, USA.

Griffin, O.M. 1985 *Vortex-Induced vibrations of marine cables and structures*. NRL Memorandum Report. Naval Research Laboratory, Washington D.C. Report 56.

Harding, B. H. 2002 More upgraded deepwater rigs on the horizon. *Offshore*, July.

Holmes, P., Lumley, J.L., Berkooz, G. 1996 *Turbulence, Coherent Structures and Symmetry*. Cambridge University Press, Cambridge, U.K.

Huse, E., Nielsen, F.G., Soreide, T. 2002. *Proceedings of the 21st International Conference on Offshore Mechanics and Arctic Engineering*, Oslo, Norway.

Kaasen, K.E. 2000 Identification of modes of VIV on a drilling riser from measurements of acceleration and rate of rotation. *International Offshore and Polar Engineering Conference*, Seattle, USA

Khalak, A., Williamson, C.H.K. 1999 Motions, forces and mode transitions in vortex-induced vibrations at low mass-damping. *Journal of Fluids and Structures* **13**, 813-851.

Kim, Y.H., Vandiver, J.K., Holler, R. 1986 Vortex-Induced vibration and drag coefficients of long cables subjected to sheared flow. *Journal of Energy Resources Technology* **108**, 77-83.

King, R., Prosser, M.J., Johns, D.J. 1973 On Vortex Excitation of Model Piles in Water. *Journal of Sound and Vibration* **29**, 169-188.

King, R. 1977 A review of vortex shedding research and its application. *Ocean Engineering*, **4**, 141-171.

Larsen, C.M., Koushan, K., Passano, E. 2002 Frequency and time domain analysis of vortex induced vibrations for free span pipelines. *Int. Conf. on Offshore Mechanics and Arctic Engineering (OMAE)*, Oslo, Norway.

Leonard, A., Roshko, A. 2001 Aspects of Flow-Induced Vibration. *Journal of Fluids and Structures* **15**, 415-425.

Lie, H., Larsen, C.M. Vandiver, J.K. 1997 Vortex-Induced Vibrations of long marine risers; model test in a rotating rig. *Proc. Of the Int. Conf. On Offshore Mechanics and Arctic Engineering*.

Moe, G., Wu, Z.-J. 1990. The Lift Force on a Cylinder Vibrating in a Current. *Journal of Offshore Mechanics and Arctic Engineering* **112**, 297-303.

Pantazopoulos, M.S. 1994 Vortex-induced vibration parameters: Critical review. *Proc. Of the 13th Int Conf on Offshore Mechanics and Arctic Engineering (OMAE)* **1**, 199-255.

Rao, S.S. 1990 *Mechanical Vibrations*. Prentice-Hall.

Sarpkaya, T. 1979 Vortex-induced oscillations, a selective review. *Journal of Applied Mechanics* **46**, 241-258.

Sarpkaya, T. 1995 Hydrodynamic Damping, Flow-Induced Oscillations, and Biharmonic Response. *Transactions of the ASME*. **117**, 232-238.

Sarpkaya, T. 2000 Conference discussion. *Bluff Body Wakes and Vortex-Induced Vibrations II (BBVIV2)*. Marseille, France.

Stansby, P.K. 1976 The locking-on of vortex shedding due to the cross-stream vibration of circular cylinders in uniform and shear flows. *Journal of Fluid Mechanics* **74(4)**, 641-665.

Sumer, B.M., Jensen, B.L., Fredsoe, J. 1991 Effect of plane boundary on oscillatory flow around a circular cylinder. *Journal of Fluid Mechanics* **225**, 271-300.

Sumer, M.B. and Fredsøe, J. 1997 *Hydrodynamics around cylindrical structures*. World Scientific.

Toebes, G. H. 1969 The unsteady flow and wake near an oscillating cylinder. *ASME Journal of Basic Engineering*, **91**, 493-502.

Vandiver J.K. 1985 Prediction of lock-in vibration on flexible cylinders in sheared flow. *Proceedings of the 1985 Offshore Technology Conference, Paper No. 5006*, Houston, USA.

Vandiver, J.K., Jong, J.-Y. 1987 The relationship between in-line and cross-flow vortex-induced vibration of cylinders. *Journal of Fluids and Structures*. **1**, 381-399.

Vandiver, J.K. 1993 Dimensionless parameters important to the prediction of vortex-induced vibration of long, flexible cylinders in ocean currents. *Journal of Fluids and Structures* **7**, 423-455.

Vandiver, J.K., Allen, D., Li, L. 1996 The occurrence of lock-in under highly sheared conditions. *Journal of Fluids and Structures* **10**, 555-561.

Vandiver, J.K. 2000. Predicting lock-in on drilling risers in sheared flows. *Flow Induced Vibration*. Ziada and Staubli (eds), Balkema, Rotterdam, ISBN 90 5809 129 5.

Venugopal, M. 1996 *Damping and Response Prediction of a Flexible Cylinder in a Current*. PhD Thesis, M.I.T., USA.

Vikestad, K. 1998 *Multi-frequency response of a cylinder subjected to vortex shedding and support motions*. Dr.Ing Thesis. N.T.N.U., Norway.

Vikestad, K., Halse, K.H. 2000 VIV lift coefficients found from response build-up for an elastically mounted dense cylinder. *Proc. Of the 10th Int. Offshore and Polar Engineering Conference*, Seattle, USA. **III**, 455-460.

Vikestad, K., Larsen, C.M., Vandiver, J.K. 2000 Norwegian Deepwater Program: Damping of vortex-induced vibrations. *Proc. Offshore Technology Conference 2000. Paper No. 11998.*, Houston, USA.

Vikestad, K., Vandiver, J.K., Larsen, C.M. 2000. Added mass and oscillation frequency for a circular cylinder subjected to vortex-induced vibrations and external disturbance. *Journal of Fluids and Structures* 14, 1071-1088.

Williamson, C.H.K., Roshko, A. Vortex formation in the wake of an oscillating cylinder. *Journal of Fluids and Structures* 2, 355-381.

Zdravkovich, M. M. 1990 On origins of hysteretic responses of a circular induced by vortex shedding. *Zeitschrift fur Flugwissenschaften Weltraumforschung* 14, 47-58.

Zdravkovich, M. M. 1997 Flow Around Circular Cylinders. Vol. 1: Fundamentals. Oxford University Press.